DOCTORAL DISSERTATION

博士論文

MODELING NAPL DISSOLUTION IN A MULTIPHASE FLUID SYSTEM IN POROUS MEDIA

相転移を含む多孔質媒体中における多相流体のモデル化

Yokohama National University

Graduate School of Urban Innovation

国立大学法人横浜国立大学大学院都市イノベーション学府

PULIGADDA LOHIT KRISHNA PRANAV

プリガッダ・ローヒト・クリシュナ・プラナヴ

March 2023

2023 年 3 月

MODELING NAPL DISSOLUTION IN A MULTIPHASE FLUID SYSTEM IN POROUS MEDIA

相転移を含む多孔質媒体中における多相流体のモデル化

by

PULIGADDA LOHIT KRISHNA PRANAV

プリガッダ・ローヒト・クリシュナ・プラナヴ

A Dissertation Submitted to the Graduate School of Urban Innovation, Yokohama National University in Partial Fulfillment of the Requirement for the Degree of

Doctor of Philosophy (Engineering)

Yokohama National University, Graduate School of Urban Innovation

国立大学法人横浜国立大学大学院都市イノベーション学府

Examination Committee

Professor, Dr. Mamoru KIKUMOTO (Chair)

Professor, Dr. Kimitoshi HAYANO

Associate Professor, Dr. Ying CUI

Professor, Dr. Takayuki SUZUKI

Associate Professor, Dr. Hiroto HIGA

March 2023

2023 年 3 月

ACKNOWLEDGEMENTS

ABSTRACT

Based on their aqueous solubilities, some Non-Aqueous Phase Liquids (NAPLs), Volatile Organic Compounds (VOCs), oils, and other chemical contaminants have been proven to dissolve in water present in the vadose zone affecting their transport phenomena such as advection, diffusion, dispersion, etc., and pose a threat to the quality of groundwater and subsurface environment in terms of public health through poisoning and spread of disease. Hence, it is necessary for us to take appropriate steps in predicting the contaminant's subsurface flow and transport to retrieve them through the implementation of effective remediation techniques. To describe a contaminant's seepage flow and transport, defining the suction (pressure)-coefficient of permeability-degree of saturation $\psi - k_r - S$ relationship of the pore phase fluids accurately is necessary.

Hence, the aims of this study are (1) to discuss the NAPL dissolution issue as a pore-scale phenomenon and provide a theoretical basis to model it quantitatively, (2) to establish a connection of suction-saturation $\psi - S$ relationship of a multiphase fluids system with the proposed NAPL dissolution theory, (3) to conduct experimental validation, (4) to check the applicability of the proposed governing equations, (5) to conduct parametric study of certain important newly proposed model parameters, and (6) to conduct numerical simulations and analyze the issue as a boundary value problem.

We model the dissolution process of NAPLs using a rate-dependent mass variation of vadose zone fluids. We focus on the pore-scale dissolution mechanism and propose a novel approach to define the NAPL dissolution rate in terms of NAPL-water specific contact surface area, which is in turn proven to depend on liquid saturation based on the theoretical study conducted in a cubic and hexagonal soil packing setting. A model connecting the NAPL dissolution formulation with the existing $\psi - S$ relationship among pore phase fluids is presented, to calculate the effective pore fluid pressures, which is later incorporated in defining the contaminant seepage flow.

We conducted experimental validation of the proposed model by comparing the decrease in NAPL saturation during dissolution process with existing results. The applicability of simplified forms

of Richard's equation to another analytical solution for fluid infiltration under different initial and boundary conditions is checked.

The effects of the type of NAPL and its wettability in defining the NAPL dissolution are studied through conducting parametric study with NAPLs that are frequently found in remediation sites for practical application. Finally, to numerically analyze the NAPL dissolution problem, we conduct Finite Element Method (FEM) simulation to solve a boundary value problem in both, NAPL-water two-phase system and gas-NAPL-water three-phase system.

TABLE OF CONTENTS

LIST OF FIGURES

LIST OF TABLES

CHAPTER 1

INTRODUCTION

1.1 Research background

1.1.1 Contamination in soil subsurface

Groundwater is the most extracted natural resource globally, with an estimated annual withdrawal rate of 982 km^3/year (J Margat, J van der Gun [2013]). A significant portion of the world's drinking water, ranging from 25% to 40%, is sourced from boreholes and dug wells (J Vrba, J van der Gun [2004]), while 38% of irrigated lands use groundwater for irrigation (S Siebert et al. [2010]).

This groundwater can be contaminated as a result of human activities or natural conditions. This can occur due to various processes such as: on–site sanitation systems, the excessive application of fertilizers and pesticides in agriculture, effluent discharged from wastewater treatment plants, leaks from sewers, petrol filling stations, a surface spill from industrial operations or an improperly maintained underground storage tank/reservoir, infiltration from urban runoff, or leaking from landfills etc. Groundwater can become contaminated by organic substances from landfills, posing a threat to public health through the spread of disease or poisoning. To address these dangers, the process of groundwater remediation has been established.

According to a study by the US Environmental Protection Agency, approximately 16000 chemical spills occur per year from trucks, trains, and improperly stored underground storage tanks (Pataki et al., [2007]). The transport mechanism of various toxic contaminant fluids under the ground surface is extremely important to avoid the pollution of soil and groundwater. Various mechanisms, such as interphase mass transfer, diffusion, adsorption, precipitation, and decay, impact the movement of pollutants in groundwater. Subsequently, under the proper conditions, if the contaminants creating a plume accumulate on the top of the groundwater table, the movement of water and dispersion within the aquifer spreads the pollutant over a wider area. The advancing boundary of a pollutant plume, also known as the plume edge, can reach groundwater wells, making the water unsafe for human and wildlife

consumption. Hence, it is crucial to understand their movement in identifying and implementing appropriate and effective groundwater remediation techniques.

1.1.2 NAPL contamination

Among all the contaminants, the Non–Aqueous Phase Liquids (NAPLs), both Light NAPLs (LNAPLs) and Dense NAPLs (DNAPLs) cause numerous detrimental effects to the quality of groundwater in different forms such as diffusion, advection, and dispersion. Toxicology studies have found that many volatile organic chemicals present in both landfills and groundwater can cause adverse health effects.

The behavior of NAPLs (Non-Aqueous Phase Liquids) in the subsurface is influenced by their fluid density. LNAPLs, such as petroleum hydrocarbons, are lighter than water and float on the groundwater table, present in unsaturated ground. On the other hand, DNAPLs, such as chlorinated solvents, are denser than water, sinking until they reach an impermeable layer, and exist in the saturated ground, as illustrated in Figure 1-1 (i). LNAPLs create a gas-NAPL-water three-phase system, while DNAPLs form an NAPL-water two-phase system, as depicted in Figure 1-1 (ii). Due to groundwater flow and variations in unsaturated hydraulic properties, these NAPLs can also spread laterally.
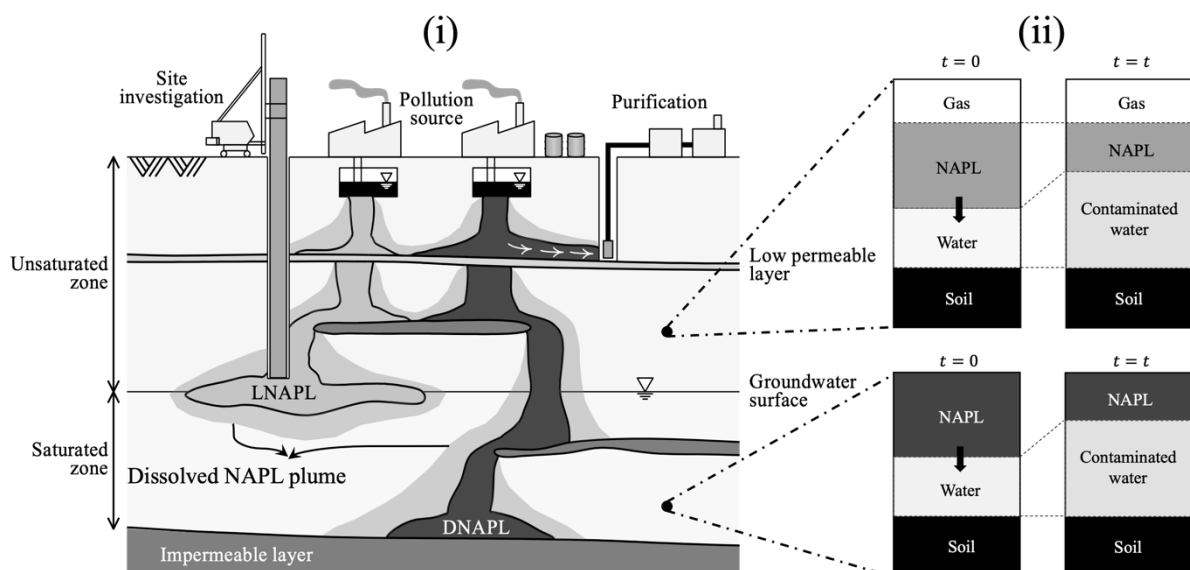
Figure 1-1: (i) Schematic figure of contamination of unsaturated shallow ground by LNAPL and

So far, numerous case histories of NAPL contaminated sites have been reviewed and described in published literature, consulting reports, and personal communications with investigators in NAPL remediations. The review indicates that the monitoring wells can contain no observable NAPL. The thickness of NAPL in wells typically decreases as the water table rises and increases as the water table falls (Kemblowski and Chiang [1988, 1990], Hunt et al. [1989]). As a result, NAPLs may suddenly appear or disappear in monitoring wells across a site, as shown in Figure 1-2. Furthermore, if the groundwater table level drops below its normal range of fluctuation, NAPLs may no longer be present in the monitoring wells. Although these observations do not apply to all NAPL sites, their frequent occurrence requires additional technical attention.
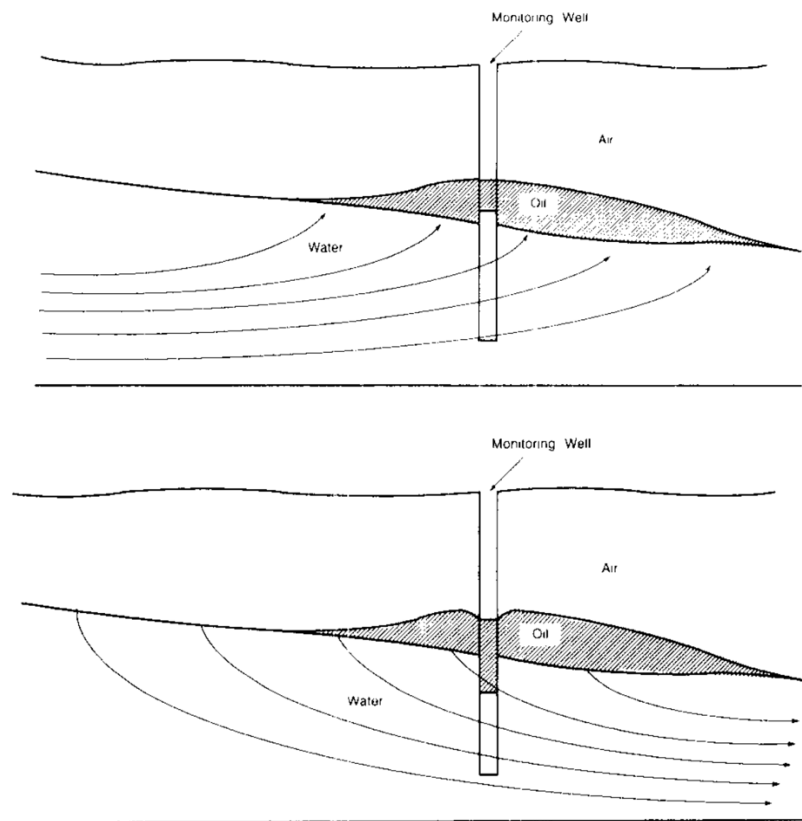
Figure 1-2: Hydrocarbon thickness decrease and increase for rising and falling interfaces

(Kemblowski and Chiang, [1990])

When these hazardous liquids enter the ground surface, they form an NAPL–water two–phase system in the saturated ground or a gas–NAPL–water three–phase system in the unsaturated ground as shown in the Figure 1-1 (ii). The NAPL travels first through the unsaturated zone, under three-phase

(Gas-NAPL-Water) flow conditions, displacing gas and water. When the NAPL comes across layers with lower permeability (e.g. silt or clay layers, or densely packed sand) or smaller pores, it will flow primarily horizontally until it reaches a more permeable layer. If the NAPL travels downward in either the unsaturated or saturated zones, it may create ganglia having low enough saturation level, as illustrated in Figure 1-3.
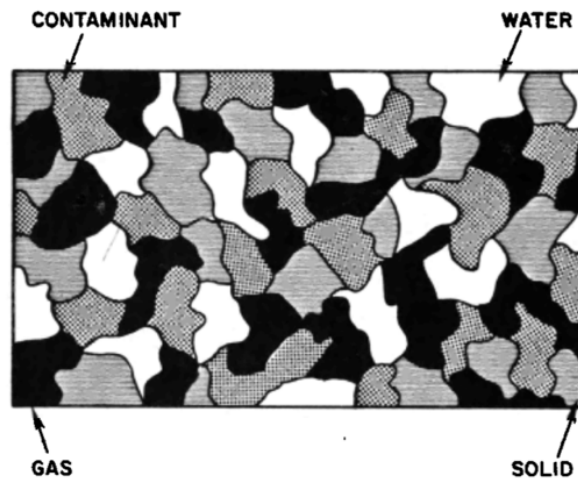
Figure 1-3: Heterogeneous distribution of pore phase fluids in the vadose zone (Abriola et al., [1985])

1.1.3 Remediation techniques

Groundwater remediation techniques can be divided into three major categories: biological, physical, and chemical treatment technologies depending on the parameters of contaminants such as physical, inorganic chemical, organic chemical, bacteriological, radioactive etc. Biological methods include treatment technologies such as bioaugmentation, biosparging, bioventing, bioslurping, phytoremediation, permeable reactive barriers which use biological organisms etc. Physical methods involve pumping and treating, air sparging, monitoring–well oil skimming, dual phase vacuum extraction etc. Chemical precipitation, ion exchange method, chemical oxidation, carbon absorption, surfactant enhanced recovery, permeable reactive barriers which use chemical processes etc. falls under the category of chemical treatment technologies. Variation in the selection of employing a specific type of remediation technique such as biological, physical, or chemical treatment technology, or a combination of different procedures varies with the type of contaminant(s) and the extent to which the

contaminant(s) spread inside the ground. To address the difficulties of direct measurement, indirect, non-invasive methods have been developed to assess field saturations.

1.2 NAPL dissolution

Both light non-aqueous phase liquids (LNAPLs) and dense non-aqueous phase liquids (DNAPLs) can dissolve into the water (miscible) phase over time, creating a plume and becoming a persistent source of contamination based on their water solubility. Most NAPLs (e.g., gasoline, BTEX etc.) present at remediation sites and in practical engineering applications consist of multicomponent forms with two or more toxic chemicals having different characteristics such as aqueous solubility and density. Some NAPLs have water solubility that greatly exceeds drinking water standards, leading to contamination of the unsaturated zone by NAPLs and their ongoing transport to groundwater, which has become a significant environmental issue in many industrialized nations. In either case of LNAPL or DNAPL contamination, the vicinity of NAPL layer to groundwater and surrounding soil suggests the possibility of dissolution. For simplicity, in this thesis, we present the illustrations of an LNAPL only. We also consider single component NAPLs and focus on the pore-scale dissolution phenomenon so as to extend the dissolution framework of NAPLs to other toxic soluble liquids which may be extremely soluble to be considered as an NAPL. Hence, the effective designs of remediation strategies require reliable modeling of NAPL flow and transport while capturing the dissolution process.

Non-equilibrium conditions, which affect the rate of transfer of mass between phases, can play a role in both active remediation and natural attenuation of NAPL contamination (Grathwohl [1998], Libelo et al. [1998], Reichert et al. [1998], Stauffer et al. [1998]). This can limit the effectiveness of treatment efforts, particularly under certain conditions such as high groundwater velocity, as indicated by recent studies (e.g. Powers et al. [1992]). The transfer of mass between fluid phases in a multiphase system is the main factor that governs the transport of contaminants in the interface between the phases.

NAPLs can also be divided based on their aqueous solubilities with their range varying from completely insoluble (aqueous solubility < 2.45 mg/L) to freely soluble (aqueous solubility > 3.9e+4 mg/L),

a list of which can be found in Newell et al. [1995] and Huling and Weaver [1991]. The following tables suggest the characteristics of NAPLs that determines the tendency of dissolution.

Table 1-1: Solubility characteristics of NAPLs (Pharmacopeia of the United States of America [2009])

Term	Aqueous solubility [mg/L]
Very soluble	15.87e+5
Freely soluble	6.5e+5
Soluble	3.9e+4
Sparingly soluble	
Slightly soluble	2.1e+3
Very slightly soluble	2e+2
Insoluble	2.45

1.3 Concluding remarks of introduction

Modeling the movement of contaminants in the subsurface can be an economical way to aid in cleaning up and managing contaminated sites. However, the lack of experimental data has negatively impacted the evaluation of existing models. To use models, it's important that they can accurately predict contaminant behavior and evaluate the level of uncertainty related to those predictions.

In order to accurately estimate the flow of NAPLs in a three-phase system, it is important to have a reliable model for the permeability of the three fluids involved. The permeability coefficients are largely dependent on the saturation levels of the fluids, so it is necessary to correctly describe the relationship between matric suction or capillary pressures and the saturation levels of the void fluids. This is achieved using the Darcy's law to associate the velocity in terms of pressure head (suction) and coefficient of permeability. The entire system is solved using the governing flow equation derived from the law of conservation of mass by substituting the degree of saturation and velocity through divergence theory. Hence, to evaluate the coefficient of permeability in Darcy's law, defining the entire system

involving suction–degree of saturation, $\psi - S$ relationship accurately is necessary. However, it is known that the $\psi - S$ relationship is affected by the dissolution phenomenon. The main focus of the current study is to capture this behavior in a multiphase fluid system.

1.4 Notations, symbols, and abbreviations

Bold letters are used to represent vectors. NAPL and oil are used interchangeably. The subscripts and superscripts, 'g', 'n', 'w', 'l' are used to represent gas, NAPL, water, and liquid (NAPL + water) phases respectively. The subscripts are used to represent the kind of system and the superscript represents the pore fluid in question (Eg., ψ_{gn} represents the suction between gas and NAPL, and S_{gnw}^{l} represent the saturation of liquid in a gas-NAPL-water three-phase system). $\nabla \cdot (\ \ )$, $\dot{}$ represents a partial differentiation in the spatial and temporal dimension respectively.

a_{nw}^{max}	*Maximum specific contact surface area between NAPL and water phases*
a_{nw}	*Specific contact surface area between NAPL and water phases*
C_n^{eq}	*Equilibrium aqueous phase concentration of NAPL*
C_n^w	*Concentration of NAPL present in the water phase*
C_n	*Total concentration of NAPL present in the system*
D_t	*Vertical dispersion coefficient*
k_d	*Mass transfer coefficient*
k_l	*Lumped mass transfer rate*
k_n^d	*Effective mass transfer rate*
k_n	*Equilibrium partitioning mass transfer coefficient*
k_r	*Coefficient of permeability*

k_r	Mass transfer rate
K_v^g	Compressibility of gas
K_w	Saturated permeability
l_c	Length of the pool
$m_n^{d,max}$	Maximum mass of NAPL dissolved in water at equilibrium state
m_n^d	Mass of NAPL dissolved
M_i	Mass balance index
m_w^0	Initial mass of water present in the system
q_{in}	Flow rate coming into the system
q_{out}	Flow rate going out of the system
S	Degree of saturation
S_e	Effective saturation of soil
S_{max}	Maximum degree of saturation of the wetting fluid
S_{min}	Minimum degree of saturation of the wetting fluid
S_n'	NAPL saturation at maximum NAPL-water specific contact surface area
S_n^0	Residual NAPL saturations
S_s	Specific storage coefficient
S_w'	Water saturation at maximum NAPL-water specific contact surface area
V_n^d	Volume of NAPL dissolved
V_t	Entire volume of the void space

V_w^0	Initial volume of water present in the system
V_x	Pore water velocities
β_l	Scaling parameter for three–phase characteristic curve given as a function of β_{nw} and μ
β_w	Scaling parameter for three–phase characteristic curve given as a function of β_{gn} and μ
Γ_i	Interphase mass transfer component of pore fluid, i
μ_{ri}	Relative viscosity
ρ_{ri}	Relative density of the fluid with respect to water
ρ_w^{mix}	Density of the contaminated water mixture
$\sigma_{n_i}, \sigma_{w_i}$	Exponents
C	Specific water capacity
$D(\Theta)$	Diffusivity function
g	Acceleration due to gravity
h	Total head
$K(\Theta)$	Hydraulic conductivity function
m	Fitting parameters for characteristic curve proposed by van Genuchten
n	Fitting parameter for characteristic curve proposed by van Genuchten
p	Pore fluid pressure
t	Time
v	Darcy's velocity

y	Depth	
z	Pressure head	
α	Material parameter for characteristic curve proposed by van Genuchten	
θ	Contact angle	
θ	Volumetric fluid content	
Θ	State variable in terms of θ	
μ	Relative magnitude of NAPL pressure to water pressure and air pressure	
ρ	Density	
ϕ	Porosity of the medium	
ψ	Suction	
ψ	Suction defined as the pressure difference between two void fluids	
ω	NAPL-water specific contact surface area	

Frequently appearing words are abbreviated as follows.

BTEX	*Benzene, Toluene, Ethylbenzene, Xylene*
BV	*Bio Venting*
CMLS	*Chemical Movement in Layered Soils model*
DNAPL	*Dense Non–Aqueous Phase Liquid*
ET	*Evapo–Transpiration*
FEM	*Finite Element Method*

LNAPL	*Light Non–Aqueous Phase Liquid*
NAPL	*Non-Aqueous Phase Liquids*
PCB	*Poly–Chlorinated Biphenyls*
PCE	*Per–Chloro Ethylene*
PRZM-2	*Pesticide Root Zone Model*
QB	*Quadratic Bezier*
RITZ	*Regulatory and Investigative Treatment Zone model*
SESOIL	*SEasonal SOIL compartment model*
SVE	*Soil Vapour Extraction*
SWCC	*Soil Water Characteristic Curve*
TCE	*Tri–Chloro Ethylene*
US EPA	*United States Environmental Protection Agency*
UTCHEM	*University of Texas Chemical Compositional Simulator*
VC	*Vinyl Chloride*
VIP	*Vadose zone Interactive Process model*
VLEACH	*Vadose zone LEACHing model*
VOC	*Volatile Organic Compounds*
WHO	*World Health Organization*

CHAPTER 2

LITERATURE REVIEW

2.1 Contaminant plume flow and transport

R N Bhargava [2019] had summarized succinctly, the governing mechanisms of petrochemical fate and subsurface transport mathematically. Chevalier et al. [1999], Oostrom et al. [2007], and specially Essaid et al. [2015] have summarized the research focusing on multidimensional, multifluid contaminant flow and transport, NAPL dissolution and volatilization, and organic contaminant biodegradation and remediation unlike several other compilations and reviews of flow and transport solely in an gas-water two-phase system such as Assouline [2013], DiCarlo [2013], Nielsen et al. [1986], Rolston [2007], van Genuchten et al. [2014] etc.

Chevalier et al. [1998] performed experiments to measure the thickness of an LNAPL spill in the subsurface and how it changes the capillary fringe. They also derived an equation to estimate the vertical thickness of the NAPL based on the displacement pressure in groundwater flow direction.

The suction–coefficient of permeability–degree of saturation, ($\psi - k_r - S$), an interdependent relationship, is crucial in predicting the movement of NAPLs in porous media. In this series of relationships, this thesis focuses on the $\psi - S$ relationship as it has not been defined precisely, especially in a multiphase system capturing NAPL dissolution. Extensive research has been conducted for accurately depicting the $k_r - S$ relationship (e.g., Gardner [1958], Mualem, [1976]) and $\psi - S$ relationship (e.g., van Genuchten [1980], Fredlund and Xing [1994]) for a two-phase system. Parker and Lenhard [1987] attempted to explain the coefficient of permeability–degree of saturation, $k_r - S$ relationship in the three–phase system by the extension of the model for two–phase system based on the assumption that the fluid entrapment process is similar to that in both systems. Some attempts were also made to describe the $\psi - S$ relationship in a three–phase system (e.g., Parker and Lenhard [1990], Eckberg and Sunada, [1984]). As pointed out by Nakamura and Kikumoto [2014], Parker and Lenhard [1987a, 1987b, 1990] had several limitations such as: (a) difficulty in describing the NAPL transport

phenomena due to its comparatively low spreading coefficient, (b) lack of an arbitrary phase transition to the water–air two-phase relationship because it depends on the premise that NAPL exists, and (c) not being able to predict the capillary behavior of the gas–NAPL–water three-phase system in soils when the NAPL saturation is low. The experimental work done by Eckberg and Sunada [1984] in the three–phase system was verified by extending a two–phase system capillary pressure versus saturation data. Nakamura and Kikumoto [2014, 2018] proposed a rational model for multiphase fluids incorporating transition among arbitrary two– and three–phase systems by smoothening the $\psi - S$ characteristic curves using the quadratic Bezier curve concept. Eventually, following Nakamura and Kikumoto [2014, 2018], Puligadda and Kikumoto [2021, 2022] were successful in modeling a multiphase fluid system capturing the phenomenon of hysteresis. Throughout this literature review, the consideration of interphase mass transfer was ignored in defining $\psi - S$ relationship.

It is important to note that the soil-water characteristic curve (SWCC), which describes the relationship between water content and soil suction, is crucial in understanding the behavior of unsaturated soil. The SWCC is used to estimate various properties of unsaturated soils, including hydraulic conductivity, shear strength, volume change, and aqueous diffusion functions (Pham et al. [2003]). In this regard, the basis of this thesis mainly lies in the importance of $\psi - k_r - S$ functional relationship which describes the fluid flow in soil subsurface considering NAPL dissolution.

2.2 Interphase mass transfer

2.2.1 Modeling

Early models generally assumed equilibrium between concentrations in all phases (e.g., Abriola and Pinder [1985a], Adenekan et al. [1993], Baehr [1987], Baehr and Corapcioglu [1987], Panday et al. [1995], Sleep and Sykes [1993a], Cline et al. [1991], Mackay et al. [1991], Simon A Michelle [2003], Sato and Nakajima [1979], Jury et al. [1990]) as shown in equation 2-1. Several researchers focused on estimating the partitioning coefficients of NAPL to predict its amount present in the soil accurately for

remediation using partitioning tracer tests (Jin et al. [1995], Wang et al. [1998], Lee et al. [1998], Schubert et al. [2007]).

$$C_n^{eq} = k_n C_n \qquad (2-1)$$

Furthermore, the mass transfer coefficient (k_n) is determined by equation 2-2 as reported by Powers and Heermann [1999].

$$k_n = n\sqrt{\frac{4D_t V_x}{\pi l_c}} \qquad (2-2)$$

where l_c is the length of the pool, D_t is the vertical dispersion coefficient, corresponding to respective pore water velocities, V_x.

The equilibrium NAPL aqueous phase concentration is reached after a considerable period of time (sometimes taking up to several years) depending on the properties of NAPL and is generally given by aqueous solubility. Hence, it is reasonable to assume that equilibrium conditions do not occur in many subsurface remediation systems. Nonequilibrium mass transfer of a dissolved constituent across fluid phases was also represented as a first-order rate-limited process by (Cussler [1984], [Sleep and Sykes, 1989]).

$$\dot{C_n^w} = k_n^d\left(C_n^{eq} - C_n^w\right) \qquad (2-3)$$

A detailed summary and review of the available NAPL dissolution modeling is given in Essaid et al. [2015] and Jia et al. [1999].

2.2.2 Experimental investigation

Experimental investigations were carried out by several researchers such as Miller et al. [1990], Broholm et al. [1999], Powers et al. [1998], Powers et al. [1992], Nambi and Powers [2000], Ramezanzadeh et al. [2020], Mobile et al. [2016], Bahar et al. [2018] to explore the influence of porous

media characteristics, NAPL type, and more importantly, aqueous phase velocities on NAPL dissolution rates until steady state is reached. Studies conducted by Hunt et al. [1998a] and Powers et al. [1991] have demonstrated that the rate of mass transfer between two liquids may be significantly slowed down in field conditions. Nambi and Powers [2000] conducted NAPL dissolution experiments for a range of conditions by varying the grain size of sand, initial NAPL saturations, and size and number of the coarse lenses and found that the variation in effective permeabilities and interfacial area for mass transfer affected the NAPL concentration at the sampling port. Nambi and Powers [2003] developed a new correlation based on experimental data for predicting rate limited mass transfer within a NAPL source zone entrapped in heterogeneous systems.

Several researchers have conducted experiments to examine the impact of various factors on NAPL dissolution rates, including porous media characteristics, type of NAPL, and groundwater velocity. These studies have shown that liquid-liquid mass transfer can be a limiting factor, especially in field conditions. Research by Nambi and Powers [2000] showed that the grain size of sand, initial NAPL saturations, and the size and number of coarse lenses all influenced NAPL concentration. Nambi and Powers [2003] developed a correlation to predict rate-limited mass transfer in NAPL source zones trapped in heterogeneous systems based on experimental data.

Broholm et al. [1999] investigated the fate of a multicomponent chlorinated solvent after its injection in a sandy aquifer i.e., the variation of concentration of NAPL due to dissolution over a space-time continuum through the sample experimentally. As a result, contour maps of different components of NAPL were shown to spread across the sample site.

However, most of these NAPL dissolution experiments were not straightforward to compare simulation results with due to one or more of the following reasons:

(1) they were not conducted in a closed system having rigid boundaries,

(2) they included a set of complicated boundary value problems with samples taken at a distant location (inside and/or outside of the soil specimen) from the fluid drainage point,

(3) analysis was mainly conducted to check the effect on multiple empirical parameters, rather than seepage flow variables.

Khasi et al. [2019] explored the continuum based experimental approaches for NAPL dissolution and modelled them at a pore scale by the introduction of a new empirical parameter. Although they provided a complex pore-scale network theory to model NAPL dissolution, they conducted a simple flow experiment to verify their contaminant transport theory in porous media, which we use later on to conduct our model validation. One of the important experimental conclusions which is used in developing our model was drawn from Geller and Hunt [1993] where they mention the importance of NAPL ganglia size and NAPL-water area of contact, besides the type of NAPL and Darcy's velocity, in the dissolution process. Agaoglu et al. [2015] evaluated various factors such as NAPL saturation, the extent of interaction between the NAPL and aqueous phase, NAPL's distribution in the porous media at the small scale, grain size heterogeneity, the size of the study area or domain, and the heterogeneity of the porous media at a small scale to understand the impact of NAPL-to-aqueous phase mass transfer (referring specifically to dissolution) and validate their findings with the experiments performed by Nambi and Powers [2000]. In this way, Agaoglu et al. [2015], Powers et al. [1991], Geller and Hunt [1993], Anwar and Matsubayashi [2000] etc. showed that the importance of interphase NAPL mass transfer in contaminant transport, and multiphase flow, has been recognized for decades.

2.3 FEM modeling

Models can be useful in evaluating technology in some cases, specifically numerical models related to groundwater flow and contaminant transport. There are various numerical models such as those by Harbaugh et al. [2000], Zheng and Wang [1999], Voss [1984], and Delshad et al. [1996] which discuss the contaminant seepage flow and transport in the soil subsurface along with groundwater flow. A finite difference numerical solution for 1 dimensional vertical flow to solve nonlinear partial differential equations was developed in Corapcioglu and Baehr [1987]. In their study, Yu and Li [2019]

created a three-dimensional numerical simulation to examine the flow of two non-miscible phases in subsurface water. They compared their simulation results with those produced by a commercially available software called FLAC.

2.4 Limitations in the current research so far

Some of the limitations present in most of the existing models include but are not limited to the following.

1) Mainly considered final equilibrium state without any focus on the rate form of NAPL dissolution,

2) The pore-scale mechanism of time dependent NAPL dissolution phenomenon was not explained,

3) Mass transfer formulation based on empirical parameters such as Reynold's number, Sherwood's number, Peclet's number, Schmidt's number etc. -- not only difficult to predict, but also impractical and unreliable,

4) Effect of NAPL dissolution process on contaminant seepage flow variables without using empirical parameters was not considered, and

5) Inability in establishing a connection of NAPL dissolution theory with the pressure-degree of saturation, $p - S$ relationship in both, a three-phase (gas-NAPL-water) and a two-phase (gas-water) system.

2.5 Research objectives

Hence, in this paper, we divide the research objectives into the following five parts.

1) Approach the NAPL dissolution phenomenon by analyzing it as a pore-scale mechanism,

2) Propose a rate-limited NAPL dissolution model based on the analysis of NAPL-water specific contact surface area,

3) Apply the proposed concept to the existing contaminant seepage flow and transport theory (Nakamura and Kikumoto [2014, 2018]),

4) Conduct experimental validation using the tetrachloroethylene (TCE) dissolution rate results (Khasi et al. [2019]), and

5) Conduct Finite Element Method simulation to analyze the given issue as a boundary value problem.

CHAPTER 3

THEORETICAL FRAMEWORK FOR MODELING INTERPHASE MASS TRANSFER OF MULTIPHASE FLUIDS IN POROUS MEDIA

3.1 Theoretical basis

The rationality of proposed mass transfer theory is based on a theoretical study of NAPL-water specific contact surface area, a_{nw}, which is an important factor affecting the extent of NAPL dissolution based on Geller and Hunt [1993]. Emphasis on the main part of modeling by analyzing the variation of a_{nw} with liquid saturations is checked, which is used in the formulation of lumped mass transfer rate. For this, we analyze the arc lengths created by pore phase fluids based on their varying surficial area in 2-D AutoCAD™ illustrations that we created in two different types of soil packing settings – cubic and hexagonal.

3.1.1 Contact angle measurement

A reasonable NAPL-water contact angle (θ_{nw}) and gas-NAPL contact angle (θ_{gn}) must be considered to carry out the theoretical study. It has been reported by several researchers that a large uncertainty is associated with the measurement of contact angle (Mahadevan [2012], Bikkina [2012], Iglauer et al. [2014], Palamara et al. [2015]), and that there is a scarcity of available data for contact angle values due to the complexity of the underlying phenomena and the challenging nature of the experimental measurement (Adamson and Gast [1997], Butt and Kappl [2006]). Considering the interfacial tension values of general NAPLs, a reasonable estimate of contact angles were derived influenced by the works of Hirasaki [1993] and Ryder [2007]: $\theta_{nw} = 7°$ and $\theta_{gn} = 14°$ illustrated in Figure 3-2 and Figure 3-6 for cubic and hexagonal soil packing respectively.

It is also important to consider the effect of changes in pressure on interfacial contact angle. Based on an extensive literature review, the variation of contact angle with pressure for liquids (in solid lines) and gases (in dashed lines) is indicated in Figure 3-1. Measurements did not show any significant impact of pressure on the contact angle of brine and liquid hydrocarbon on quartz (Rajayi and Kantzas [2011], Wang and Gupta [1995]), mica (Hansen et al. [2000]) or calcite (Hansen et al. [2000]). Studies have reported that the initial contact angle remains mostly unchanged under different pressures (Bernardin et al. [1997], Hansen et al. [2000]). For any pressure changes at high pressure (in the order of ~20 Mpa), significant changes in wettability are only expected for gases or supercritical fluids, but not for liquids.
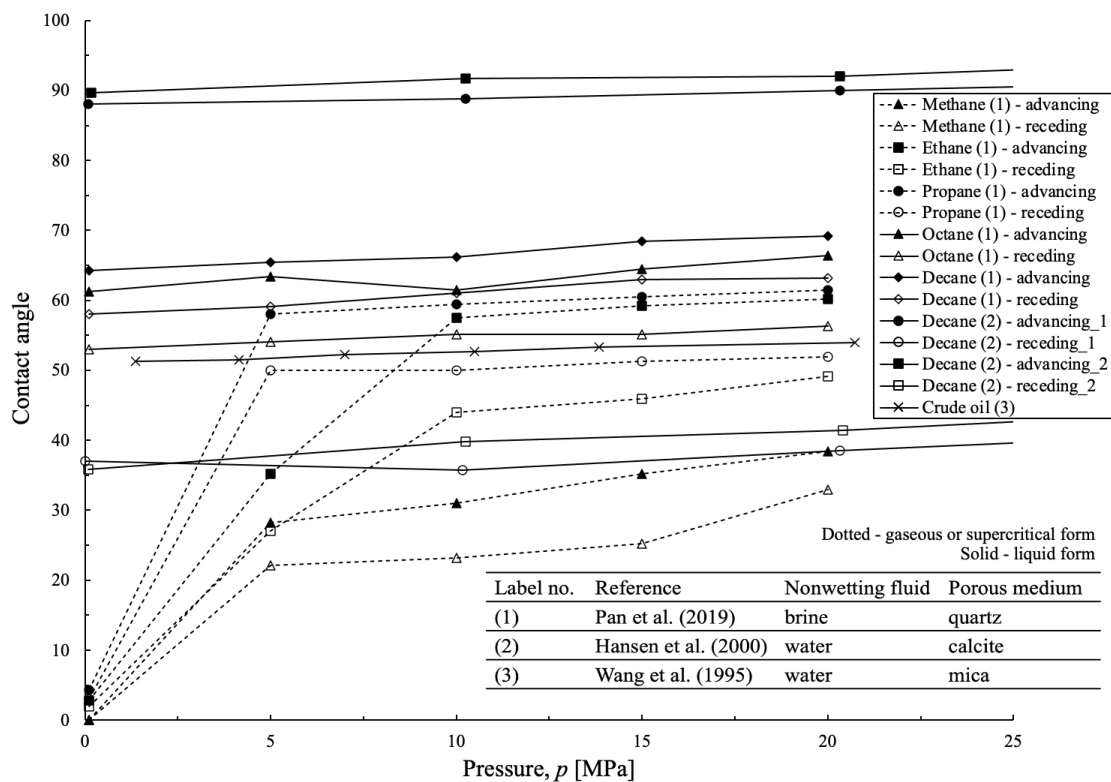
Figure 3-1: Effect of pressure on contact angles of liquids based on experimental studies by Pan et al. [2009], Hansen et al. [2000], and Wang et al. [1995]

Based on the above literature review, a few assumptions are made to make the theoretical study simpler and more straightforward.

1) Soil particle surfaces are molecularly smooth to avoid heterogeneities in contact angle measurements.

2) The effect of pressure on the contact angles is negligible i.e., contact angles remain constant throughout the study.

3) Advancing and receding contact angles are ignored and only equilibrium contact angles are considered, i.e., hysteresis phenomenon is ignored.

3.1.2 Relationship between fluid saturation and NAPL-water interfacial contact area

For each soil packing case, we start with the condition where the void space is only filled with NAPL and water with varying proportions (Figure 3-3 (a) and Figure 3-7 (a) for cubic and hexagonal soil packing respectively). Then, we increase the saturation of gas while continuing to vary NAPL and water saturations (Figure 3-3 (b), 3-3 (c), 3-3 (d), 3-3 (e) and Figure 3-7 (b), 3-7 (c), 3-7 (d), 3-7 (e) for cubic and hexagonal soil packing respectively). It is to be noted that the configuration of void fluids will be based on the fluid wettabilities. The results obtained are consolidated for varying fluid saturations in a single 3-D Figure for cubic (Figure 3-5) and hexagonal (Figure 3-9) soil packing respectively. The drawings are made in AutoCAD™ software to calculate

a) the NAPL-water arc length, which when extended to a 3-D soil packing, is directly proportional to the specific contact surface area of NAPL-water interface.

b) the surficial area of a liquid, which is directly proportional to the volume occupied by that liquid or its saturation in an extended 3-D soil packing.

A relationship is drawn between the NAPL-water specific contact surface area and the NAPL and water saturation in each case represented in Figure 3-4 (a) and Figure 3-4 (b) for cubic soil packing, and Figure 3-8 (a) and Figure 3-8 (b) for hexagonal soil packing respectively. It is known and observed that, a_{nw} reduces to zero if any one liquid or both the liquids cease to exist in the void space. An increase in the gas saturation leaves less void space for the liquids to occupy causing a leftward shift of

the specific contact surface area vs NAPL/water saturation curve. In each case, a nonlinear relationship between a_{nw} and liquid saturations was observed with maximum NAPL-water arc length or specific contact surface area is reached for (i) an arbitrary NAPL/water saturation in an NAPL-water two-phase system, and (ii) an arbitrary NAPL and water saturation in a gas-NAPL-water three-phase system. The maximum NAPL-water specific contact surface area is higher in a hexagonal packing as compared to that of a cubic packing due to the arrangement of fluids in the void space.
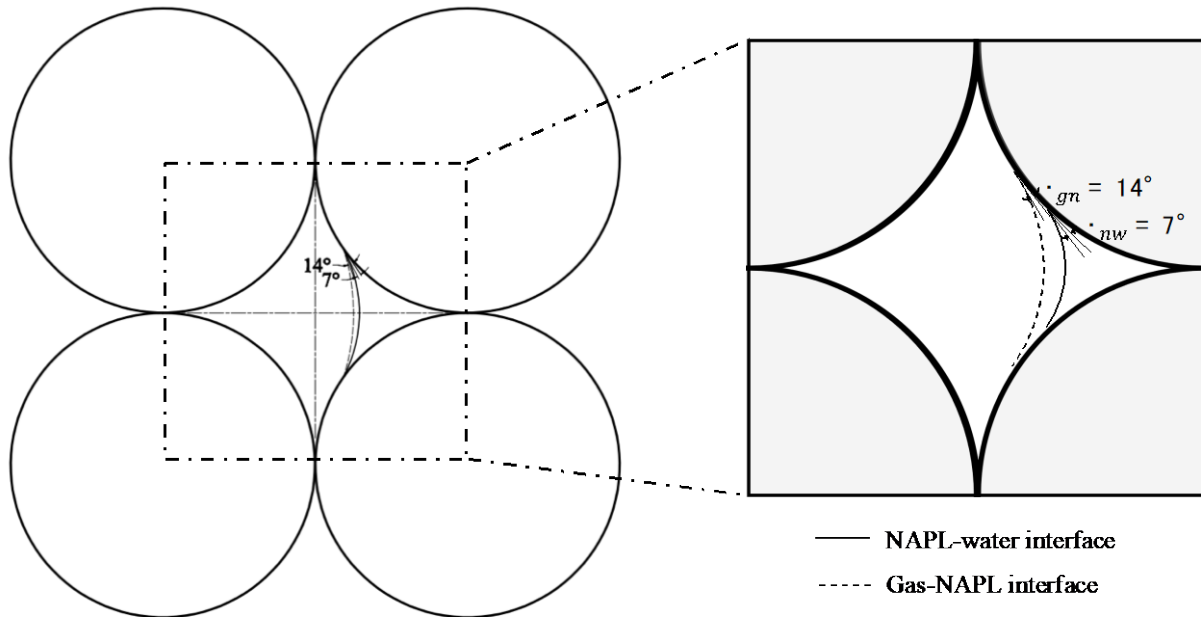
Figure 3-2: Cubic soil packing with NAPL-water contact angle - 7° and gas-NAPL contact angle - 14°

(c) $S_g = 0.266$

(d) $S_g = 0.538$

(e) $S_g = 0.722$
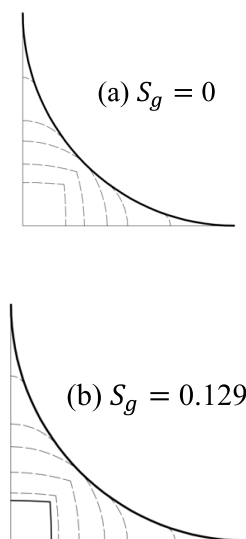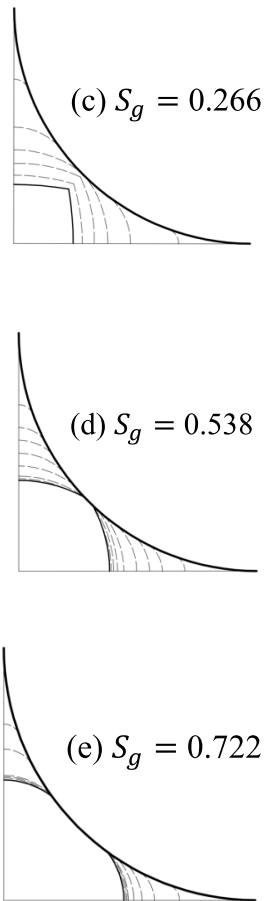
Figure 3-3: Axisymmetric void space of cubic soil packing with varying gas saturations
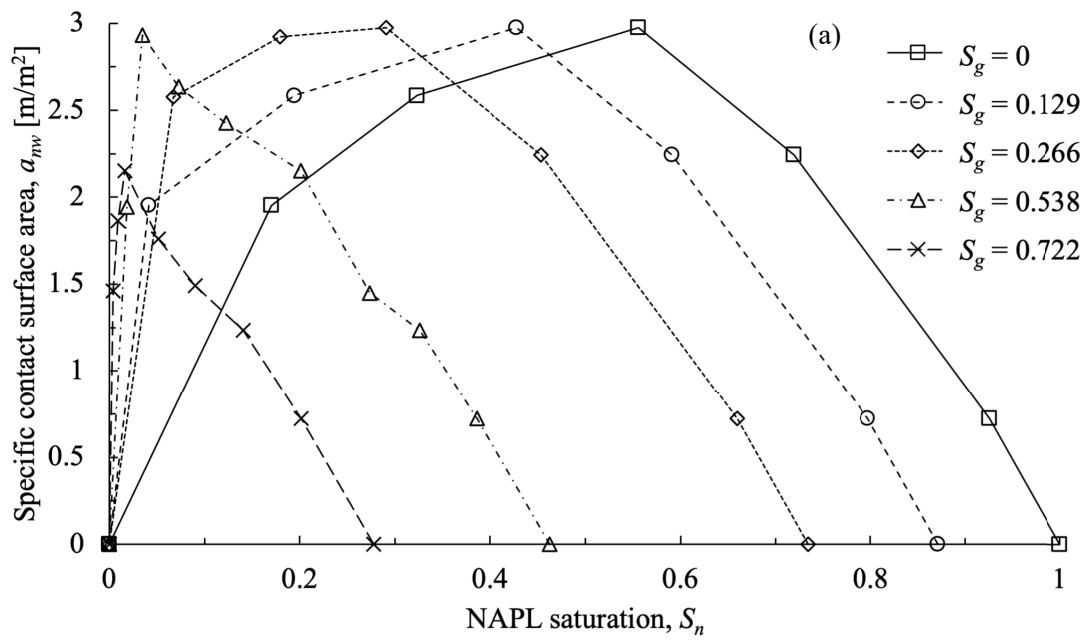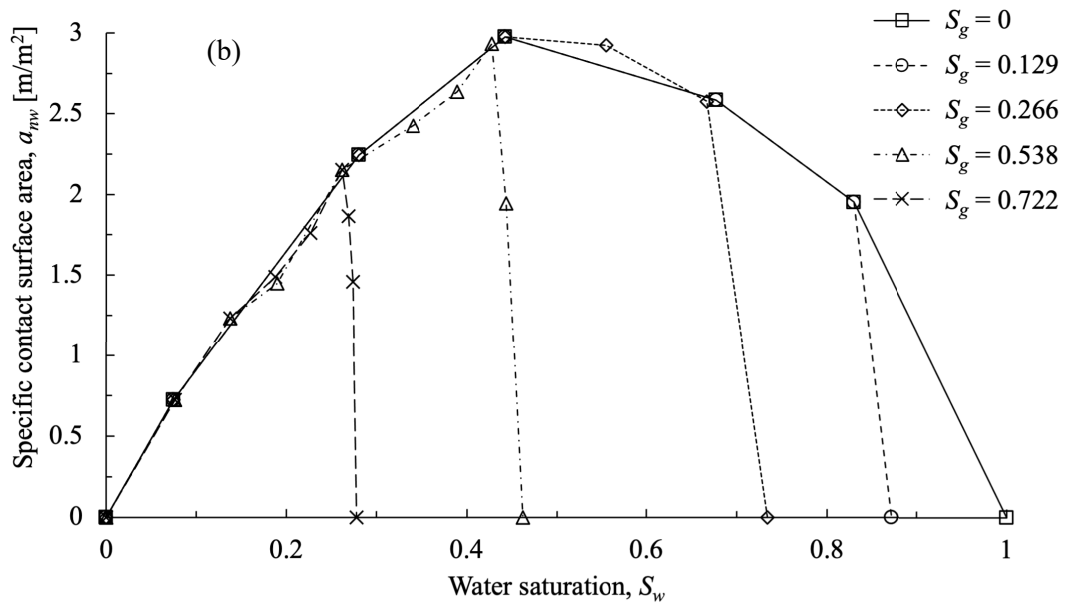
Figure 3-4: Variation of NAPL-water specific contact surface area with (a) NAPL saturation and (b) water saturation in cubic soil packing
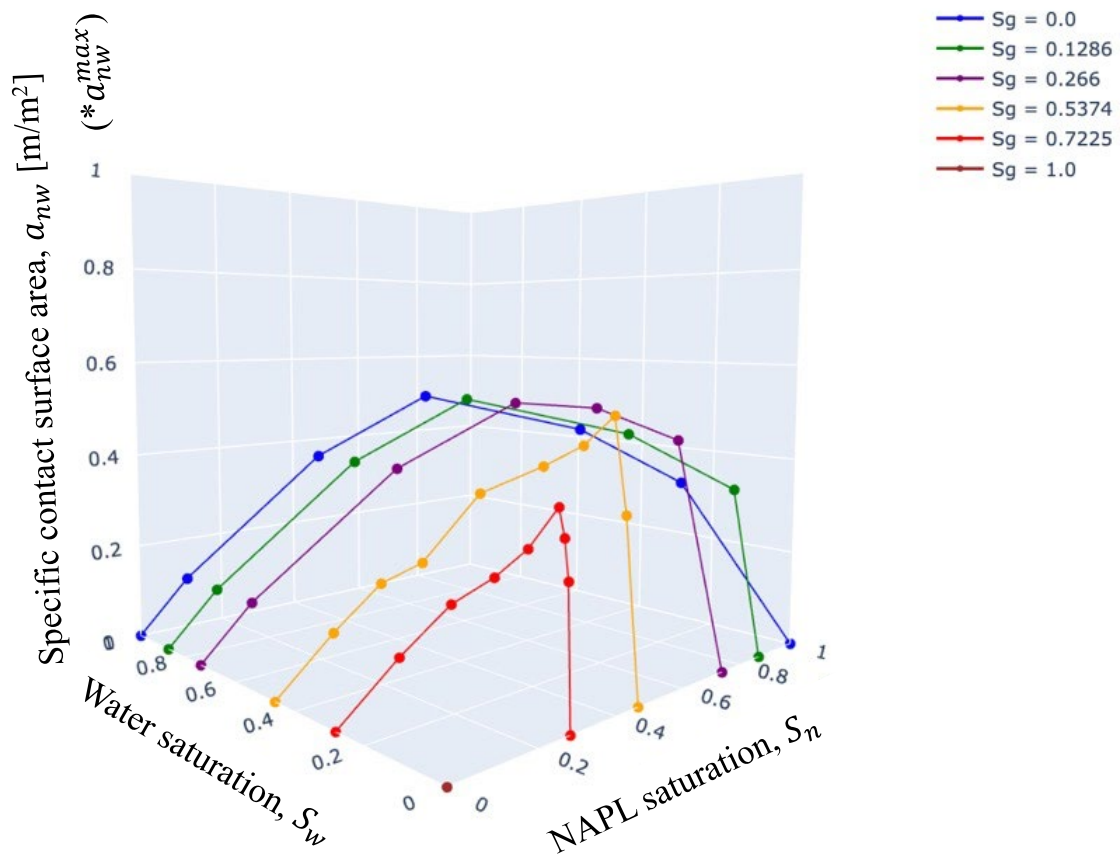
Figure 3-5: Variation of NAPL-water specific contact surface area with fluid saturations in cubic soil
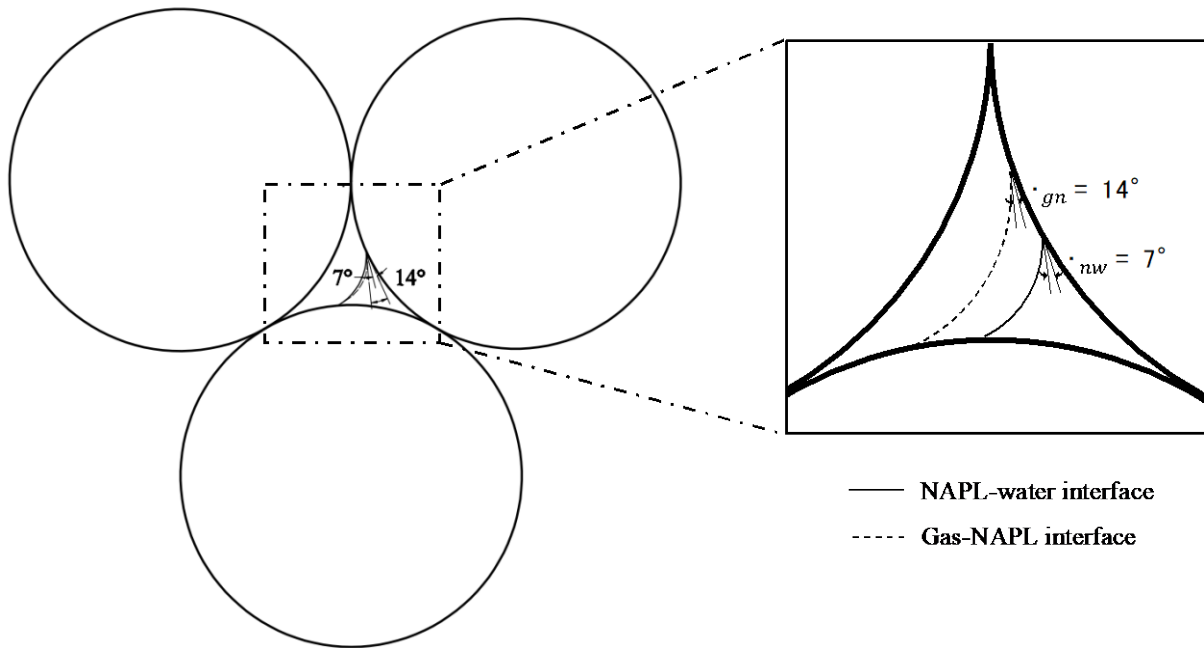
Figure 3-6: Hexagonal soil packing with NAPL-water contact angle - 7° and gas-NAPL contact angle

- 14°
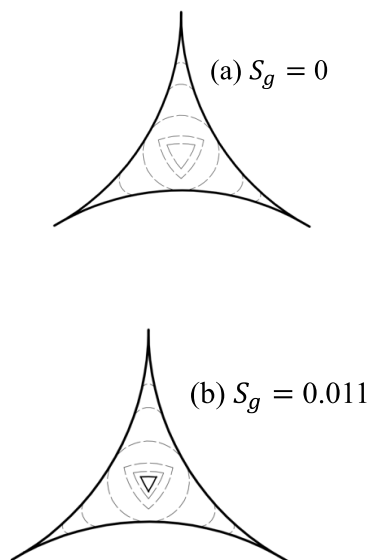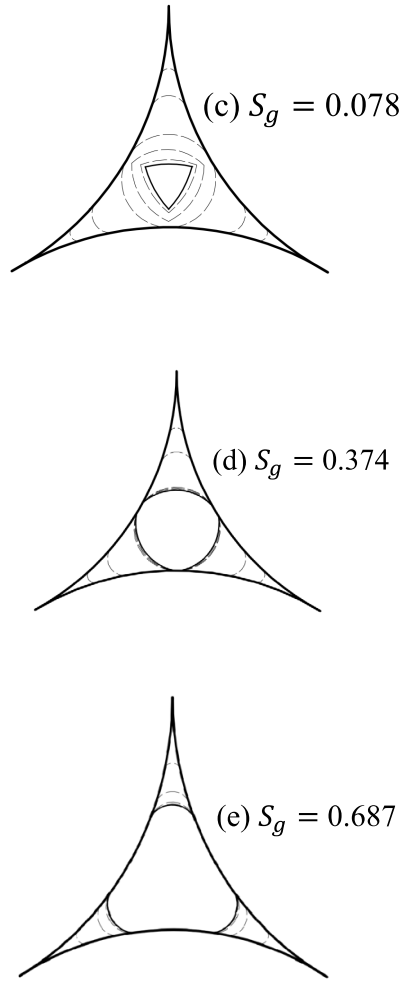
Figure 3-7: Axisymmetric void space of hexagonal soil packing with varying gas saturations
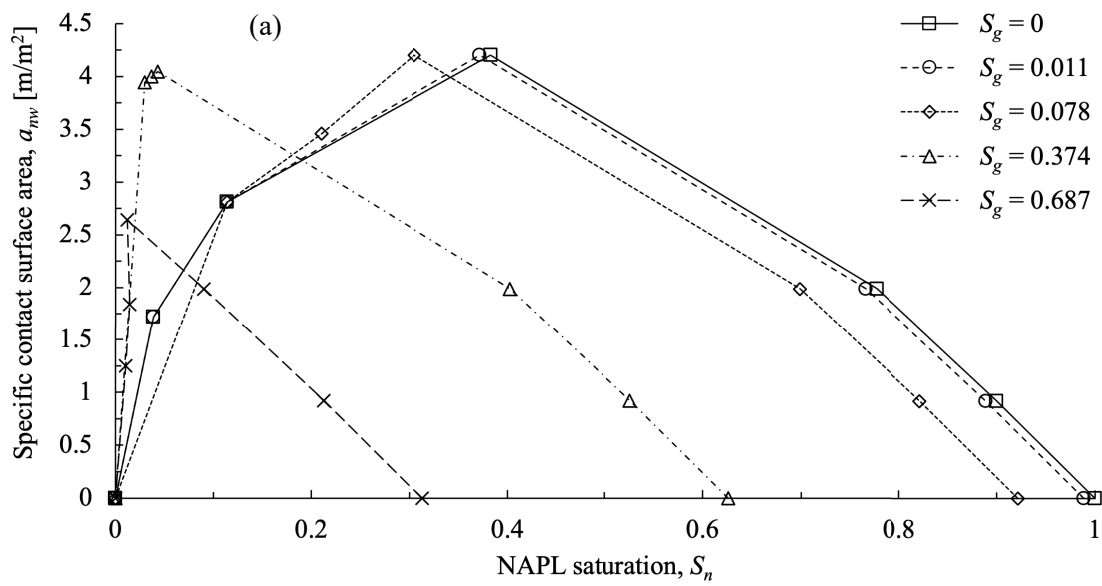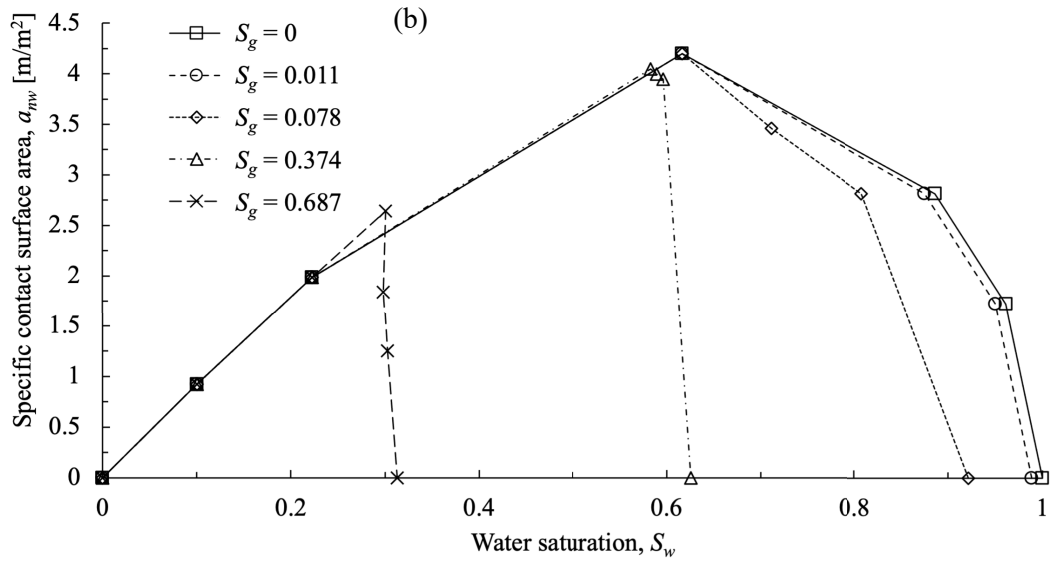
Figure 3-8: Variation of NAPL-water specific contact surface area with (a) NAPL saturation and (b)

water saturation in hexagonal soil packing
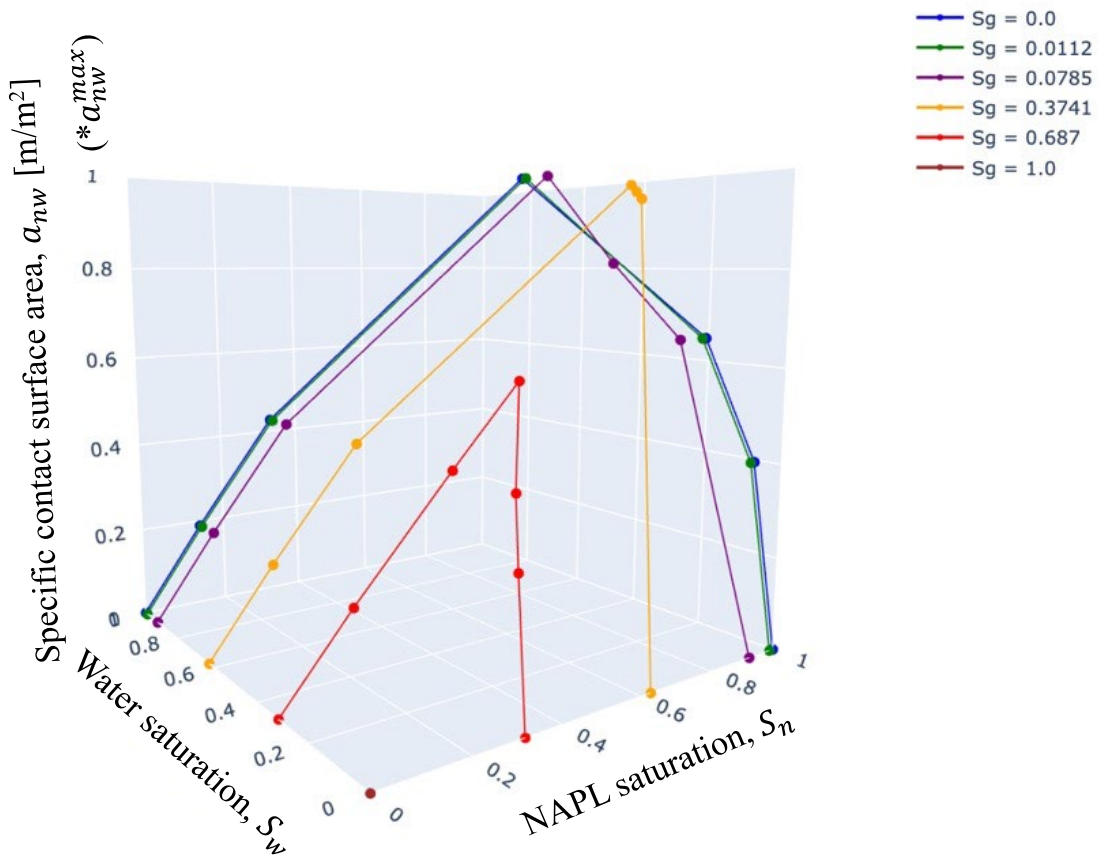
Figure 3-9: Variation of NAPL-water specific contact surface area with fluid saturations in hexagonal

3.2 Formulation of NAPL dissolution theory

The following assumptions are made in the formulation of NAPL dissolution theory:

1) No molecular/chemical interaction between NAPLs and the surrounding soil skeleton.

2) NAPLs dissolved in water are present as blobs and retain the volume of NAPL.

3) For simplicity, closed system with rigid boundaries is assumed i.e., fluids can neither enter nor escape the system.

4) Gas, if present in the system, behaves as an ideal gas.

A rational model defining the variation of a_{nw} during the course of NAPL dissolution is vital to model the interphase mass transfer. Based on the results obtained in section 3.1, a_{nw} in an NAPL-water two-phase system is defined as a function of NAPL saturation as per equation 3-1 and equation 3-2, and reaches a maximum value, a_{nw}^{max} at an arbitrary NAPL saturation, S_n' as shown in the illustrative Figure 3-10. ω is a scalar multiplier defining the ratio between a_{nw} and a_{nw}^{max}, which is modeled such that its value tends to 0 when the system is completely saturated with any one fluid and reaches 1 at S_n'.

$$a_{nw} = \omega a_{nw}^{max} \qquad (3-1)$$

$$\omega = \begin{cases} \left(\dfrac{S_n}{S_n'}\right)^{\sigma_{n_1}} ; 0 \le S_n \le S_n' \\ \left(\dfrac{1-S_n}{1-S_n'}\right)^{\sigma_{n_2}} ; S_n' \le S_n \le 1 \end{cases} \qquad (3-2)$$

S_n' is a model parameter that describes the extent of water-wettability or NAPL-wettability of the porous medium in an NAPL-water two-phase system. Since NAPLs spread over the surface of water phase in a water-wet medium, the maximum specific contact surface area, a_{nw}^{max} typically occurs for $S_n' > 0.5$. Whereas, in an NAPL-wet medium, NAPLs form a lens-like structure, resulting in a_{nw}^{max} for $S_n' < 0.5$. Exponents σ_{n_i} ($i = 1, 2$) in equation 3-2 are dependent on soil particle shape and packing conditions and describe the variation of a_{nw} with change in the NAPL saturation degree.
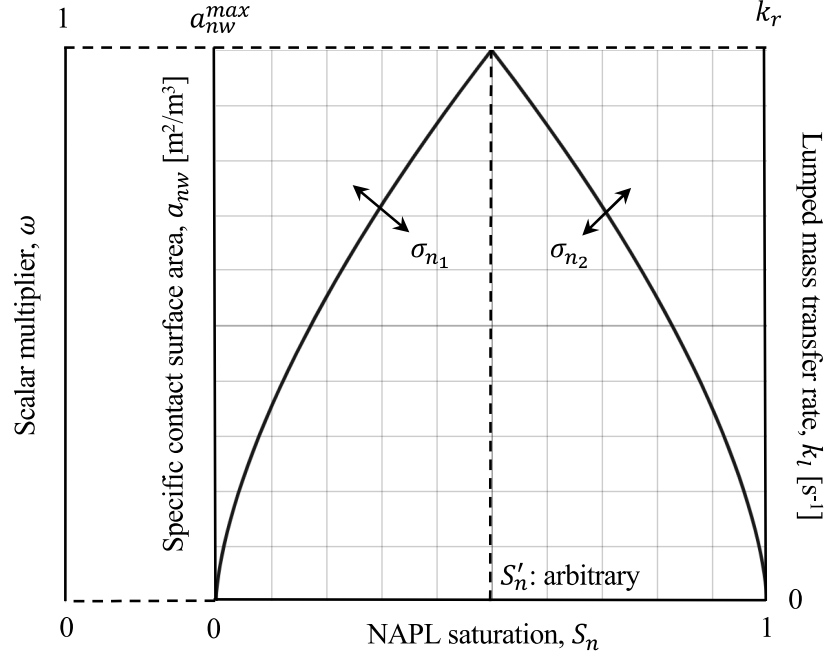
Figure 3-10: Illustrative relationship between NAPL-water specific contact surface area and NAPL

saturation for an NAPL-water two-phase system

Since the saturations of NAPL and water do not complement each other in a gas-NAPL-water three-phase system (as is the case for an NAPL-water two phase system), a_{nw} now depends on both, NAPL and water saturations. ω is modeled to become 0 when either of the liquids in the system or both of them completely cease to exist, and reaches a maximum value at an arbitrary NAPL saturation, S_n' and water saturation, S_w' as shown in the illustrative Figure 3-11. For the same reason, wettability of the medium is now defined in terms of both, S_n' and S_w'. Exponents σ_{n_j} and σ_{w_j} (j = 1, 2, 3, 4) in equation 3-3 are parameters which describe the variation of NAPL-water specific contact surface area with change in their saturation degree.

$$\omega = \frac{a_{nw}}{a_{nw}^{max}} = \begin{cases} \left(\dfrac{S_n}{S_n'}\right)^{\sigma_{n_1}} \left(\dfrac{S_w}{S_w'}\right)^{\sigma_{w_1}} & ; 0 \leq S_n \leq S_n' \; and \; 0 \leq S_w \leq S_w' \\[2mm] \left(\dfrac{S_n}{S_n'}\right)^{\sigma_{n_2}} \left(\dfrac{1-S_w}{1-S_w'}\right)^{\sigma_{w_2}} & ; 0 \leq S_n \leq S_n' \; and \; S_w' \leq S_w \leq 1 \\[2mm] \left(\dfrac{1-S_n}{1-S_n'}\right)^{\sigma_{n_3}} \left(\dfrac{S_w}{S_w'}\right)^{\sigma_{w_3}} & ; S_n' \leq S_n \leq 1 \; and \; 0 \leq S_w \leq S_w' \\[2mm] \left(\dfrac{1-S_n}{1-S_n'}\right)^{\sigma_{n_4}} \left(\dfrac{1-S_w}{1-S_w'}\right)^{\sigma_{w_4}} & ; S_n' \leq S_n \leq 1 \; and \; S_w' \leq S_w \leq 1 \end{cases} \qquad (3-3)$$
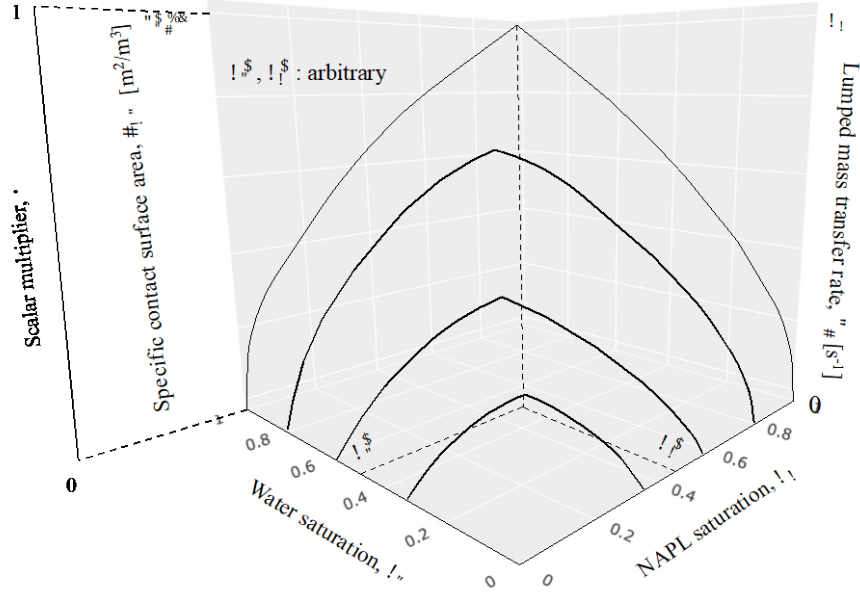
Figure 3-11: Illustrative relationship between NAPL-water specific contact surface area and NAPL saturation for a gas-NAPL-water three-phase system

A new lumped mass transfer rate, k_l is defined in terms of ω as per equation 3-4 to capture the effect of this varying a_{nw} through the course of NAPL dissolution. k_l is set to reach its maximum value, k_r when the NAPL-water specific contact surface area is maximum, i.e., when $\omega = 1$.

$$k_l = \omega k_r \qquad (3-4)$$

We express an analogous equation to equation 2-3 in order to define mass transfer rate more directly, starting with the rate of change in masses and then proceed with the calculation of the changes in volumes, saturations, and pressures as shown in the following set of equations.

$$\frac{\partial m_n^d}{\partial t} = -k_l\left(m_n^{d,\,max} - m_n^d\right) \qquad (3-5)$$

$$m_n^{d,\,max} = k_d m_w^0 = k_d V_w^0 \rho_w \qquad (3-6)$$

m_n^d is the mass of NAPL dissolved at the current time step, t; $m_n^{d,\,max}$ represents the maximum mass of NAPL dissolved in water at equilibrium state and is directly proportional to the total initial mass of water present in the system, m_w^0 i.e., a greater amount of NAPL mass is dissolved with more water present in the system. As shown in equation 3-6, a mass transfer coefficient, k_d is used to determine the fraction of maximum mass of NAPL dissolved per total initial mass of water present in the system. In a closed system, following the assumption 2, the NAPL dissolved volume is given as below.

$$\frac{\partial V_n^d}{\partial t} = \frac{1}{\rho_n} \frac{\partial m_n^d}{\partial t} \tag{3-7}$$

The NAPL and water saturations are updated with the fundamental definition of saturation in porous media. For a closed system with rigid boundaries, the volume of gas remains constant during the course of NAPL dissolution process. Due to this, the Boyle's law is now reduced to equation 3-8.

$$p_g^{t+dt} = p_g^t \tag{3-8}$$

The pressure values of liquids are then updated using modified van Genuchten's relationship as proposed by Nakamura and Kikumoto (2014).

$$\begin{Bmatrix} \frac{\partial p_w}{\partial t} \\ \frac{\partial p_n}{\partial t} \end{Bmatrix} = \begin{bmatrix} \frac{\partial S_w}{\partial p_w} & \frac{\partial S_w}{\partial p_n} \\ \frac{\partial S_n}{\partial p_w} & \frac{\partial S_n}{\partial p_n} \end{bmatrix}^{-1} \begin{Bmatrix} \frac{\partial S_w}{\partial t} \\ \frac{\partial S_n}{\partial t} \end{Bmatrix} \tag{3-9}$$

3.3 Finite Element Method formulation

A set of governing equations are formulated to analyze the NAPL dissolution issue as a boundary value problem. The governing Richard's equations are defined by a unique $\psi - k_r - S$ relationship among pore phase fluids to solve for the contaminant seepage flow and transport. A detailed derivation of these governing equations 3-10 to 3-12 and analyzing through Finite Element Method (FEM) is provided in Appendix A2. It is to be noted that ψ-based form is used to conduct simulations in this thesis since it is rather comprehensible to provide the initial and boundary conditions in terms of pore fluid pressure and flux. Further, although θ-based form is more accurate in terms of maintaining the mass balance of pore phase fluids, abrupt change in saturation degree distribution in the soil profile can cause numerical instability, especially when implemented in the COMSOL Multiphysics™ software. Furthermore, the difficulty to implement a mixed-form in the software leads us to have ψ-based form to be the most compatible method in running the simulations. Details about the different forms of governing equations with their respective advantages and limitations is provided in Table 4-2, and a summary of the governing equations for seepage flow in the ψ-based form is shown as below.

Water:

$$\nabla \cdot v_w - \phi \dot{S_w} = 0 \qquad\qquad (3-10)$$

NAPL:

$$\nabla \cdot v_n - \phi \dot{S_n} = 0 \qquad\qquad (3-11)$$

Gas:

$$\nabla \cdot v_g - \phi \dot{S_g} - \phi S_g \frac{\dot{p_g}}{K_v^g} = 0 \qquad\qquad (3-12)$$

where, v_i represents the Darcy's velocity of the fluid, i,

ϕ represents the porosity of the medium,

S_i represents the degree of saturation of the fluid, i, and

K_v^g defines the compressibility of gas.

The $\psi - k_r - S$ relationship is governed by three individual relationships as:

1) Darcy's velocity flux defining the $p - k_r$ relationship:

$$v_i = -\frac{k_{ri} K_w}{\mu_{ri}} \nabla \left(\frac{p_i}{\rho_w g} + \rho_{ri} z \right) \qquad\qquad (3-13)$$

where, k_{ri} represents the relative permeability of the fluid, i,

K_w represents the saturated permeability,

μ_{ri} defines the relative viscosity,

p_i is the pressure of the fluid, i,

ρ_w is the density of water,

g is the acceleration due to gravity,

ρ_{ri} is the relative density of the fluid with respect to water, and

z represents the pressure head.

2) Modified van Genuchten's suction-saturation $\psi - S$ relationship (Refer to the appendix-A1)

3) Mualem's law defining $k_r - S$ relationship:

$$k_{ri} = S_i \left\{ 1 - \left(1 - S_i^{\frac{1}{m}} \right)^m \right\}^2 \qquad\qquad (3-14)$$

where m is the van Genuchten's parameter of the porous medium

However, Appendix A2 and equations 3-10 to 3-12 only discusses the governing equations for seepage flow and transport without considering NAPL dissolution. Hence, we build upon this theory and derive the governing equation for contaminant transport in a simple seepage flow considering NAPL dissolution for each pore phase fluid as below. The equation for law of conservation of mass is evolved to now have an additional mass exchange term to represent NAPL dissolution.

$$q_{in} - q_{out} = \left(\frac{\partial \theta}{\partial t} \pm \frac{\dot{V}_n^d}{V_t} \right) V_t \qquad (3-15)$$

where V_t represents the entire volume of the void space

The above equation 3-15 is expanded for each constituent as follows.

Water:

$$v_w^x dydz + v_w^y dxdz + v_w^z dxdy - \left(v_w^x + \frac{\partial v_w^x}{\partial x} dx \right) dydz - \left(v_w^y + \frac{\partial v_w^y}{\partial y} dy \right) dxdz$$
$$- \left(v_w^z + \frac{\partial v_w^z}{\partial z} dz \right) dxdy = \left(\frac{\partial \theta_w}{\partial t} - \frac{\dot{V}_n^d}{V_t} \right) dxdydz \qquad (3-16)$$

Applying equation 3-7, we get,

$$\left(\frac{\partial v_w^x}{\partial x} + \frac{\partial v_w^y}{\partial y} + \frac{\partial v_w^z}{\partial z} \right) dxdydz = \left(-\frac{\partial \phi S_w}{\partial t} - \frac{1}{V_t \rho_n} \frac{\partial m_n^d}{\partial t} \right) dxdydz \qquad (3-17)$$

$$\nabla \cdot \boldsymbol{v_w} + \phi \left(\frac{\partial S_w}{\partial t} \right) = \frac{-1}{V_t \rho_n} \frac{\partial m_n^d}{\partial t} \qquad (3-18)$$

NAPL:

$$v_n^x dydz + v_n^y dxdz + v_n^z dxdy - \left(v_n^x + \frac{\partial v_n^x}{\partial x} dx \right) dydz - \left(v_n^y + \frac{\partial v_n^y}{\partial y} dy \right) dxdz$$
$$- \left(v_n^z + \frac{\partial v_n^z}{\partial z} dz \right) dxdy = \left(\frac{\partial \theta_n}{\partial t} + \frac{\dot{V}_n^d}{V_t} \right) dxdydz \qquad (3-19)$$

Applying equation 3-7, we get,

$$\left(\frac{\partial v_n^x}{\partial x} + \frac{\partial v_n^y}{\partial y} + \frac{\partial v_n^z}{\partial z} \right) dxdydz = \left(-\frac{\partial \phi S_n}{\partial t} + \frac{1}{V_t \rho_n} \frac{\partial m_n^d}{\partial t} \right) dxdydz \qquad (3-20)$$

$$\nabla \cdot \boldsymbol{v_n} + \phi \left(\frac{\partial S_n}{\partial t} \right) = \frac{1}{V_t \rho_n} \frac{\partial m_n^d}{\partial t} \qquad (3-21)$$

Gas:

The governing equation for gas remains the same as in equation 3-12 since, in a closed system with rigid boundaries, because gas is not undergoing any changes due to NAPL dissolution maintaining the law of conservation of mass to remain unchanged.

CHAPTER 4

MODEL VALIDATION AND APPLICABILITY

4.1 Experimental validation

The NAPL dissolution experiment conducted by Khasi et al. [2019] was used to validate our proposed model. In the experiment, water was made to flow at three different constant rates (0.05 cc/min, 0.01 cc/min, and 0.1 cc/min) into a completely NAPL saturated micromodel which was monitored with a digital microscope to measure the fluid saturations at different times. Equal pore volumes of water were passed into the micromodel specimen, and the residual NAPL saturations (S_n^0) in each case was evaluated by the end of this phase displacement process. S_n^0 in each case was evaluated to be 0.4442, 0.4143, and 0.3566 for flow rates 0.01 cc/min, 0.05 cc/min, and 0.1 cc/min respectively. The dissolution of NAPL was analyzed starting from this point for different periods of time based on the residual saturations (203.76 hours for S_n^0 =0.4442, 40.75 hours for S_n^0 =0.4143, 8.15 hours for S_n^0 =0.3566). Later, in their paper, they analyzed the fluid flow and reactive transport using a pore-scale network model, also in two stages: phase displacement and dissolution. We extracted the data for the rate of change of fluid saturation at different NAPL inflow rates and compared with our proposed model with the parameters presented in Table 4-1. The comparison of experimental NAPL saturation variation with time with the simulation results is shown in Figure 4-1. A qualitative resemblance in the decrease of NAPL saturation tendency is seen in all the cases, especially when initial NAPL saturation was relatively close to S_n' due to the exponential variation in a_{nw} with NAPL saturation. For the same reason, it is also observed that the case with a relatively less S_n^0 reaches an asymptotic saturation state sooner. This can be understood better from Figure 4-2 (a) which shows the rate of change of specific contact surface area and the lumped mass transfer rate, and Figure 4-2 (b) which shows the variation of specific contact surface area with NAPL saturation in the three given experimental cases for NAPL-water two-phase system. A peak in the evolution of lumped mass transfer rate is seen to reach sooner for the case with S_n^0 closest to the applied S_n'.

Table 4-1: Material parameters used for experimental validation with Khasi et al. [2019]

Material parameters		
Soil	ϕ	0.45
	V_t [m³]	$0.025 \times 0.018 \times 0.000296$
NAPL	ρ_n [kg/m³]	1600
Interphase mass transfer parameters	k_r [1/s]	1.5e-4
	k_d	0.14
	S_n'	0.335
	σ_{n_i}	25
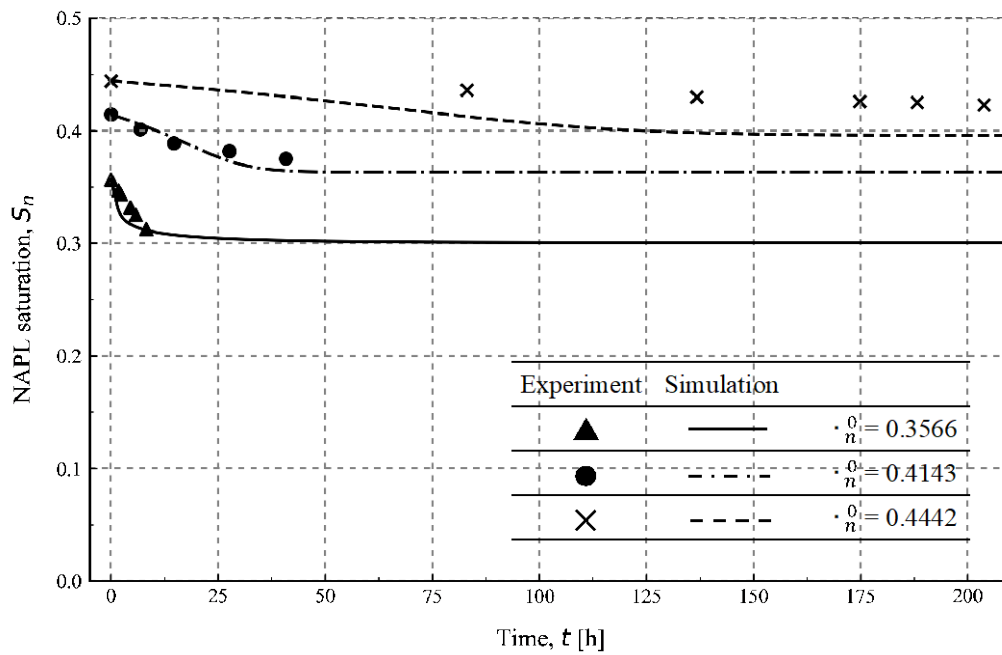
Figure 4-1: Validation of NAPL dissolution rate experimental results from Khasi et al. [2019] with the

proposed model
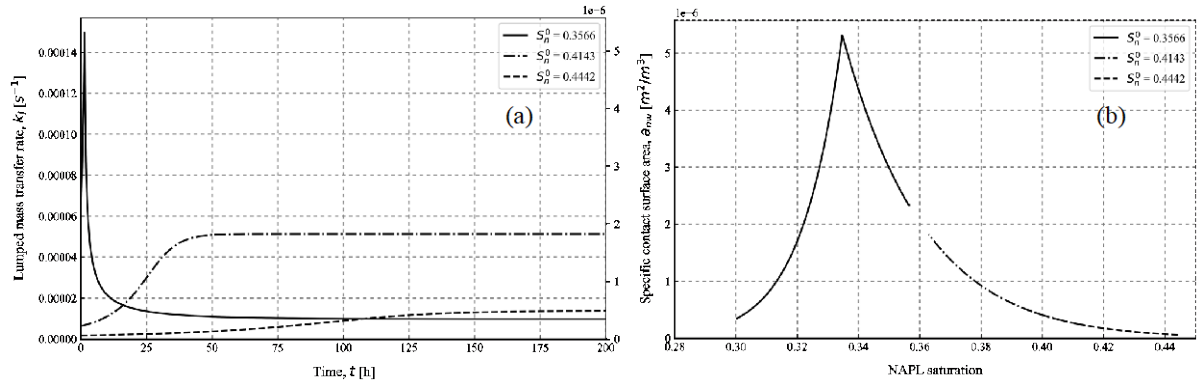
Figure 4-2: (a) Rate of change of specific contact surface area, and (b) Variation of specific contact surface area with NAPL saturation

4.2 Applicability

The simplified form of governing equations for liquid phases in a multiphase fluid system (equations 3-29, 3-32) follows from the seepage flow derived from Richard's equation as given below.

$$\mathbf{\nabla} \cdot \mathbf{v_i} + \phi \left(\frac{\partial S_i}{\partial t} \right) = \Gamma_i \qquad (4-1)$$

where Γ_i defines the interphase mass transfer of component 'i' by dissolution and is given by equation 4-2. The positive or negative sign indicates the mass loss or gain respectively.

$$\Gamma_i = \pm \frac{1}{V_t \rho_{mix}} \frac{\partial m_n^d}{\partial t} \qquad (4-2)$$

Since gas is compressible, its movement is solved by assuming the complementary of liquid present in the system.

It is well-known that solving Richard's equation leads us to two different kinds of governing equations: pressure head (ψ) - based form and the volumetric fluid content (θ) - based form (refer to Appendix A2). The difficulties in solving for Richard's equation numerically through these two forms have been thoroughly discussed by several researchers, and a brief overview of the advantages and limitations in each form is provided in the Table 4-2. Some have proposed a class of exact and approximate analytical solutions (Rogers et al. [1983], Fleming et al. [1984], Havercamp et al. [1990],

Barry et al. [1993], Ross and Parlange [1994], Broadbridge and White [1998], Chen and Dai [2015], Hayek [2016]) to solve it.

Table 4-2: Overview of the advantages and limitations of ψ-based and θ-based form

Method	Advantages	Limitations
ψ-based form	a) Even in heterogeneous ground, the value of the pressure head in the ground changes continuously, so it can be used. b) It can be used for both saturated and unsaturated regions.	Mass balance can't be satisfied strictly.
θ-based form	The conservation of mass is strictly maintained.	a) In the saturation region, the specific moisture capacity is 0, causing the moisture diffusion coefficient to be infinite making the relationship invalid. b) In heterogeneous ground, it is difficult to use because the value of volumetric moisture content in the ground may be discontinuous.

The applicability of the proposed model is discussed with the analytical solution of Richard's equation proposed in Hayek [2016]. Their analytical solution is written is in terms of Θ, a state variable describing the dimensionless volumetric water content as per equation 4-4. The analytical solution produced from equation 4-3 for a simple rainfall infiltration is compared with the numerical solutions of both, Θ-based form and ψ-based form.

$$\frac{\partial \Theta}{\partial t} = \frac{\partial}{\partial z}\left(D(\Theta)\frac{\partial \Theta}{\partial z}\right) - \frac{\partial K(\Theta)}{\partial z} \qquad (4-3)$$

$$\Theta = \frac{\theta - \theta_r}{\theta_s - \theta_r} \tag{4-4}$$

Where $D(\Theta)$ is the diffusivity function and $K(\Theta)$ is the hydraulic conductivity function, defined as below.

$$D(\Theta) = \frac{nK_s}{a(\theta_s - \theta_r)} \Theta^{n-1} \tag{4-5}$$

$$K(\Theta) = \frac{K_s}{(\theta_s - \theta_r)} \Theta^n \tag{4-6}$$

The interrelated $\psi - k_r - \theta$ relationships are given by equations 4-7 to 4-9. These relationships are used to convert the governing Richard's equation from Θ-based form to ψ-based form.

$$\psi = \frac{n}{a} ln\left(\frac{\theta - \theta_r}{\theta_s - \theta_r}\right) \tag{4-7}$$

$$k_r = \left(\frac{\theta - \theta_r}{\theta_s - \theta_r}\right)^n \tag{4-8}$$

$$k_r = e^{a\psi} \tag{4-9}$$

Different initial and boundary conditions were used to model the fluid infiltration over a semi-infinite soil domain in one dimension in both, ψ- and θ-based forms, details of which are provided in Table 4-3.

*Table 4-3: Initial and boundary conditions of **ψ**-based and **θ**-based form in Hayek et al. [2016]*

Condition		Initial condition	Boundary condition
Constant boundary condition	ψ -based form	$\psi(z, 0) = \frac{n}{a} ln\left(\frac{\theta_i - \theta_r}{\theta_s - \theta_r} + \varepsilon\right)$	$\psi(0, t) = \frac{n}{a} ln\left(\frac{\theta_s - \delta - \theta_r}{\theta_s - \theta_r} + \varepsilon\right)$
	θ -based form	$\theta(z, 0) = \theta_r + (\theta_* - \theta_r)\left\{1 - \left[1 - exp\left(-\frac{\theta_* - \delta - \theta_r}{\theta_* - \theta_r}\right)\right]e^{\left(-\frac{a(n-1)z}{n}\right)}\right\}^{\frac{1}{n-1}}, z \geq 0$	$\theta(0, t) = \theta_* - \delta, t \geq 0$
Time varying	ψ -based form	$\psi(z, 0) = \frac{n}{a} ln(\varepsilon)$	$\psi(0, t) = \frac{n}{a} ln\left(\frac{\theta_0 - \theta_r}{\theta_s - \theta_r} + \varepsilon\right)$

| boundary condition | θ -based form | $\theta\,(z,\,0) = \theta_r,\ z \geq 0$ | $\theta\,(0,\,t) = \theta_r, + (\theta_* - \theta_r)\left[1 - exp\left(-\frac{a(n-1)Vt}{n}\right)\right]^{\frac{1}{n-1}}$ |

We used COMSOL MultiPhysics™ software to numerically simulate the same conditions as that of Hayek [2016]. This model assumes a depth dependent initial condition similar to that of Vanderborght [2005], Zlotnik et al. [2007], and Hayek [2015]. In the first case with constant boundary condition, we tried to infiltrate water into a semi-saturated soil system, and follows the initial condition provided in the Table 4-3. In the second case with time-varying boundary condition, we infiltrated water into a completely dry soil with initial condition as its driest state. The rainfall infiltration is set to decrease with time due to the boundary conditions at the wetting surface. In each of the cases, we simulated the Θ-based form and ψ-based form of Richard's equation to prove the applicability of the basis of proposed model to other forms of governing equations which haven't been defined by modified van Genuchten's $p - S$ relationship, Mualem's $k_r - S$ law, or Darcy's law.
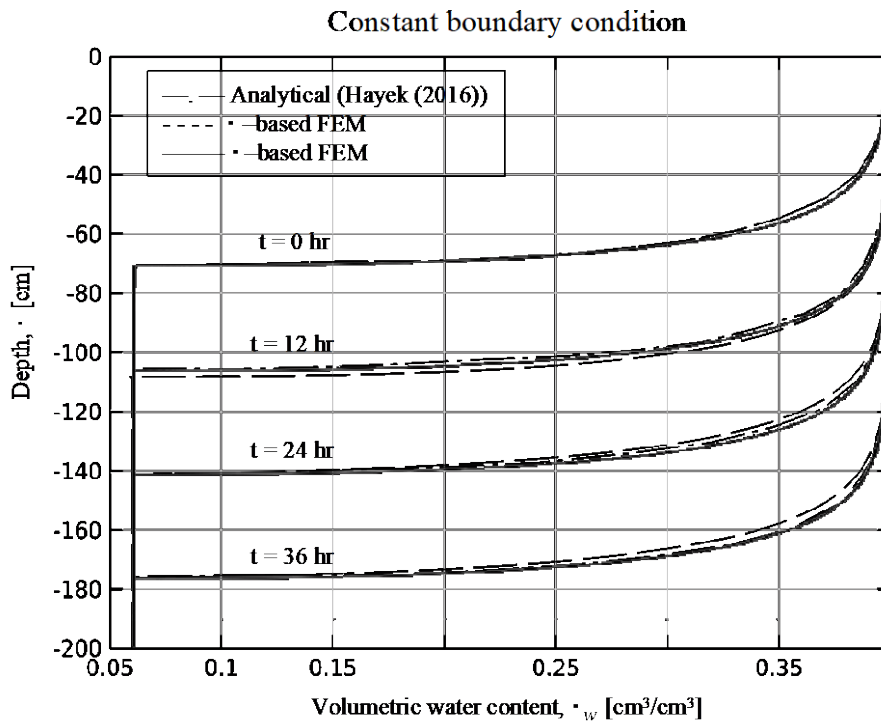
Figure 4-3: Comparison of FEM infiltration simulation with Hayek et al. [2016] analytical solution

for a constant boundary condition
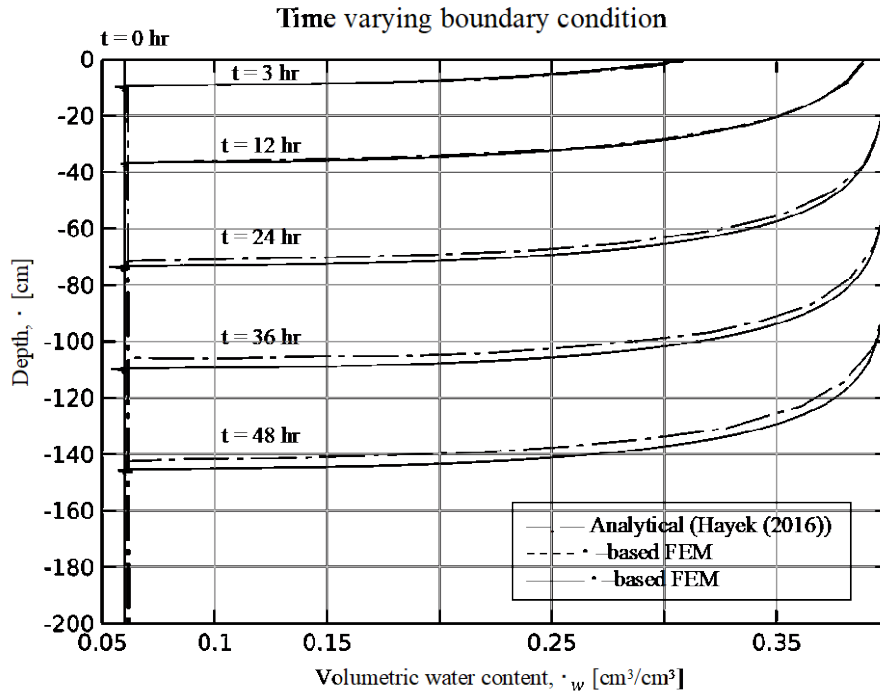
Figure 4-4: Comparison of FEM infiltration simulation with Hayek et al. [2016] analytical solution

for a time varying boundary condition

CHAPTER 5

RESULTS AND DISCUSSION

5.1 Parametric study

Two parameters were considered while conducting the parametric study to help understand the importance of mass transfer effects. For simplicity, an NAPL-water two-phase system is considered to emphasize the effect of the below parameters on the simulation. Material parameters and applied conditions shown in Table 5-1 and Table 5-2 respectively were used for conducting the below parametric studies.

Table 5-1: Material parameters used in the parametric study

Material parameters		
Porosity, ϕ		0.45
	S_{max}	1.0
	S_{min}	0.0
van Genuchten's parameters	α [1/kPa]	0.038
	m	0.656
	n	2.91
	β_{aw}	1.0
Scaling parameters for two-phase fluid systems	β_{an}	2.76
	β_{nw}	1.77

Table 5-2: Applied conditions used in the parametric study of (a) Mass transfer coefficient, k_d, (b) NAPL saturation at maximum specific contact surface area, S'_n

Initial conditions (a)	
Parameter	k_d

Fig. no.		13-16 (a)		
Chemical		Tetrahydrofuran	Phenol	O-cresol
Interphase mass transfer variables	k_r [1/s]	1.5e-4		
	k_d	0.30	0.084	0.031
	S_n'	0.55		
	σ_{n_i}	20		
Pressure [kPa]	NAPL	98.0		
	Water	75.5		
NAPL density [kg/m³]		889.2	1057.6	1050
Total volume [m³]		0.025 × 0.018 × 0.000296		
Area of cross-section [m²]		5.328e-6		
Time [h]		200		

Initial conditions (b)

Parameter		S_n'		
Fig. no.		13-16 (b)		
Condition		NAPL-wet	Intermediate-wet	Water-wet
Interphase mass transfer variables	k_r [1/s]	1.5e-4		
	k_d	0.30		
	S_n'	0.45	0.50	0.55, 0.60
	σ_{n_i}	20		
Pressure [kPa]	NAPL	98.0		
	Water	77.0		
NAPL density [kg/m³]		889.2		
Total volume [m³]		0.025 × 0.018 × 0.000296		

Area of cross-section [m^2]	5.328e-6
Time [h]	200

5.1.1 Mass transfer coefficient

The objective of this parametric study was to emphasize the effect of dissolution on some of the most soluble NAPLs and organic liquid contaminants. For this purpose, three chemicals – tetrahydrofuran, phenol, and o-cresol, having some of the highest mass transfer coefficients (or aqueous solubilities) and those that are most commonly found on remediation sites were considered for this study. The aqueous solubility and density data for these chemicals were derived from Newell et al. [1995] and Huling and Weaver [1991].

The quantity of NAPL dissolved in each case given by Figure 5-1 (a) followed the trend based on aqueous solubilities. The variation of total masses of water and NAPL present in the system over the course of dissolution for varying mass transfer coefficient is shown in Figure 5-2 (a) and Figure 5-3 (a) respectively. Despite mass transfer rate remaining the same in all cases, a difference in the rate of dissolution before reaching the maximum NAPL dissolved quantity is observed. This is because, although the maximum values of lumped mass transfer rate and NAPL-water specific contact surface area remains the same in all the three cases as shown in Figure 5-4 (a-i), the rate of dissolution was faster for the case with higher mass transfer coefficient due to a higher $m_n^{d,max}$, and this is reflected in Figure 5-4 (a-ii). It is seen how a higher mass transfer coefficient can cause a higher lumped mass transfer rate of NAPL dissolution and changes in its saturation. Due to dissolution, a reduction in the contaminant saturation is also seen to follow the trend according to aqueous solubilities of the respective contaminants as shown in Figure 5-5 (a), and the corresponding change in the contaminant fluid pressure can be seen in Figure 5-6 (a).

5.1.2 NAPL saturation at the maximum NAPL-water specific contact surface area

Four cases are simulated with maximum NAPL-water specific contact surface area occurring at different fluid saturations (S_n'= 0.45, 0.50, 0.55, 0.60) to emphasize the importance and analyze the effects of wettability of the porous medium or the newly proposed parameter, S_n' on the dissolution phenomenon. As discussed in section 3, a change in S_n' from 0.45 to 0.60 implies a change in wettability of the porous medium from being NAPL-wet to a water-wet medium.

The quantity of NAPL dissolved in each case is given by Figure 5-1 (b). The variation of total masses of water and NAPL present in the system over the course of dissolution for varying S_n' is shown in Figure 5-2 (b) and Figure 5-3 (b) respectively. Although the maximum amount of NAPL dissolved tends to reach the same asymptotic value, the rate at which dissolution occurs is different, because NAPL can dissolve in a water wet medium easily due to its high a_{nw} in the applied conditions. It is observed from Figure 5-4 (b-i) that the case with S_n' closest to the initial NAPL saturation will reach the maximum NAPL-water specific contact surface area quicker causing dissolution rate to be at its highest soon. This is also reflected in the rate of change of NAPL-water specific contact surface area/lumped mass transfer rate in Figure 5-4 (b-ii). Finally, the rate of change of liquid saturation shown in Figure 5-5 (b) explains the dissolution effect being more severe in the case of water-wet medium than in an NAPL-wet medium since the initial state represents a relatively water-wet medium. Finally, the rate of change of NAPL pressure is plotted in Figure 5-6 (b) to show the influence of contaminant fluid pressure on NAPL dissolution based on wettability of the porous medium. Since the modified van Genuchten's equation proposed by Nakamura and Kikumoto [2014] is applied only for NAPLs following the Leverett's [1941] assumption of fluid wettability, the change in NAPL pressure in Figure 5-6 (b) is not plotted for NAPL-wet medium with S_n'=0.45.
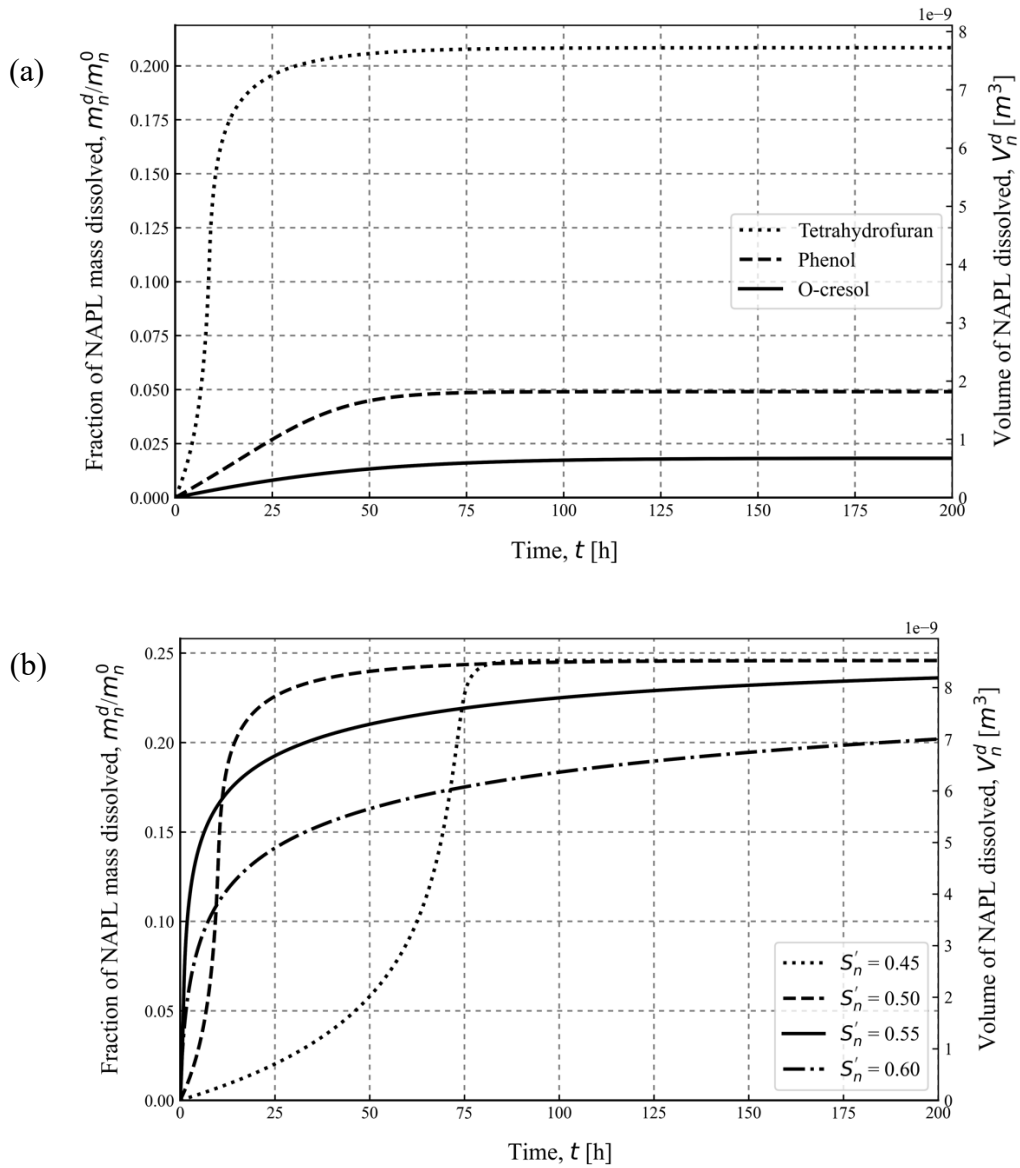
Figure 5-1: Rate of change of dissolved NAPL mass and volume with varying (a) mass transfer coefficients and (b) NAPL saturation at maximum NAPL-water specific contact surface area

(a)

(b)
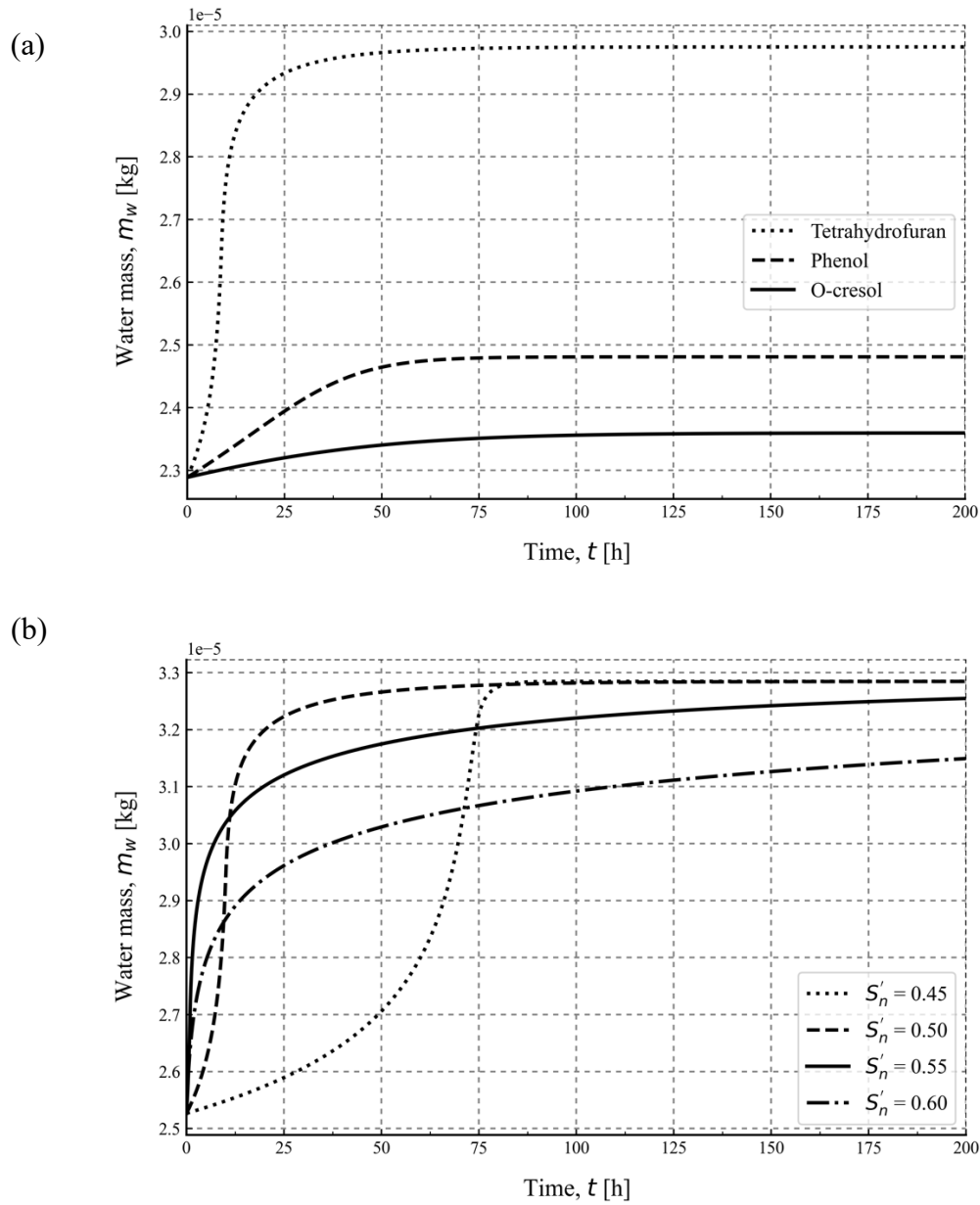
Figure 5-2: Variation in mass of water present in the system during the course of dissolution for varying (a) mass transfer coefficients and (b) NAPL saturation at maximum NAPL-water specific contact surface area

(a)

(b)
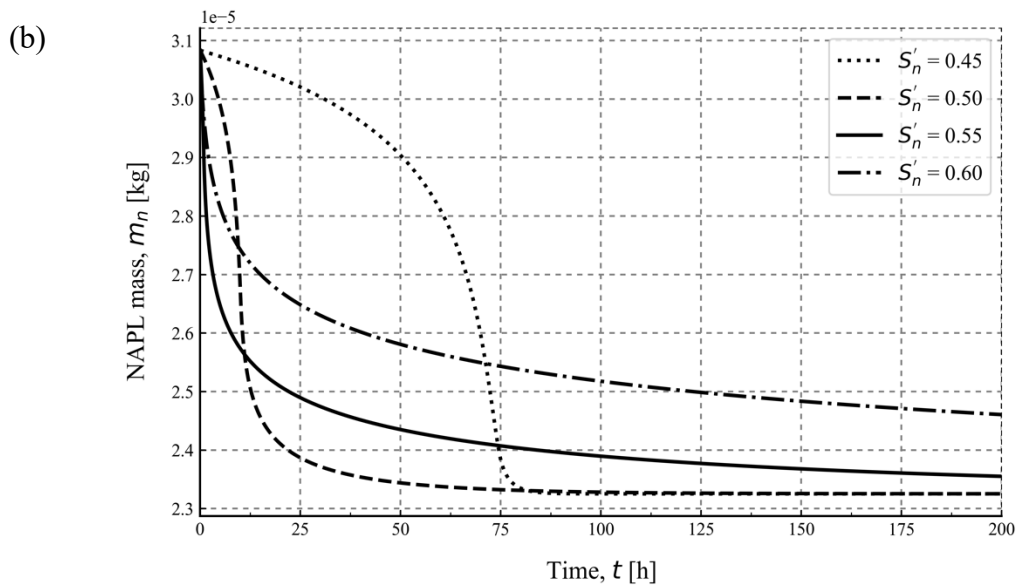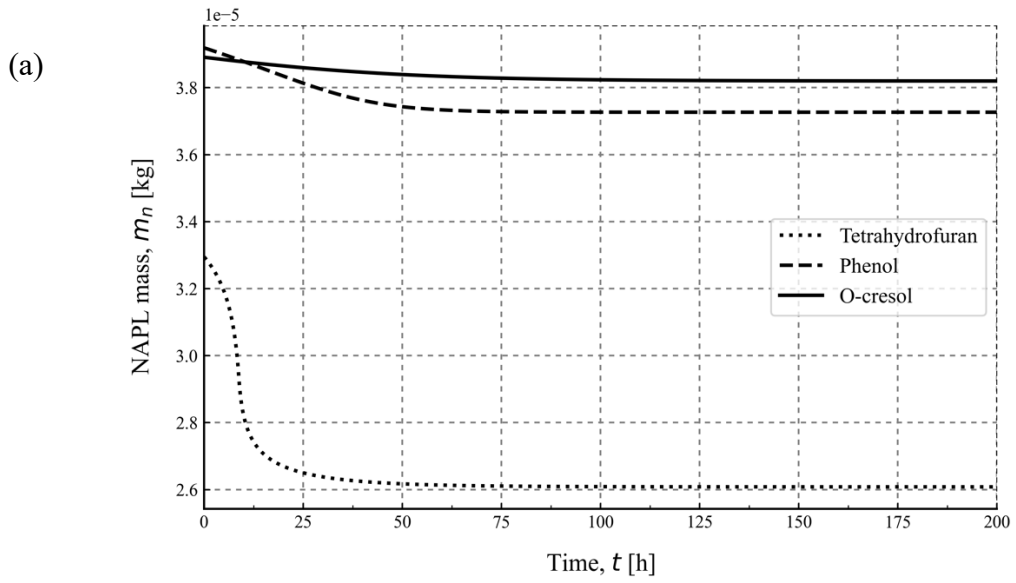
Figure 5-3: Variation in mass of NAPL present in the system during the course of dissolution for varying (a) mass transfer coefficients and (b) NAPL saturation at maximum NAPL-water specific contact surface area
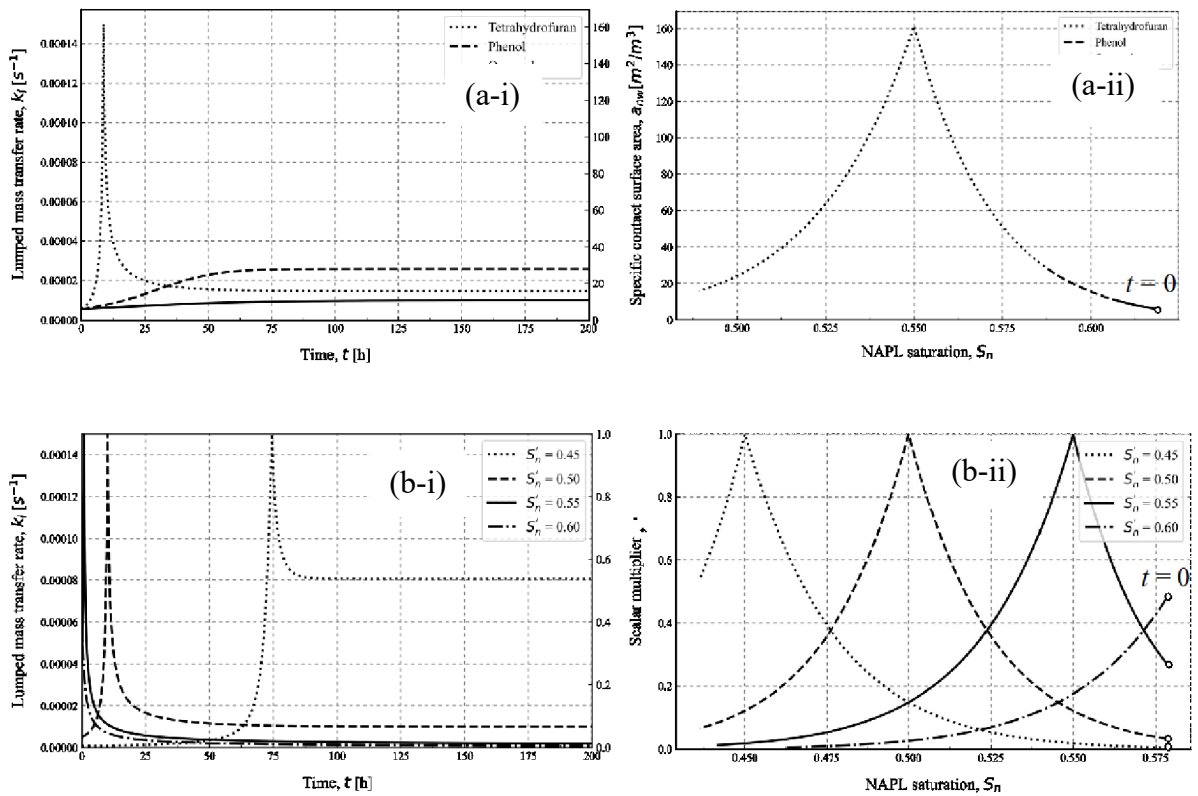
Figure 5-4: Variation of NAPL-water specific contact surface area/scalar multiplier and lumped mass transfer rate with time and NAPL saturation for varying mass transfer coefficients ((a-i) and (a-ii) respectively) and varying NAPL saturation at maximum NAPL-water specific contact surface area ((b-i) and (b-ii) respectively)

(b)
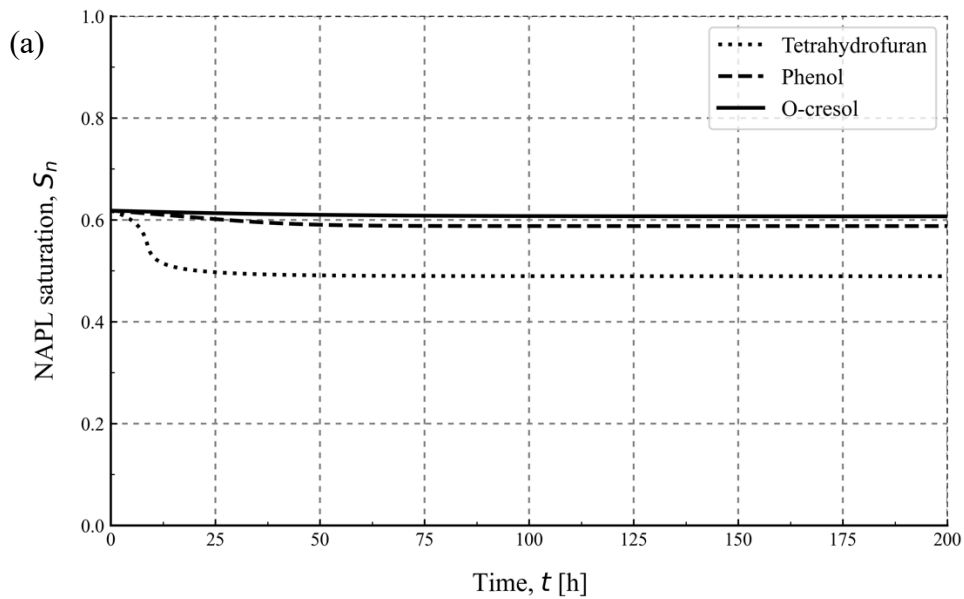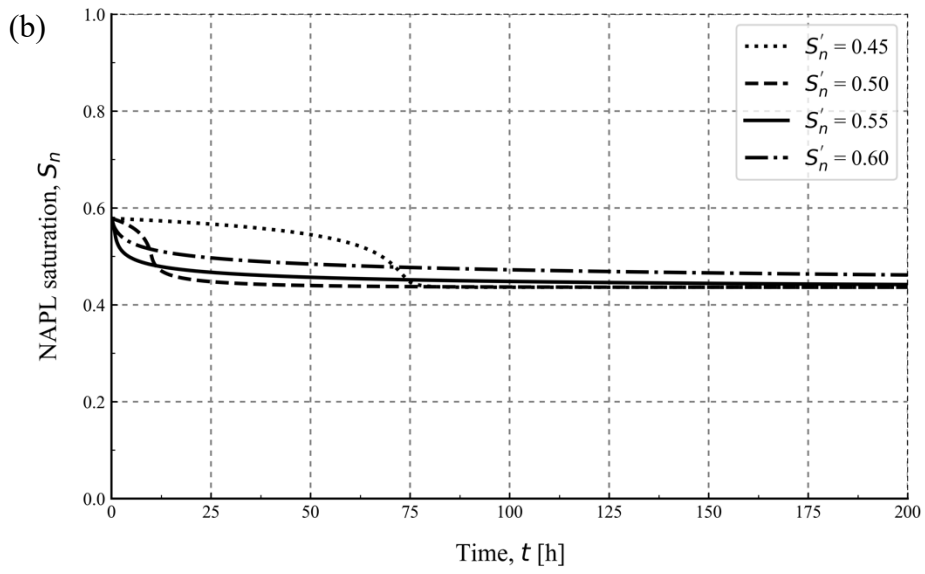
Figure 5-5: Rate of change of NAPL saturation with varying (a) mass transfer coefficients and (b)

NAPL saturation at maximum NAPL-water specific contact surface area

(a)
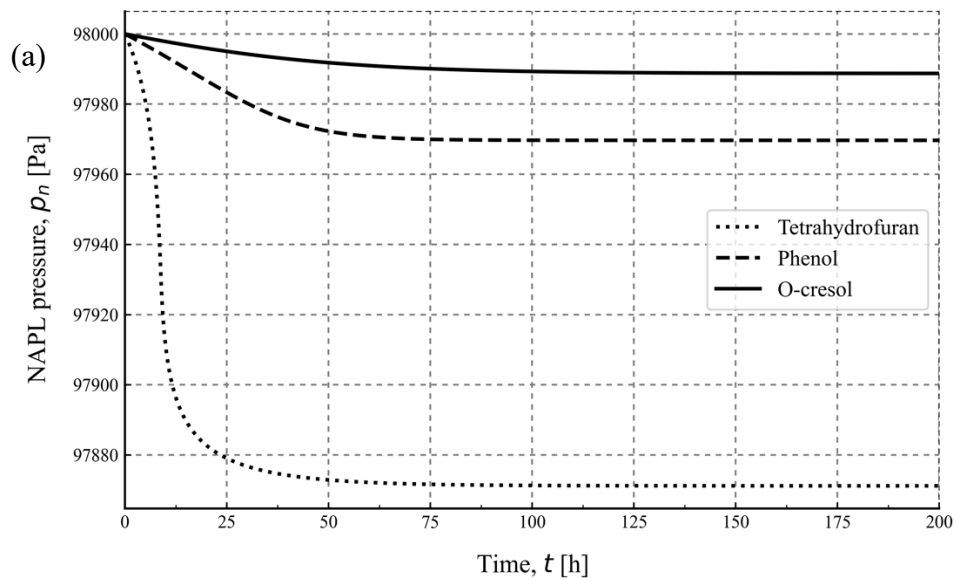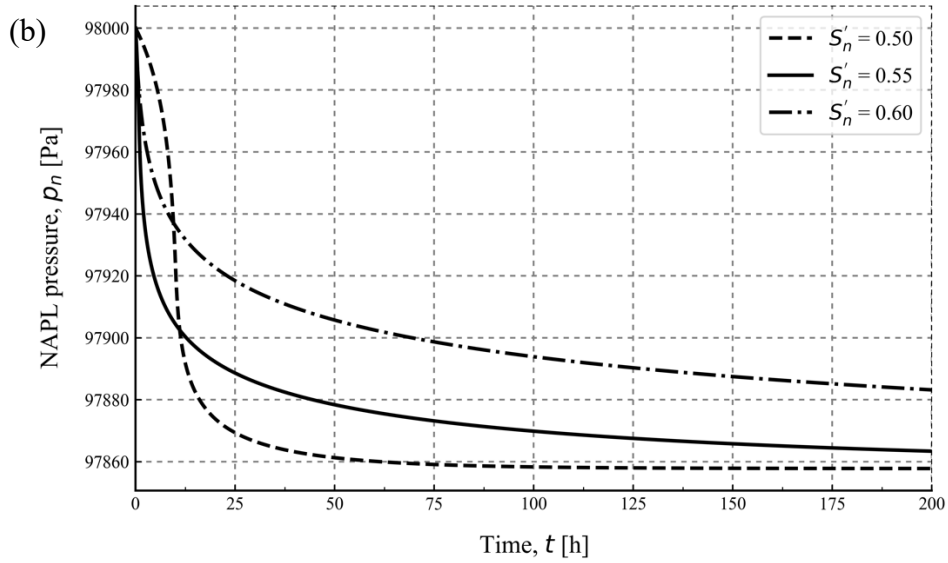
Figure 5-6: Rate of change of water pressure with varying (a) mass transfer coefficients and (b) NAPL saturation at maximum NAPL-water specific contact surface area

5.2 Finite Element Simulation results

Finite element method (FEM) simulations are conducted to check the applicability of the proposed model to a boundary value problem. The simulations are conducted for both, an NAPL-water two-phase system and a gas-NAPL-water three-phase system using COMSOL Multiphysics™ software. In both the cases, simulations were conducted under simple initial and boundary conditions to emphasize the importance of NAPL dissolution in contaminant seepage flow and transport. The simple conditions include 1-dimensional fluid flow in the soil specimen and a closed system with rigid boundaries. A new state variable, mass balance index (M_i) of water is defined to check the conservation of mass of pore fluids during the course of NAPL dissolution. M_i is a ratio of the mass gained by water until any time, t, as compared to the mass lost by NAPL until that time during the course of NAPL dissolution.

$$M_i = \frac{m_w^t - m_w^0}{m_n^0 - m_n^t}$$

The value of M_i is ideally always equal to 1, and any deviation from it implies that the law of conservation of mass of water is not strictly satisfied. The variation in M_i with the simulation time

62

measures the numerical error in the system which is used to define the accuracy of the simulation. Besides, a comparison with analytical solutions for most of the results also emphasizes the accuracy of the FEM simulation results.

For an NAPL-water two-phase system (referred to with the suffix (a) in the Figures and tables hereon), a 5-metre-long specimen is considered with the groundwater table present at depth, $y = 0.5$ m. For a gas-NAPL-water three-phase system (referred to with the suffix (b) in the Figures and tables hereon), same length of the soil specimen is considered with the groundwater table present at depth, $y = 0.5$ m and NAPL surface present at depth, $y = 2.0$ m.

The material properties and initial conditions are defined in Table 5-3 and 5-4 (a, b) respectively. An illustration of the applied initial conditions and boundary conditions is shown in Figure 5-7 (a, b). The corresponding boundary conditions for both, the two- and three-phase system, have been maintained to be the same, and are defined in Table 5-5. The mesh properties and time steps considered in running the simulation for both (a) and (b) are shown in Table 5-6 which define the spatial and temporal discretization in the soil specimen.

Table 5-3: Material parameters applied in simulating both, (a) NAPL-water two-phase system and (b) gas-NAPL-water three-phase system

Material parameters			
	Porosity, ϕ		0.6
		S_{max}	1.0
		S_{min}	0.0
Soil	van Genuchten's parameters	α [1/kPa]	0.38
		m	0.656
		n	2.91
	Total volume, V_t [m^3]		5.0
	Saturated permeability, K_w [m/s]		0.01
Interface	Area of crosssection [m^2]		5.0

63

NAPL	Density, ρ_n [kg/m^3]	876.5

Table 5-4: Initial conditions applied in simulating (a) NAPL-water two-phase system and (b) gas-NAPL-water three-phase system

Initial conditions (a)

Water pressure, p_w [Pa]	$-\rho_w g(y-11.814)$
NAPL pressure, p_n [Pa]	$-\rho_n g(y-13.409)$
Variance σ_n	20
Saturation at maximum area, S'_n	0.5
Mass transfer coefficient, k_d	0.1
Mass transfer rate, k_r [1/s]	0.008
Time, t [h]	1000

Initial conditions (b)

Water pressure, p_w [Pa]		$-\rho_w g(y-11.814)$
NAPL pressure, p_n [Pa]		$-\rho_n g(y-13.409)$
Gas pressure, p_g [Pa]		90000
Exponent	σ_n	7
	σ_w	7
Saturation at maximum area	S'_n	0.1
	S'_w	0.6
Mass transfer coefficient, k_d		0.067
Mass transfer rate, k_r [1/s]		2e-5
Time, t [h]		1000

(i) Pressure **(ii) Saturation** **(iii) Boundary conditions**

5.0

NAPL

Water

No flux:
$\cdot . \cdot \cdot = 0$
$\cdot . \cdot \cdot = 0$

(a)

$(\cdot - 11.814)$
$(\cdot - 13.409)$

Height, $\cdot$ [m]

0.5

0.0

Pressure, $\cdot$ [Pa] $\cdot_w$

Fixed pressure head:
$\cdot_w = 115.78$ kPa
$\cdot_n = 115.18$ kPa

(i) Pressure **(ii) Saturation** **(iii) Boundary conditions**

5.0

Gas

NAPL

Water

No flux:
$\cdot . \cdot \cdot = 0$
$\cdot . \cdot \cdot = 0$

(b)

$(\cdot - 11.814)$
$(\cdot - 13.409)$
$\cdot = 90000$ Pa

Height, $\cdot$ [m]

0.5

0.0

Pressure, $\cdot$ [Pa] $\cdot_w$

Fixed pressure head:
$\cdot_w = 115.78$ kPa
$\cdot_n = 115.18$ kPa
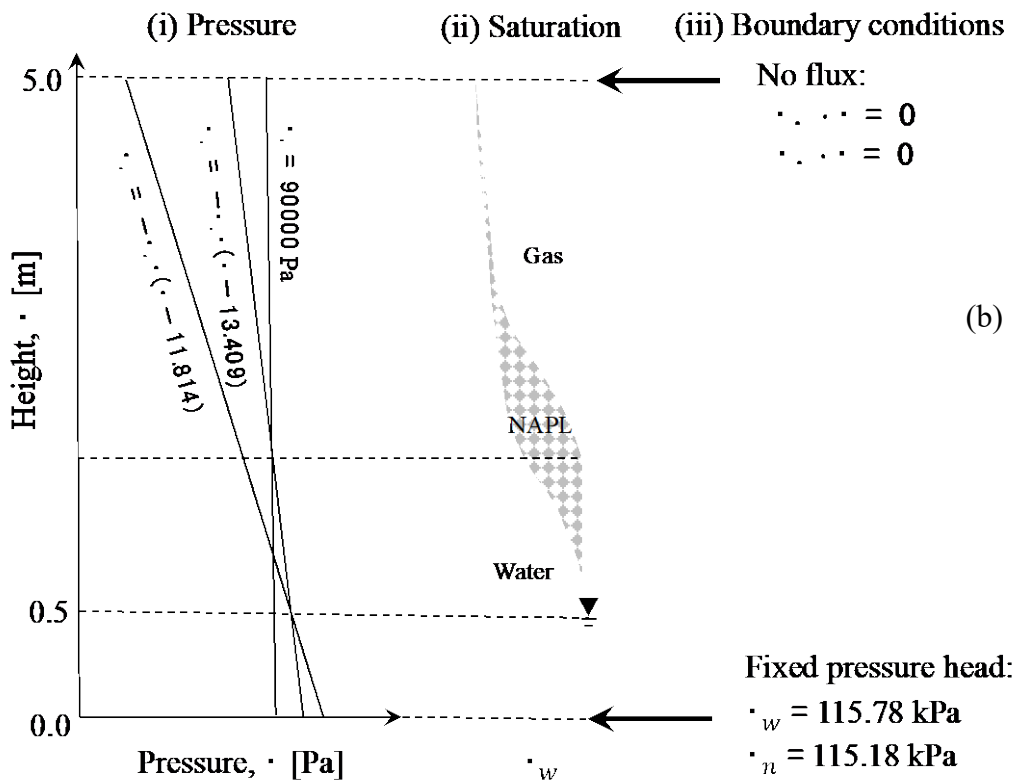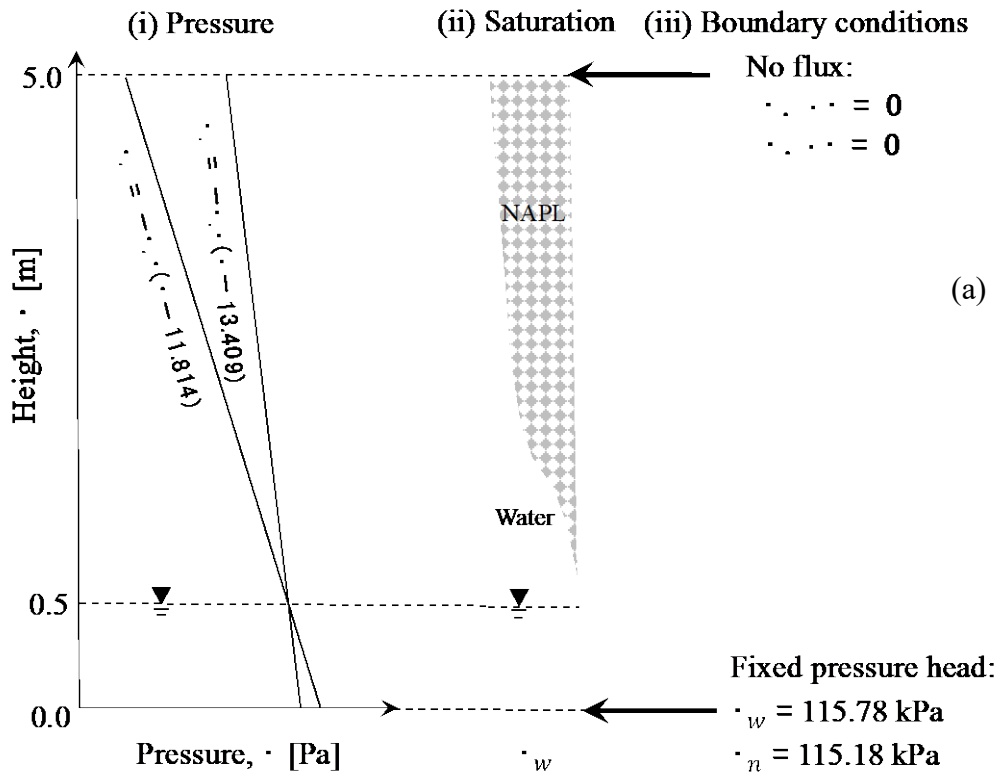
Figure 5-7: Illustration of (i) applied conditions, (ii) saturation distribution, and (iii) boundary conditions in the 1-D soil specimen in (a) NAPL-water two-phase system and (b) gas-NAPL-water three-phase system

Table 5-5: Boundary conditions applied simulating NAPL-water two-phase system

Boundary conditions		
Boundary	**Water**	**NAPL**
I	$v_w \cdot n = 0$	$v_n \cdot n = 0$
II	$p_w = 115777.2$ Pa	$p_n = 115179.28$ Pa

Table 5-6: Mesh properties and time steps used in simulating NAPL-water two-phase system

	Mesh vertices	101
Mesh properties	Edge elements	100
	Vertex elements	2
	Element length ratio	1.0
Time discretization	Time step [h]	0.1
	Time step ratio	1.0

The results are presented in a systematic way starting with pressure distribution in the soil profile. The initial and final stages of the pore fluid pressure distribution are shown in the Figure 5-8 (a, b). The initial static states in both the cases (a) and (b) match well with the analytical solutions. A "no flux" (Neumann) boundary condition at the top boundary does not allow any change in pressure, whereas applying a constant pressure (Dirichlet) boundary condition at the bottom boundary fixes the pressure at the bottom-most node and causes a sudden pressure change. The change caused in the fluid pressure distribution curves due to NAPL dissolution drifts from the initial static states as shown in the Figure 5-8 (a, b).
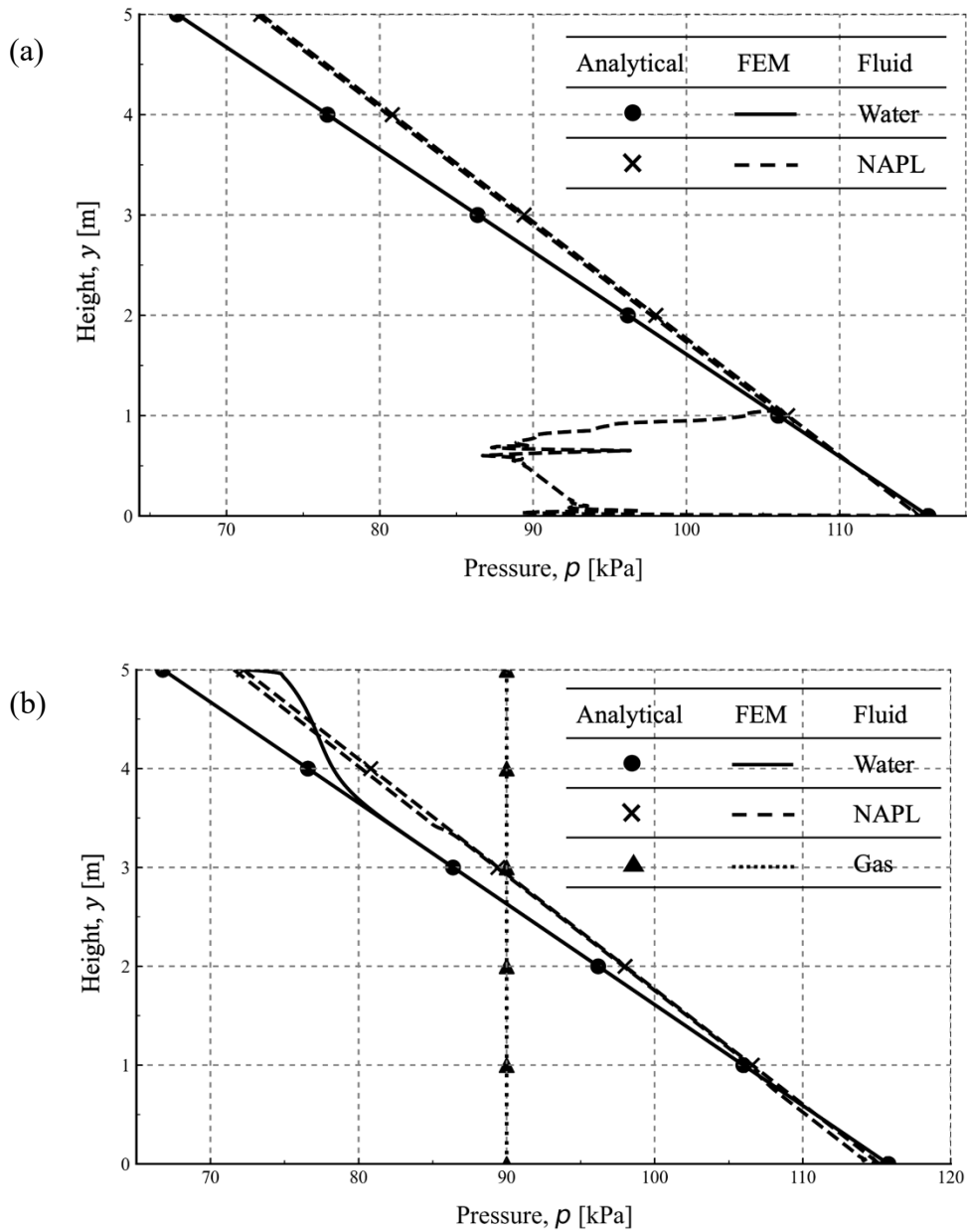
Figure 5-8: Pore fluid pressure distribution in (a) NAPL-water two-phase system and (b) gas-NAPL-water three-phase system

The next series of simulation results show the pore fluid saturation distribution in the soil profile. Similar to the pressure distribution curves, both the initial static state and final stages of the saturation distribution are shown in Figure 5-9 (a, b), and the initial static states in both the cases (a) and (b) match well with the analytical solutions. A closed system with rigid boundaries will not allow any change in

fluid saturation inside the system, so the change caused in fluid saturation distribution can only be attributed to the changes caused inside the system i.e., NAPL dissolution. In both the cases (a) and (b), a decrease in NAPL saturation and increase in water saturation is observed while the total liquid saturation remained constant.
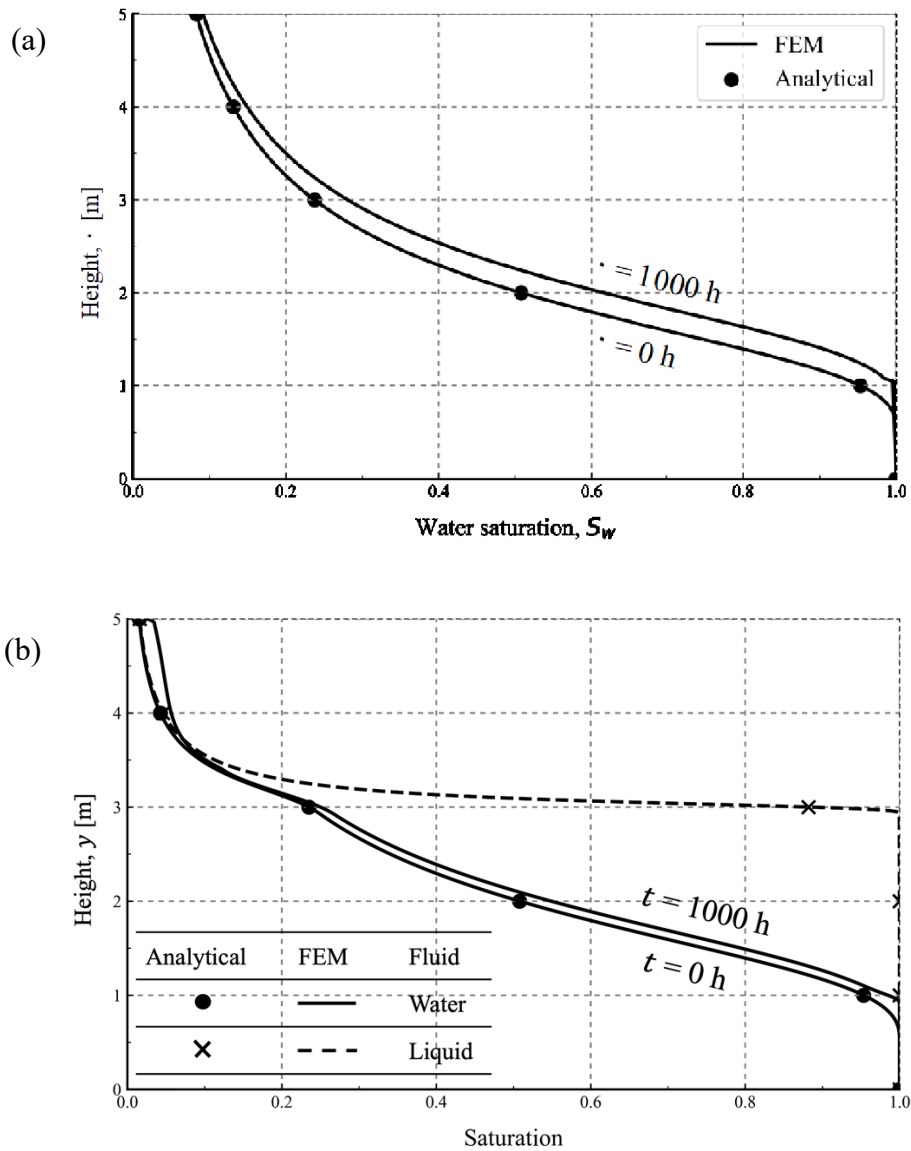
Figure 5-9: Pore fluid saturation distribution in (a) NAPL-water two-phase system and (b) gas-NAPL-water three-phase system

Relative permeability distribution of the soil profile is shown to reflect the effect of change in saturation distribution. The FEM and analytical solutions of relative permeability profiles at the initial static were also drawn to check the accuracy of the simulation in Figure 5-10 (a, b).
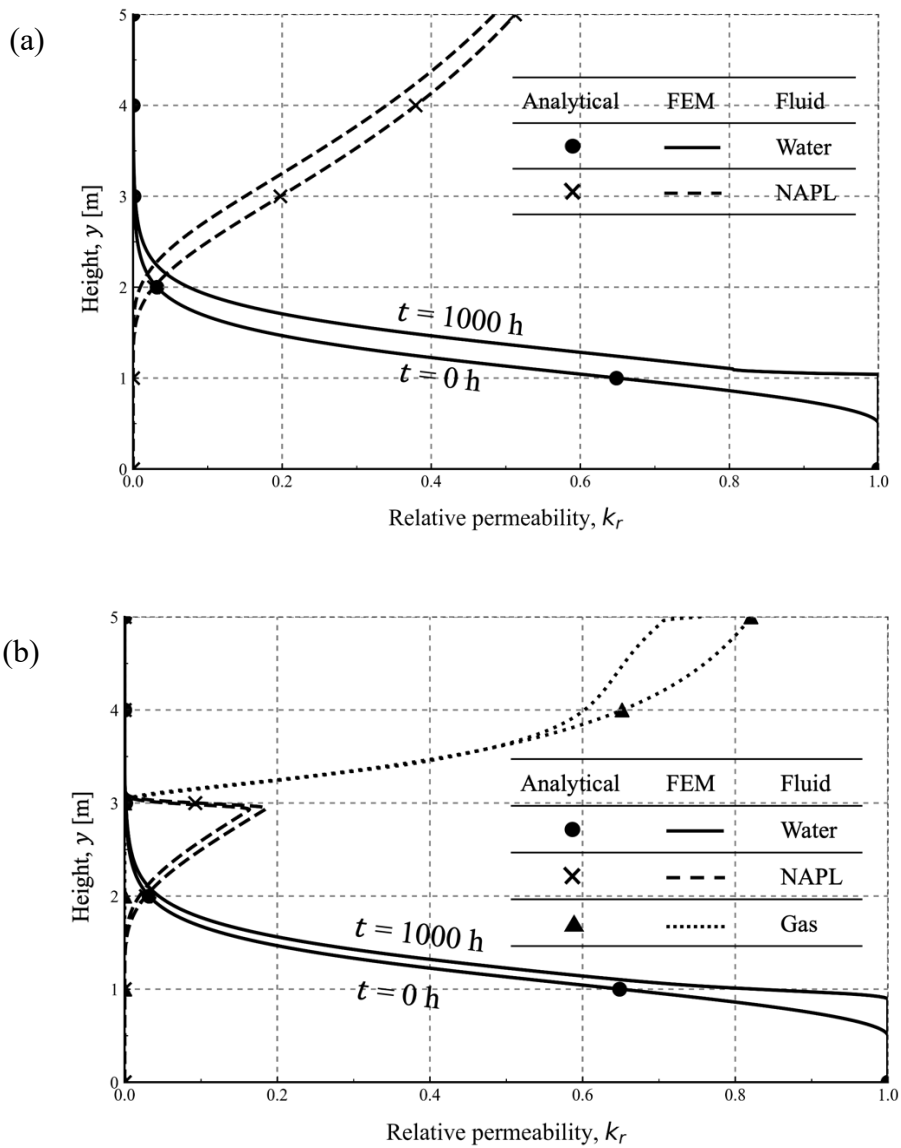
Figure 5-10: Pore fluid relative permeability distribution in (a) NAPL-water two-phase system and

(b) gas-NAPL-water three-phase system

Next, a good fit between the FEM solution of soil water characteristic curve (SWCC) of the NAPL-water two-phase system and the analytical solution is shown in Figure 5-11. These results from Figure 5-8 to Figure 5-11 prove the validity of the soil properties and the applied initial conditions to follow as per the analytical solution.
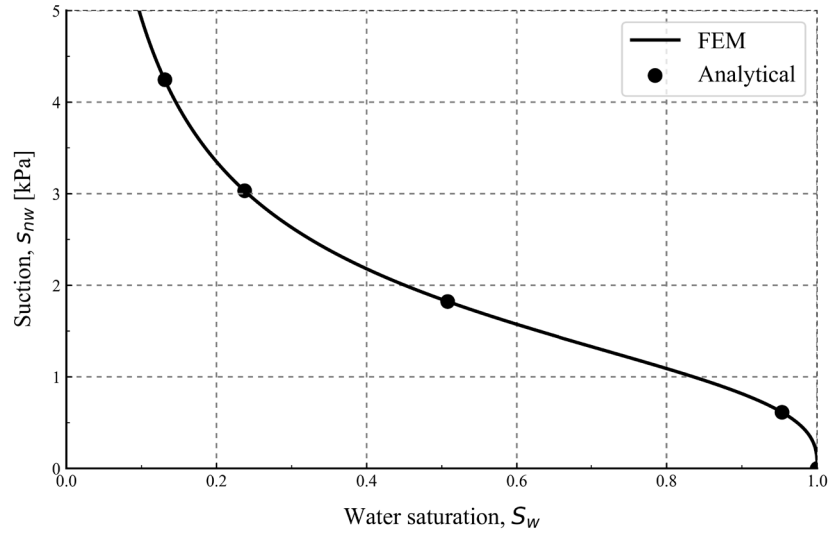
Figure 5-11: Soil water characteristic curve for (a) NAPL-water two-phase system

Hereon, we analyze the NAPL dissolution process and its effects on mass, volume, and saturation of all the pore phase fluids. Figure 5-12 (a, b) show the comparison of FEM and analytical solutions of the rate of change of the amount of NAPL dissolved. Both (a) and (b) show a good enough fit with the analytical solution.

(a)

(b)
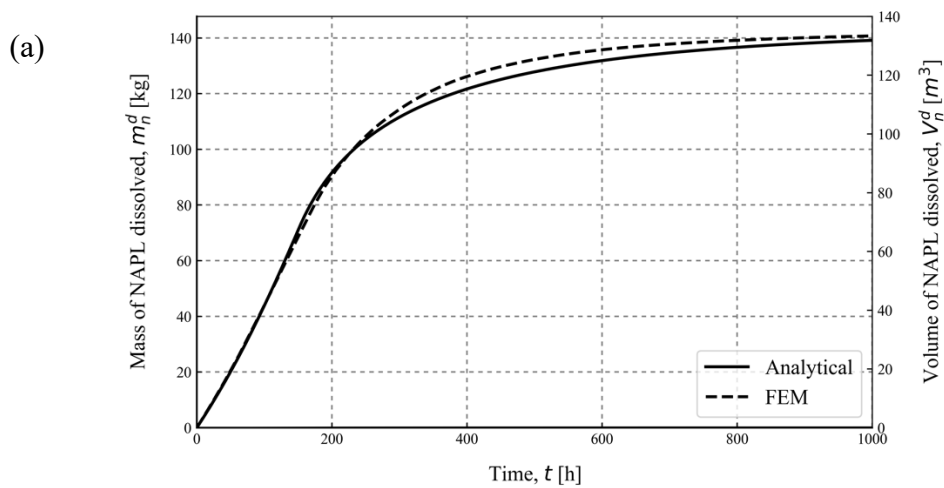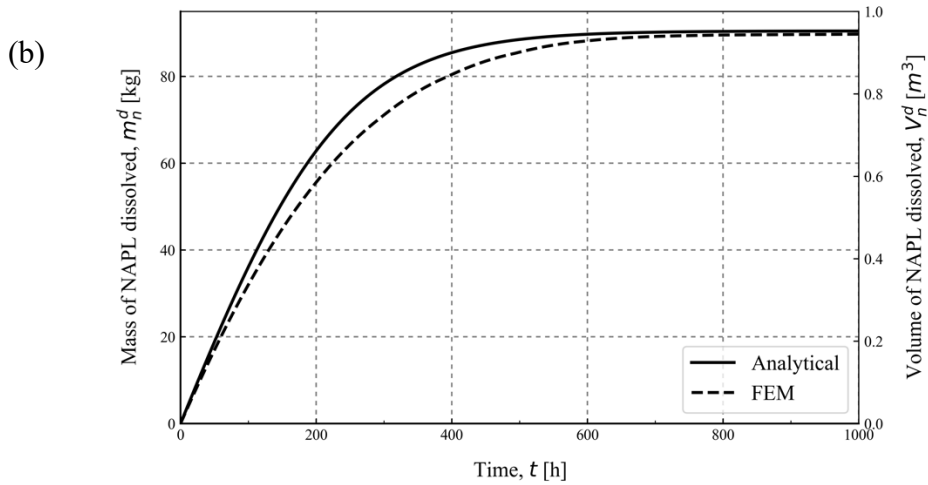
Figure 5-12: Amount of NAPL dissolved in (a) NAPL-water two-phase system and (b) gas-NAPL-

water three-phase system

Figure 5-13 (a, b) show the rate of change of the total mass of fluids present in the system. Although the initial total masses of fluids present in the system are recorded properly, both (a) and (b) have a small variation of the FEM solution as compared to the analytical solution during the course of NAPL dissolution causing the law of conservation of mass to not satisfy strictly. The reason for this numerical error could be due to the application of ψ-based form to solve for the contaminant seepage flow and transport as discussed in the Table 4-2.

(a)

(b)

Mass [kg]

Analytical	FEM	Fluid
●	——	Water
✕	- - -	NAPL

Time, t [h]
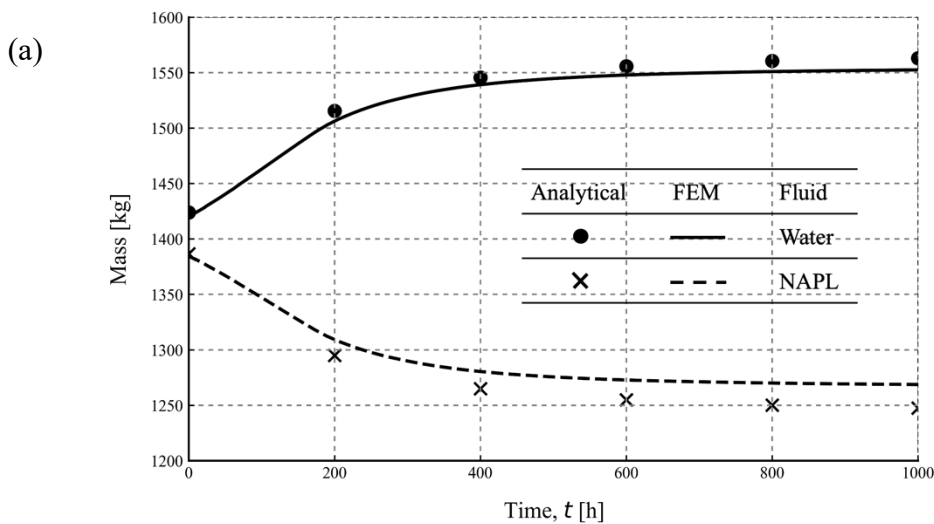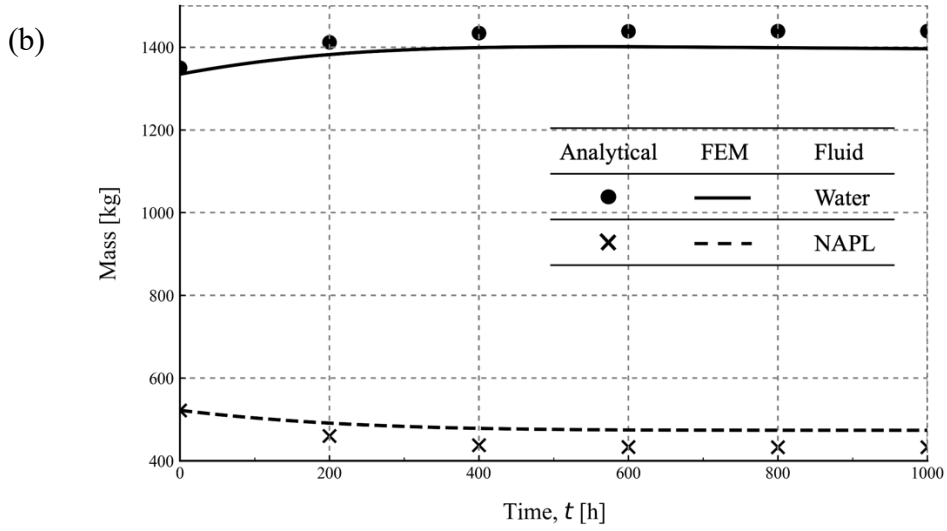
Figure 5-13: Variation in the pore fluid masses in (a) NAPL-water two-phase system and (b) gas-

NAPL-water three-phase system

The rate of change of fluid saturations are shown in Figure 5-14 (a, b) and compared with the analytical solution. The small numerical error discussed earlier is reflected in the rate of change of total fluid saturation.

(a)

Water saturation, S_w

Time, t [h]

(b)
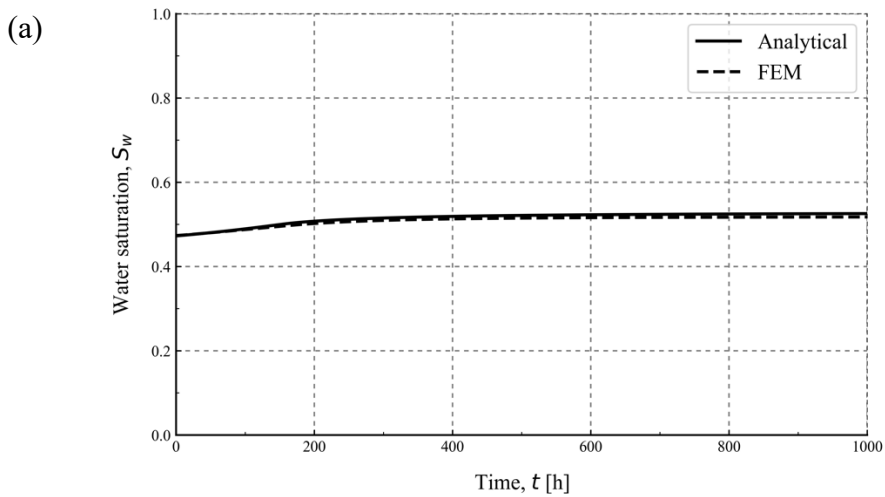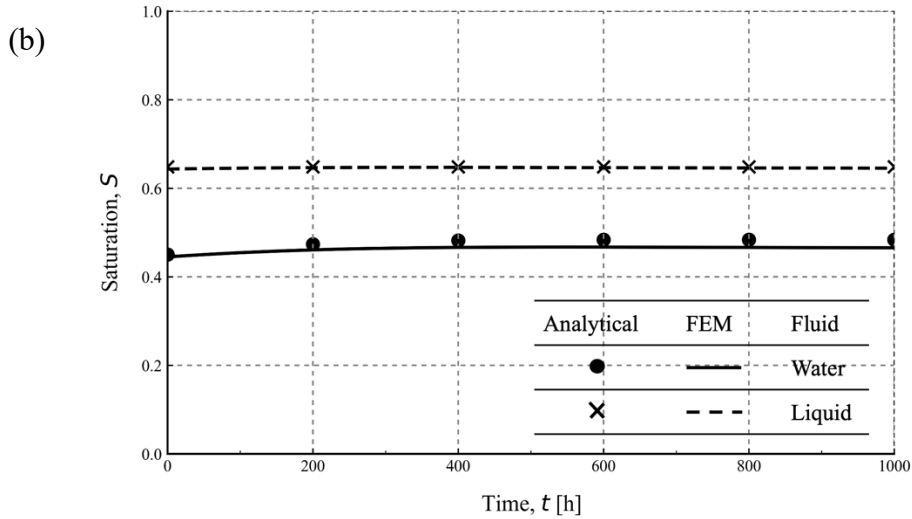
Figure 5-14: Variation in the total pore fluid saturations in (a) NAPL-water two-phase system and (b)

gas-NAPL-water three-phase system

Finally, the slope of curves in Figure 5-15 (a, b) resemble the variation in mass balance index (M_i). In the simulation (a), the change in the masses of NAPL and water seem to be equivalent to each other at all times, but in the case of a gas-NAPL-water three-phase system, the increase in the mass of water seems to be higher than the decrease in the mass of NAPL during the course of NAPL dissolution. Although a clear reason could not be identified as to why the curve tends to reach the ideal state in the ending stage of simulation period, some slight additional mass is being added to the water phase. The possible reason for this behaviour could be due to the implementation of ψ-based form for the FEM governing equations.

(a)
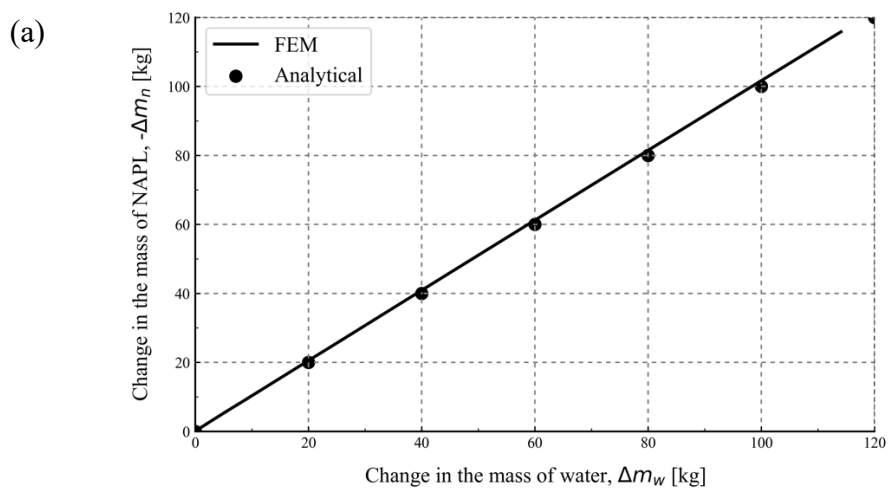
(b)
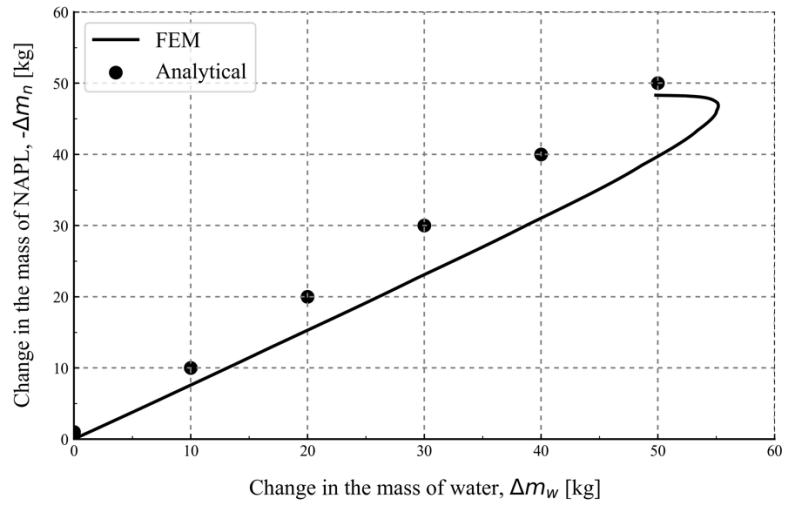
Figure 5-15: Mass gained by water phase vs mass lost by NAPL for (a) NAPL-water two-phase

system and (b) gas-NAPL-water three-phase system

CHAPTER 6

CONCLUDING REMARKS AND FUTURE RESEARCH

In this thesis, a multiphase system model considering the phenomenon of NAPL dissolution was proposed and analyzed. Also, the limitations of the existing models for porous media in describing NAPL dissolution while capturing pressure–saturation relationships were overviewed. In this final chapter, the principles findings and novelties of this research are summarized and prospect for future research are discussed.

6.1 Contributions

The key findings and the novelty of this thesis are summarized as follows.

First, a novel concept to capture NAPL dissolution effect is presented as a pore-scale phenomenon. The vital role that NAPL-water specific contact surface area plays in defining the extent of NAPL dissolution is well-explained, along with its formulation based on a theoretical analysis of NAPL-water specific contact surface area variation with liquid saturations.

Second, the NAPL dissolution theory is connected to the existing pressure-saturation relationship proposed by Nakamura and Kikumoto [2014]; which helped model both a two–phase and three–phase system in a simple and effective way.

Third, experimental validation was conducted to show the rate of change of NAPL saturation variation to capture the realistic behaviour.

Fourth, applicability of the proposed numerical solution was checked by comparing its simplified form of Richard's equation with the analytical solution proposed by Hayek [2016].

Fifth, a rational parametric study is conducted to analyze the effects of some important newly proposed model parameters which vary with the type of NAPL and fluid wettability on NAPL dissolution.

Finally, Finite Element Method simulations to model NAPL dissolution phenomenon were conducted in both, NAPL-water two-phase and gas-NAPL-water three-phase systems to analyze the given issue as a boundary value problem.

6.2 Future research

The dynamic variation of the NAPL-water specific contact surface area caused by soil heterogeneities affects the complex NAPL dissolution mechanism; hence, for future research activities in the related field, there is a need to implement the magnitude of exponents, and fluid saturation with maximum NAPL-water specific contact surface area properly depending on the soil and fluid types. Apart from the soil heterogeneity effects, the effects of soil deformation and application of hysteresis model proposed by Puligadda and Kikumoto [2021, 2022] can be considered as a part of future research to develop the model further.

BIBLIOGRAPHY

[1] "The EPA's environmental justice strategy," *Epa.gov*, 1995. [Online]. Available: https://www.epa.gov/sites/default/files/2015-02/documents/ej_strategy_1995.pdf. [Accessed: 15-Aug-2022].

[2] Committee on Ground Water Cleanup Alternatives, Commission on Geosciences, Environment and Resources, Division on Earth and Life Studies, National Research Council, and National Academy of Sciences, *Alternatives for ground water cleanup*. Washington, D.C., DC: National Academies Press, 1994.

[3] C. J. G. Darnault, J. A. Throop, D. A. DiCarlo, A. Rimmer, T. S. Steenhuis, and J.-Y. Parlange, "Visualization by light transmission of oil and water contents in transient two-phase flow fields," *J. Contam. Hydrol.*, vol. 31, no. 3–4, pp. 337–348, 1998.

[4] C. T. Miller, M. M. Poirier-McNeil, and A. S. Mayer, "Dissolution of trapped nonaqueous phase liquids: Mass transfer characteristics," *Water Resour. Res.*, vol. 26, no. 11, pp. 2783–2796, 1990.

[5] *Interstate Technology & Regulatory Council, Integrated DNAPL Site Strategy Team*. Washington, D.C., 2011.

[6] Washington, D. C. : Interstate Technology & Regulatory Council, Integrated DNAPL Site Strategy Team, "Integrated DNAPL Site Strategy IDSS-1," 2011.

[7] S. E. Powers, L. M. Abriola, and W. J. Weber Jr, "An experimental investigation of nonaqueous phase liquid dissolution in saturated subsurface systems: Steady state mass transfer rates," *Water Resour. Res.*, vol. 28, no. 10, pp. 2691–2705, 1992.

[8] M. M. Broholm, K. Broholm, and E. Arvin, "Sorption of heterocyclic compounds from a complex mixture of coal-tar compounds on natural clayey till," *J. Contam. Hydrol.*, vol. 39, no. 3–4, pp. 201–226, 1999.

[9] S. E. Powers, I. M. Nambi, and G. W. Curry Jr, "Non-aqueous phase liquid dissolution in heterogeneous systems: Mechanisms and a local equilibrium modeling approach," *Water Resour. Res.*, vol. 34, no. 12, pp. 3293–3302, 1998.

[10] I. M. Nambi and S. E. Powers, "NAPL dissolution in heterogeneous systems: an experimental investigation in a simple heterogeneous system," *J. Contam. Hydrol.*, vol. 44, no. 2, pp. 161–184, 2000.

[11] M. Ramezanzadeh, M. Aminnaji, F. Rezanezhad, M. H. Ghazanfari, and M. Babaei, "Dissolution and remobilization of NAPL in surfactant-enhanced aquifer remediation from microscopic scale simulations," *Chemosphere*, vol. 289, no. 133177, p. 133177, 2022.

[12] M. A. Mobile, M. A. Widdowson, and D. L. Gallagher, "Multicomponent NAPL source dissolution: evaluation of mass-transfer coefficients," *Environ. Sci. Technol.*, vol. 46, no. 18, pp. 10047–10054, 2012.

[13] M. Mobile *et al.*, "In-situ determination of field-scale NAPL mass transfer coefficients: Performance, simulation and analysis," *J. Contam. Hydrol.*, vol. 187, pp. 31–46, 2016.

[14] T. Bahar, F. Golfier, C. Oltéan, E. Lefevre, and C. Lorgeoux, "Comparison of theory and experiment for NAPL dissolution in porous media," *J. Contam. Hydrol.*, vol. 211, pp. 49–64, 2018.

[15] S. Khasi, M. Ramezanzadeh, and M. H. Ghazanfari, "Experimentally based pore network modeling of NAPL dissolution process in heterogeneous porous media," *J. Contam. Hydrol.*, vol. 228, no. 103565, p. 103565, 2020.

[16] J. T. Geller and J. R. Hunt, "Mass transfer from nonaqueous phase organic liquids in water-saturated porous media," *Water Resour. Res.*, vol. 29, no. 4, pp. 833–845, 1993.

[17] G. F. Pinder and L. M. Abriola, "On the simulation of nonaqueous phase organic compounds in the subsurface," *Water Resour. Res.*, vol. 22, no. 9S, pp. 109S-119S, 1986.

[18] A. E. Adenekan, T. W. Patzek, and K. Pruess, "Modeling of multiphase transport of multicomponent organic contaminants and heat in the subsurface: Numerical model formulation," *Water Resour. Res.*, vol. 29, no. 11, pp. 3727–3740, 1993.

[19] A. L. Baehr and M. Y. Corapcioglu, "A compositional multiphase model for groundwater contamination by petroleum products: 2. Numerical solution," *Water Resour. Res.*, vol. 23, no. 1, pp. 201–213, 1987.

[20] A. L. Baehr, "Selective transport of hydrocarbons in the unsaturated zone due to aqueous and vapor phase partitioning," *Water Resour. Res.*, vol. 23, no. 10, pp. 1926–1938, 1987.

[21] S. Pandy, P. A. Forsyth, R. W. Falta, Y.-S. Wu, and P. S. Huyakorn, "Considerations for robust compositional simulations of subsurface nonaqueous phase liquid contamination and remediation," *Water Resour. Res.*, vol. 31, no. 5, pp. 1273–1289, 1995.

[22] B. E. Sleep and J. F. Sykes, "Compositional simulation of groundwater contamination by organic compounds: 1. Model development and verification," *Water Resour. Res.*, vol. 29, no. 6, pp. 1697–1708, 1993.

[23] P. V. Cline, J. J. Delfino, and P. S. C. Rao, "Partitioning of aromatic constituents into water from gasoline and other complex solvent mixtures," *Environ. Sci. Technol.*, vol. 25, no. 5, pp. 914–920, 1991.

[24] D. Mackay, W. Y. Shiu, A. Maijanen, and S. Feenstra, "Dissolution of non-aqueous phase liquids in groundwater," *J. Contam. Hydrol.*, vol. 8, no. 1, pp. 23–42, 1991.

[25] A. Sato and T. Nakajima, "Partition coefficients of some aromatic hydrocarbons and ketones in water, blood and oil," *Br. J. Ind. Med.*, vol. 36, no. 3, pp. 231–234, 1979.

[26] W. A. Jury, D. Russo, G. Streile, and H. El Abd, "Evaluation of volatilization by organic chemicals residing below the soil surface," *Water Resour. Res.*, vol. 26, no. 1, pp. 13–20, 1990.

[27] M. Jin *et al.*, "Partitioning tracer test for detection, estimation, and remediation performance assessment of subsurface nonaqueous phase liquids," *Water Resour. Res.*, vol. 31, no. 5, pp. 1201–1211, 1995.

[28] Z. Wang, J. Feyen, and D. E. Elrick, "Prediction of fingering in porous media," *Water Resour. Res.*, vol. 34, no. 9, pp. 2183–2190, 1998.

[29] C. M. Lee, S. L. Meyers, C. L. Wright, J. T. Coates, P. A. Haskell, and R. W. Falta, "NAPL compositional changes influence partitioning coefficients," *Environ. Sci. Technol.*, vol. 32, no. 22, pp. 3574–3578, 1998.

[30] M. Schubert, K. Lehmann, and A. Paschke, "Determination of radon partition coefficients between water and organic liquids and their utilization for the assessment of subsurface NAPL contamination," *Sci. Total Environ.*, vol. 376, no. 1–3, pp. 306–316, 2007.

[31] "Reichert, B, Hoetzl, H, Weber, K and Eiswrth, M (1998). Factors controlling the natural attenuation of BTEX. IAHS Publication 250: 237-244."

[32] E. L. Libelo, T. B. Stauffer, T. Shelley, C. A. Antworth, W. G. Macintyre, and G. Bugna, "Processes contributing to natural attenuation of fuel hydrocarbons in groundwater : a field study with known initial conditions," in *Groundwater quality : remediation and protection (Tübingen, 21-25 September 1998)*, 1998, pp. 221–227.

[33] T. B. Stauffer, E. L. Libelo, W. G. MacIntyre, J. M. Boggs, and R. Stapleton, "A field study to quantitate important chemical and biological processes in natural attenuation," in *Contaminated Soil 1998*, p. 1: 94-100.

[34] S. A. Bradford, T. J. Phelan, and L. M. Abriola, "Dissolution of residual tetrachloroethylene in fractional wettability porous media: correlation development and application," *J. Contam. Hydrol.*, vol. 45, no. 1–2, pp. 35–61, 2000.

[35] S. A. Bradford and L. M. Abriola, "Dissolution of residual tetrachloroethylene in fractional wettability porous media: incorporation of interfacial area estimates," *Water Resour. Res.*, vol. 37, no. 5, pp. 1183–1195, 2001.

[36] H. I. Essaid, B. A. Bekins, and I. M. Cozzarelli, "Organic contaminant transport and fate in the subsurface: Evolution of knowledge and understanding," *Water Resour. Res.*, vol. 51, no. 7, pp. 4861–4902, 2015.

[37] C. Jia, K. Shing, and Y. C. Yortsos, "Visualization and simulation of non-aqueous phase liquids solubilization in pore networks," *J. Contam. Hydrol.*, vol. 35, no. 4, pp. 363–387, 1999.

[38] K. Nakamura and M. Kikumoto, "Modeling water–NAPL–air three-phase capillary behavior in soils," *SOILS AND FOUND.*, vol. 54, no. 6, pp. 1225–1235, 2014.

[39] K. Nakamura and M. Kikumoto, "New concept to describe three-phase capillary pressure–degree of saturation relationship in porous media," *J. Contam. Hydrol.*, vol. 214, pp. 1–15, 2018.

[40] L. K. P. Puligadda and M. Kikumoto, "Modeling hysteresis of water–NAPL–air suction–saturation relationship in porous media," *Jpn. Geotech. Soc. spec. publ.*, vol. 9, no. 8, pp. 387–393, 2021.

[41] E. L. Cussler, *Cussler, E. L., Diffusion: Mass Transfer in Fluid Systems*. New York: Cambridge University Press, 1984.

[42] B. E. Sleep and J. F. Sykes, "Modeling the transport of volatile organics in variably saturated media," *Water Resour. Res.*, vol. 25, no. 1, pp. 81–92, 1989.

[43] M. Y. Corapcioglu and A. L. Baehr, "A compositional multiphase model for groundwater contamination by petroleum products: 1. Theoretical considerations," *Water Resour. Res.*, vol. 23, no. 1, pp. 191–200, 1987.

[44] S. E. Powers and S. E. Heerman, "A Critical Review: The Effect of Ethanol in Gasoline on the Fate and Transport of BTEX in the Subsurface," in *Potential Ground and Surface Water Impacts*, G. Cannon and D. Rice, Eds. 1999.

[45] M. T. van Genuchten, "A closed-form equation for predicting the hydraulic conductivity of unsaturated soils," *Soil Sci. Soc. Am. J.*, vol. 44, no. 5, pp. 892–898, 1980.

[46] J. Mahadevan, "Comments on the paper titled 'Contact angle measurements of CO2–water-quartz/calcite systems in the perspective of carbon sequestration': A case of contamination?," *Int. J. Greenhouse Gas Control*, vol. 7, no. 7, pp. 261–262, 2012.

[47] P. K. Bikkina, "Reply to the comments on 'Contact angle measurements of CO2–water–quartz/calcite systems in the perspective of carbon sequestration,'" *Int. J. Greenhouse Gas Control*, vol. 7, no. 7, pp. 263–264, 2012.

[48] S. Iglauer, A. Salamah, M. Sarmadivaleh, K. Liu, and C. Phan, "Contamination of silica surfaces: Impact on water–CO2–quartz and glass contact angle measurements," *Int. J. Greenhouse Gas Control*, vol. 22, pp. 325–328, 2014.

[49] D. R. Palamara, T. Neeman, A. N. Golab, and A. Sheppard, "A statistical analysis of the effects of pressure, temperature and salinity on contact angles in CO 2 –brine–quartz systems," *Int. J. Greenhouse Gas Control*, vol. 42, pp. 516–524, 2015.

[50] "Adamson and Gast, 1997 A.W. Adamson, A.B. Gast Physical Chemistry of Surfaces (sixth ed.), John Wiley & Sons, New York (1997)." .

[51] H.-J. Butt, M. Farshchi-Tabrizi, and M. Kappl, "Using capillary forces to determine the geometry of nanocontacts," *J. Appl. Phys.*, vol. 100, no. 2, p. 024312, 2006.

[52] M. Rajayi and A. Kantzas, "Effect of Temperature and Pressure on Contact Angle and Interfacial Tension of Quartz/Water/Bitumen Systems," *J Can Pet Technol*, vol. 50, no. 06, pp. 61–67, 2011.

[53] W. Wang and A. Gupta, "Investigation of the effect of temperature and pressure on wettability using modified pendant drop method," in *All Days*, 1995.

[54] G. Hansen, A. A. Hamouda, and R. Denoyel, "The effect of pressure on contact angles and wettability in the mica/water/n-decane system and the calcite+stearic acid/water/n-decane system," *Colloids Surf. A Physicochem. Eng. Asp.*, vol. 172, no. 1–3, pp. 7–16, 2000.

[55] J. D. Bernardin, I. Mudawar, C. B. Walsh, and E. I. Franses, "Contact angle temperature dependence for water droplets on practical aluminum surfaces," *Int. J. Heat Mass Transf.*, vol. 40, no. 5, pp. 1017–1033, 1997.

[56] C. Rogers, M. P. Stallybrass, and D. L. Clements, "On two phase filtration under gravity and with boundary infiltration: application of a bäcklund transformation," *Nonlinear Anal. Theory Methods Appl.*, vol. 7, no. 7, pp. 785–799, 1983.

[57] Ross and Parlange, "COMPARING EXACT AND NUMERICAL SOLUTIONS OF RICHARDS' EQUATION FOR ONE-DIMENSIONAL INFILTRATION AND DRAINAGE," *Soil Sci.*, vol. 157, no. 6, p. 341, 1994.

[58] Haverkamp, Parlange, Starr, Schmitz, and Fuentes, "INFILTRATION UNDER PONDED CONDITIONS: 3. A PREDICTIVE EQUATION BASED ON PHYSICAL PARAMETERS," *Soil Sci.*, vol. 149, no. 5, p. 292, 1990.

[59] Fleming, Parlange, and Hogarth, "SCALING OF FLUX AND WATER CONTENT RELATIONS: COMPARISON OF OPTIMAL AND EXACT RESULTS," *Soil Sci.*, vol. 137, no. 6, p. 464, 1984.

[60] X. Chen and Y. Dai, "An approximate analytical solution of Richards' equation," *Int. J. Nonlinear Sci. Numer. Simul.*, vol. 16, no. 5, pp. 239–247, 2015.

[61] P. Broadbridge and I. White, "Constant rate rainfall infiltration: A versatile nonlinear model: 1. Analytic solution," *Water Resour. Res.*, vol. 24, no. 1, pp. 145–154, 1988.

[62] V. A. Zlotnik, T. Wang, J. L. Nieber, and J. Šimunek, "Verification of numerical solutions of the Richards equation using a traveling wave solution," *Adv. Water Resour.*, vol. 30, no. 9, pp. 1973–1980, 2007.

[63] D. A. Barry, J.-Y. Parlange, G. C. Sander, and M. Sivaplan, "A class of exact solutions for Richards' equation," *J. Hydrol. (Amst.)*, vol. 142, no. 1–4, pp. 29–46, 1993.

[64] M. Hayek, "Analytical solution to transient Richards' equation with realistic water profiles for vertical infiltration and parameter estimation: A MODEL FOR VERTICAL INFILTRATION AND PARAMETER ESTIMATION," *Water Resour. Res.*, vol. 52, no. 6, pp. 4438–4457, 2016.

[65] G. J. Hirasaki, "Structural interactions in the wetting and spreading of van der Waals fluids," *J. Adhes. Sci. Technol.*, vol. 7, no. 3, pp. 285–322, 1993.

[66] J. L. Ryder, "EXPERIMENTAL INVESTIGATION OF THE FACTORS AFFECTING THE WETTABILITY OF AQUIFER MATERIALS," The University of Michigan, Michigan, USA, 2007.

[67] J. Margat and J. van der Gun, *Groundwater around the world: A geographic synopsis*, 1st Edition. Boca Raton, FL: CRC Press, 2013.

[68] J. Vrba and J. Van Der Gun, "The world's groundwater resources. World Water Development Report 2, contribution to Chapter 4," *International Groundwater Resources Assessment Centre (IGRAC)*, vol. 2, 2004.

[69] G. E. Pataki and E. M. Crotty, *New York State Spill Response Program for Petroleum and Hazardous Materials*. 2007.

[70] S. Siebert *et al.*, "Groundwater use for irrigation – a global inventory," *Hydrol. Earth Syst. Sci.*, vol. 14, no. 10, pp. 1863–1880, 2010.

[71] M. W. Kemblowski and C. Y. Chiang, "Hydrocarbon thickness fluctuations in monitoring wells," *Ground Water*, vol. 28, no. 2, pp. 244–252, 1990.

[72] M. W. Kemblowski and C. Y. Chiang, "Analysis of the measured free product thickness in dynamic aquifers," in *Proceedings of Petroleum Hydrocarbons and Organic Chemicals in Ground Water: Prevention, Detection, and Restoration, A Conference and Exposition, The Westin Galleria*, vol. 1, Houston, Texas, 1988.

[73] T.-C.-J. Yeh, "Zhu Hydraulic/partitioning tracer tomography for characterization of dense nonaqueous phase liquid source zones Water Resour," *Water Resour. Res*, vol. 43, no. 6, 2007.

[74] L. M. Abriola, S. A. Bradford, J. Lang, and C. L. Gaither, "Volatilization of binary nonaqueous phase liquid mixtures in unsaturated porous media," *Vadose Zone J.*, vol. 3, no. 2, pp. 645–655, 2004.

[75] C.-O. Ng, C. C. Mei, and D. W. Ostendorf, "A model for stripping multicomponent vapor from unsaturated soil with free and trapped residual nonaqueous phase liquid," *Water Resour. Res.*, vol. 35, no. 2, pp. 385–406, 1999.

[76] T. Saba and T. H. Illangasekare, "Effect of groundwater flow dimensionality on mass transfer from entrapped nonaqueous phase liquid contaminants," *Water Resour. Res.*, vol. 36, no. 4, pp. 971–979, 2000.

[77] E. Park and J. C. Parker, "Evaluation of an upscaled model for DNAPL dissolution kinetics in heterogeneous aquifers," *Adv. Water Resour.*, vol. 28, no. 12, pp. 1280–1291, 2005.

[78] E. Libelo, T. Shelley, and G. Bugna, "Processes contributing to natural attenuation of fuel hydrocarbons in groundwater: A field study with known initial conditions," *IAHS Publication*, vol. 250, pp. 221–227, 1998.

[79] Reichert, B, Hoetzl, H, Weber, K and Eiswrth, M, *Factors controlling the natural attenuation of BTEX. 250: 237-244*. IAHS Publication, 1998.

[80] T. B. Stauffer and R. Stapleton, "A field study to quantitate important chemical and biological processes in natural attenuation. 6. International FZK/TNO Conference," *ConSoil '*, vol. 98, pp. 17–21, 1998.

[81] S. A. Bradford, R. A. Vendlinski, and L. M. Abriola, "The entrapment and long-term dissolution of tetrachloroethylene in fractional wettability porous media," *Water Resour. Res.*, vol. 35, no. 10, pp. 2955–2964, 1999.

[82] S. E. Powers, L. M. Abriola, J. S. Dunkin, and W. J. Weber Jr, "Phenomenological models for transient NAPL-water mass-transfer processes," *J. Contam. Hydrol.*, vol. 16, no. 1, pp. 1–33, 1994.

[83] P. T. Imhoff, P. R. Jaffé, and G. F. Pinder, "An experimental study of complete dissolution of a nonaqueous phase liquid in saturated porous media," *Water Resour. Res.*, vol. 30, no. 2, pp. 307–320, 1994.

[84] S. E. Powers, C. O. Loureiro, L. M. Abriola, and W. J. Weber Jr, "Theoretical study of the significance of nonequilibrium dissolution of nonaqueous phase liquids in subsurface systems," *Water Resour. Res.*, vol. 27, no. 4, pp. 463–477, 1991.

[85] J. Kim and M. Y. Corapcioglu, "Modeling dissolution and volatilization of LNAPL sources migrating on the groundwater table," *J. Contam. Hydrol.*, vol. 65, no. 1–2, pp. 137–158, 2003.

[86] L. M. Abriola, "Modeling contaminant transport in the subsurface: An interdisciplinary challenge," *Rev. Geophys.*, vol. 25, no. 2, p. 125, 1987.

[87] L. M. Abriola, "Modeling multiphase migration of organic chemicals in groundwater systems. A review and assessment," *Environ. Health Perspect.*, vol. 83, p. 117, 1989.

[88] F. H. Chapelle, "Bioremediation of petroleum hydrocarbon-contaminated ground water: The perspectives of history and hydrology," *Ground Water*, vol. 37, no. 1, pp. 122–132, 1999.

[89] P. L. Bjerg, N. Tuxen, L. A. Reitzel, H.-J. Albrechtsen, and P. Kjeldsen, "Natural attenuation processes in landfill leachate plumes at three Danish sites," *Ground Water*, vol. 49, no. 5, pp. 688–705, 2011.

[90] H. I. Essaid, B. A. Bekins, W. N. Herkelrath, and G. N. Delin, "Crude oil at the bemidji site: 25 years of monitoring, modeling, and understanding," *Ground Water*, vol. 49, no. 5, pp. 706–726, 2011.

[91] M. Oostrom, J. H. Dane, and T. W. Wietsma, "A review of multidimensional, multifluid intermediate-scale experiments: Nonaqueous phase liquid dissolution and enhanced remediation," *Vadose Zone J.*, vol. 5, no. 2, pp. 570–598, 2006.

[92] R. N. Bharagava, Ed., *Environmental contaminants: Ecological implications and management*, 1st ed. Singapore, Singapore: Springer, 2020.

[93] M. Oostrom, J. H. Dane, and T. W. Wietsma, "A review of multidimensional, multifluid, intermediate-scale experiments: Flow behavior, saturation imaging, and tracer detection and quantification," *Vadose Zone J.*, vol. 6, no. 3, pp. 610–637, 2007.

[94] S. Assouline, "Infiltration into soils: Conceptual approaches and solutions: REVIEW: INFILTRATION INTO SOILS," *Water Resour. Res.*, vol. 49, no. 4, pp. 1755–1772, 2013.

[95] D. A. DiCarlo, "Stability of gravity-driven multiphase flow in porous media: 40 Years of advancements: Stability of Multiphase Gravity-Driven Flow," *Water Resour. Res.*, vol. 49, no. 8, pp. 4531–4544, 2013.

[96] D. R. Nielsen, M. Th. Van Genuchten, and J. W. Biggar, "Water flow and solute transport processes in the unsaturated zone," *Water Resour. Res.*, vol. 22, no. 9S, pp. 89S-108S, 1986.

[97] M. T. van Genuchten, C. Naveira-Cotta, T. H. Skaggs, A. Raoof, and E. M. Pontedeiro, "The use of numerical flow and transport models in environmental analyses," in *Application of Soil Physics in Environmental Analyses*, Cham: Springer International Publishing, 2014, pp. 349–376.

[98] L. R. Chevalier, "Experimental and numerical evaluation of LNAPL lens and polluted capillary fringe thickness," *J. Environ. Eng. (New York)*, vol. 124, no. 2, pp. 156–161, 1998.

[99] *SOILS WITH AN EMPHASIS ON GASOLINE HYDROCARBONS (PETROLEUM, FINITE DIFFERENCE, GROUNDWATER, NUMERICAL MODELING, CHLOROHYDROCARBON)*. .

[100] Y. Mualem, "A new model for predicting the hydraulic conductivity of unsaturated porous media," *Water Resour. Res.*, vol. 12, no. 3, pp. 513–522, 1976.

[101] W. R. Gardner, "Mathematics of isothermal water conduction in unsaturated soils," *Highway Res. Board, Nat. Res. Counc*, vol. 40.

[102] "Model for hysteretic constitutive relations governing multiphase flow. 1. Saturation-pressure relations," *Int. j. rock mech. min. sci. geomech. abstr.*, vol. 25, no. 4, p. A168, 1988.

[103] R. J. Lenhard and J. C. Parker, "A model for hysteretic constitutive relations governing multiphase flow: 2. Permeability-saturation relations," *Water Resour. Res.*, vol. 23, no. 12, pp. 2197–2206, 1987.

[104] J. C. Parker and R. J. Lenhard, "Determining three-phase permeability—saturation—pressure relations from two-phase system measurements," *J. Pet. Sci. Eng.*, vol. 4, no. 1, pp. 57–65, 1990.

[105] D. K. Eckberg and D. K. Sunada, "Nonsteady three-phase immiscible fluid distribution in porous media," *Water Resour. Res.*, vol. 20, no. 12, pp. 1891–1897, 1984.

[106] M. Kikumoto and K. Nakamura, "Simulation of seepage flow of non-aqueous phase liquid in vadose zone," *Environ. geotech.*, vol. 4, no. 3, pp. 171–183, 2017.

[107] L. M. Abriola and G. F. Pinder, "A multiphase approach to the modeling of porous media contamination by organic compounds: 2. Numerical simulation," *Water Resour. Res.*, vol. 21, no. 1, pp. 19–26, 1985.

[108] D. M. Mackay, D. L. Freyberg, P. V. Roberts, and J. A. Cherry, "A natural gradient experiment on solute transport in a sand aquifer: 1. Approach and overview of plume movement," *Water Resour. Res.*, vol. 22, no. 13, pp. 2017–2029, 1986.

[109] A. H. M. F. Anwar, T. H. Tien, Y. Inoue, and F. Takagi, "Mass transfer correlation for nonaqueous phase liquid volatilization in porous media," *Environ. Sci. Technol.*, vol. 37, no. 7, pp. 1277–1283, 2003.

[110] C. Jia, K. Shing, and Y. C. Yortsos, "Advective mass transfer from stationary sources in porous media," *Water Resour. Res.*, vol. 35, no. 11, pp. 3239–3251, 1999.

[111] J. F. McBride, "Dense chlorinated solvents in porous and fractured media: Model experiments: F. Schwille, translated by J. f. pankow, Lewis publishers, 121 S. main street, P.o. drawer 519, Chelsea, MI 48118. 1988. 146 p. $55.00," *J. Environ. Qual.*, vol. 19, no. 1, pp. 158–158, 1990.

[112] I. M. Nambi and S. E. Powers, "Mass transfer correlations for nonaqueous phase liquid dissolution from regions with high initial saturations: DISSOLUTION MODEL FOR HIGH NAPL SATURATIONS," *Water Resour. Res.*, vol. 39, no. 2, 2003.

[113] M. Ramezanzadeh, S. Khasi, M. Fatemi, and M. H. Ghazanfari, "Remediation of trapped DNAPL enhanced by SDS surfactant and silica nanoparticles in heterogeneous porous media: experimental data and empirical models," *Environ. Sci. Pollut. Res. Int.*, vol. 27, no. 3, pp. 2658–2669, 2020.

[114] B. Agaoglu, N. K. Copty, T. Scheytt, and R. Hinkelmann, "Interphase mass transfer between fluids in subsurface formations: A review," *Adv. Water Resour.*, vol. 79, pp. 162–194, 2015.

[115] A. H. M. F. Anwar and U. Matsubayashi, "Volatilization of non-aqueous phase liquid in porous media: Vapor phase mass transfer characteristics," *J. Groundwater Hydrol./Chikasui Gakkaishui*, vol. 42, no. 1, pp. 61–81, 2000.

[116] T. Xu, E. Sonnenthal, N. Spycher, and K. Pruess, "TOUGHREACT—A simulation program for non-isothermal multiphase reactive geochemical transport in variably saturated geologic media: Applications to geothermal injectivity and CO2 geological sequestration," *Comput. Geosci.*, vol. 32, no. 2, pp. 145–165, 2006.

[117] C. Zheng and P. P. Wang, "MT3DMS : a modular three-dimensional multispecies transport model for simulation of advection, dispersion, and chemical reactions of contaminants in groundwater systems; documentation and user's guide," 1999.

[118] A. F.-E. Simulation Model For, "A FINITE-ELEMENT SIMULATION MODEL FOR SATURATEDUNSATURATED."

[119] M. Delshad, G. A. Pope, and K. Sepehrnoori, "A compositional simulator for modeling surfactant enhanced aquifer remediation, 1 formulation," *J. Contam. Hydrol.*, vol. 23, no. 4, pp. 303–327, 1996.

[120] W. Yu and H. Li, "Development of 3D finite element method for non-aqueous phase liquid transport in groundwater as well as verification," *Processes (Basel)*, vol. 7, no. 2, p. 116, 2019.

[121] M. Hayek, "An exact explicit solution for one-dimensional, transient, nonlinear Richards' equation for modeling infiltration with special hydraulic functions," *J. Hydrol. (Amst.)*, vol. 535, pp. 662–670, 2016.

[122] S. E. Power and S. E. Heermann, "Appendix B: Modeling interface mass-transfer processes. In: Cannon, G., Rice, D. (eds) A critical review: the effect of ethanol in gasoline on the fate and transport of BTEX in the subsurface. Vol. 4, Chapter 2," in *Potential ground and surface water impacts*, 1999.

[123] H. Q. Pham, D. G. Fredlund, and S. L. Barbour, "A practical hysteresis model for the soil–water characteristic curve for soils with negligible volume change," *Géotechnique*, vol. 53, no. 2, pp. 293–298, 2003.

[124] R. G. Thomas, "Volatilization from soil," in *Handbook of Chemical PropertyEstimation Methods*, W. J. Lyman, W. F. Rheel, and D. H. Rosenblatt, Eds. New York, NY: McGraw-Hill, 1982.

[125] W. T. Hunt, J. W. Wiegand, and J. D. Trompeter, "Free gasoline thickness in monitoring wells related to ground water elevation change," in *Conference on New Field Techniques for Quantifying the Physical and Chemical Properties of Heterogenous Aquifers, National Water Wells Association*, 1989, pp. 671–692.

[126] L. K. P. Puligadda and M. Kikumoto, "Concept of effective suction for describing hysteresis of multiphase pressure–saturation relationship in porous media," *SOILS AND FOUND.*, vol. 63, no. 1, p. 101267, 2023.

[127] G. H. Scott and W. W. James, "Ground water issue, Dense Nonaqueous Phase Liquids, Office of Solid Waste andn Emergency Response," 1991.

[128] D. E. Rolston, "Historical development of soil-water physics and solute transport in porous media," *Water Sci. Technol. Water Supply*, vol. 7, no. 1, pp. 59–66, 2007.

[129] "Pharmacopeia of the United States of America, 32nd revision, and the National Formulary," pp. 1–12, 2009.

[130] P. Grathwohl, *Slow contaminant release: The necessity for enhanced/natural attenuation*, vol. 250. IAHS Publication, 1998.

[131] J. N. Charles, D. A. Steven, R. R. Randall, and G. H. Scott, "Ground water issue, Light Nonaqueous Phase Liquids, Office of Solid Waste and Emergency Response," 1995.

APPENDIX-A1: OVERVIEW OF PRESSURE-SATURATION RELATIONSHIP PROPOSED BY NAKAMURA AND KIKUMOTO [2014]

The basic model is summarized in two sections. Section A1.1 presents an overview of the modeling of a basic two-phase system, which is crucial in comprehending the modeling of the multiphase system as elaborated in Section A1.2.

A1.1 Models for two–phase system

Matric suction between gas and water in a gas–water two–phase system is the difference between the pore pressures of air, p_g and water, p_w:

$$\psi_{gw} = p_g - p_w \qquad (A1-1)$$

Following this definition, for an arbitrary two-phase system with a non-wetting fluid, i and wetting fluid, j, the suction is given by the difference between pore pressures, p_i and p_j:

$$\psi_{ij} = p_i - p_j \qquad (A1-2)$$

where i and j are g, o, or w representing gas, oil (NAPL), or water phases, respectively, in increasing order of their wettability. Saturation degree, S_{ij}^j, of the wetting fluid j in $i-j$ (gas–water, gas-NAPL, or NAPL–water) phase system is given by a straightforward extension of van Genuchten's empirical relationship:

$$\begin{aligned} S_{ij}^j &= S(\beta_{ij}\psi_{ij}) \\ &= S_{min} + (S_{max} - S_{min})\left\{1 + \left(\alpha\beta_{ij}\psi_{ij}\right)^n\right\}^{-m} \end{aligned} \qquad (A1-3)$$

where S_{min} and S_{max} are minimum and maximum degrees of saturation, respectively. α, n, and m are material parameters, wherein $m = 1–1/n$. β_{ij} is a scaling parameter defined as the ratio of interfacial tension between air and water, σ_{aw}, to that between the focused two–phase fluids, σ_{ij}.

A1.2 Models for three–phase system

According to Leverett's hypothesis [1941], a void fluid with greater wettability will tend to be present near the contact point of soil particles. Typically, the order of wettability is considered to be water > NAPL > gas. Thus, NAPL is expected to always reside between water and air, which separate each other in the void space, as suggested by Nakamura and Kikumoto [2014]. To estimate the saturation degrees for a gas-NAPL-water three-phase system, Parker and Lenhard [1987] proposed the following.

$$
\begin{aligned}
S_{gnw}^w &= S(\beta_{nw}\psi_{nw}) \\
S_{gnw}^l (&= S_{gnw}^w + S_{gnw}^n) = S(\beta_{gn}\psi_{gn})
\end{aligned}
\tag{A1-4}
$$

where superscript l represents the liquid phase. Saturation degrees of NAPL and gas are derived as:

$$
\begin{aligned}
S_{gnw}^n &= S_{gnw}^l - S_{gnw}^w \\
S_{gnw}^g &= 1 - S_{gnw}^l
\end{aligned}
\tag{A1-5}
$$

The classical approach proposed by Parker and Lenhard (1987) cannot account for the transition from a 2-phase to 3-phase system and vice versa. Additionally, it is not applicable to nonspreading NAPLs (with a spreading coefficient, $\sigma_{gw} - (\sigma_{nw} + \sigma_{gn}) < 0$), as it assumes that the NAPL layer is only stable when it spreads across the water-air interface. To address these limitations, Nakamura and Kikumoto (2014) introduced a novel approach using a new state parameter, μ, which enables the transition between arbitrary 2-phase and 3-phase systems. By incorporating μ, they were able to define S_w^{gnw} and S_l^{gnw} as functions of all the suctions (ψ_{gn}, ψ_{nw}, and ψ_{gw}), in contrast to Lenhard [1992] who only considered the gas-water capillary head, ψ_{gw}, to determine S_w^{gw}, and the NAPL-water and gas-NAPL capillary heads, ψ_{nw} and ψ_{gn}, respectively, to determine S_w^{gnw} and S_l^{gnw}. Nakamura and Kikumoto [2018] further demonstrated that a simple formulation of μ can capture the configuration of a three-phase system at thermodynamic equilibrium with an arbitrary spreading coefficient, overcoming the drawbacks of Leverett's [1941] classical model proposed.

$$
\mu = \frac{p_n - p_w}{p_g - p_w}\left(= \frac{\psi_{nw}}{\psi_{gw}}\right),
\tag{A1-6}
$$

μ is a non-dimensional parameter of a relative magnitude of NAPL pressure between air and water pressure, and it systematically describes the transition between the arbitrary 2– and 3–phase systems as shown in Table A1-1. Using the scaling functions, $\tilde{\beta}^i(\mu)$ ($i = w, l$), of the state parameter, μ, given by

quadratic Bezier curves shown in Figure A1-1, the suction–saturation relationships in equation (A1-4) were replaced as:

$$S_{gnw}^w = S\left(\widetilde{\beta^w}(\mu)\psi_{gw}\right)$$
$$S_{gnw}^l = S\left(\widetilde{\beta^l}(\mu)\psi_{gw}\right)$$

$$(A1-7)$$
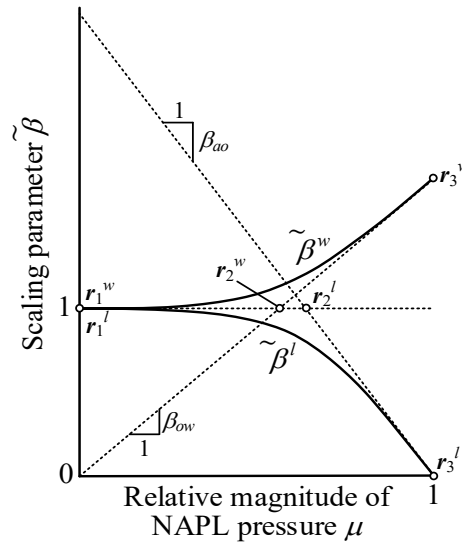
Figure A1-1. Scaling parameters $\widetilde{\beta^w}(\mu)$ and $\widetilde{\beta^l}(\mu)$ (Nakamura and Kikumoto [2014])

Table A1-1: State parameter, μ, phase system, and scaling function, $\widetilde{\beta^l}$ for arbitrary 2– and 3–phase systems

Parameter μ	Pressures p_w, p_n, p_g	Phase system	Saturations S_{gnw}^w, S_{gnw}^l	Scaling functions $\widetilde{\beta^w}, \widetilde{\beta^l}$
$\mu = 0$	$p_w = p_n < p_g$	Air–Water	$S_{gnw}^w = S_{gnw}^l = S_{gw}^w$	$\widetilde{\beta^w} = \widetilde{\beta^l} = 1 (= \beta_{gw})$
$0 < \mu < 1$	$p_w < p_n < p_g$	Air–NAPL–Water	$S_{gnw}^w < S_{gnw}^l$	$\widetilde{\beta^w}(\mu) \geq \widetilde{\beta^l}(\mu)$ (Bezier curves)
$\mu = 1$	$p_w < p_n = p_g$	NAPL–Water	$S_{gnw}^l = 1$	$\widetilde{\beta^w} = \beta_{nw}(= \sigma_{gw}/\sigma_{nw})$ $\widetilde{\beta^l} = \beta_{gn} (= \sigma_{gw}/\sigma_{gn})$

APPENDIX-A2: CALCULATION OF FLOW IN SATURATED AND UNSATURATED MEDIA (VERTICAL ONE-DIMENSIONAL)

A2.1 Saturated-unsaturated osmotic flow governing equation

Consider a fluid flow in a soil element of volume [L³], $V_t (= dxdydz)$ with inlet velocities [LT⁻¹], v_x, v_y, and v_z in the X, Y, and Z directions respectively illustrated in Figure A2-1. For a given time [T], t, if q_{in} and q_{out} represent the quantity of fluid [L³T⁻¹] flowing through the inlet and outlets respectively, and θ represents the volumetric water content [dimensionless], by the law of conservation of volume, the amount of fluid remaining in the soil element system is given as

$$q_{in} - q_{out} = \frac{\partial \theta}{\partial t} V_t \qquad (A2 - 1)$$
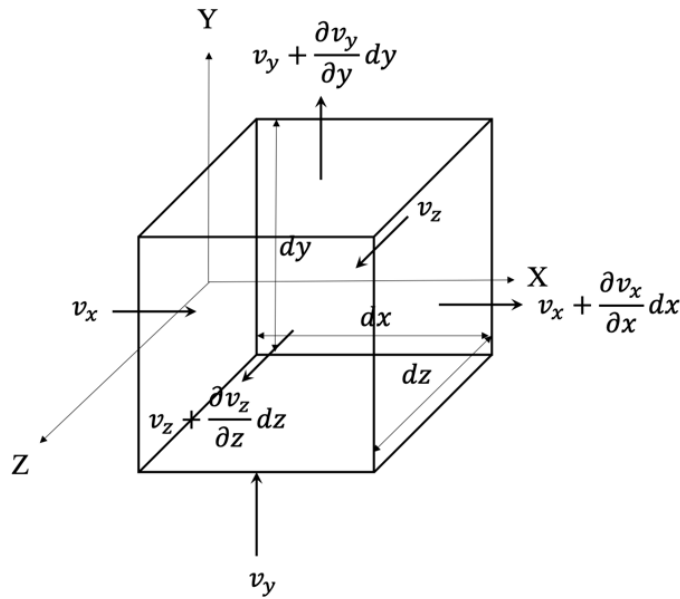
Figure A2-1: Fluid flow in porous media element

Using the definition for the amount of fluid flow,

$$v_x dydz + v_y dxdz + v_z dxdy - \left(v_x + \frac{\partial v_x}{\partial x} dx\right) dydz - \left(v_y + \frac{\partial v_y}{\partial y} dy\right) dxdz$$
$$- \left(v_z + \frac{\partial v_z}{\partial z} dz\right) dxdy = \frac{\partial \theta}{\partial t} dxdydz \qquad (A2 - 2)$$

Rearranging the terms, we get,

$$\left(\frac{\partial v_x}{\partial x} + \frac{\partial v_y}{\partial y} + \frac{\partial v_z}{\partial z}\right) dxdydz = \frac{\partial nS}{\partial t} dxdydz \qquad (A2-3)$$

where n represents the porosity, and S is the saturation of the fluid in the soil element

$$\frac{\partial v_x}{\partial x} + \frac{\partial v_y}{\partial y} + \frac{\partial v_z}{\partial z} + n\frac{\partial S}{\partial t} = 0 \qquad (A2-4)$$

Using the symbolic notation for spatial and temporal variation of partial differential equations, it can also be written as

$$\nabla v + \phi \dot{S} = 0 \qquad (A2-5)$$

For simplicity, in a one-dimensional fluid flow, this can be written as

$$\frac{\partial v}{\partial z} + \frac{\partial \theta}{\partial t} = 0 \qquad (A2-6)$$

This is the governing equation or the strong form of Finite Element Method (FEM) for porous media fluid flow.

Now, from the Darcy's law of fluid flow,

$$v = -K\frac{\partial h}{\partial z} \qquad (A2-7)$$

Here, K is coefficient of permeability [L/T], h is total head [L].

Substituting Equation $A2-7$ in Equation $A2-6$, we get,

$$\frac{\partial}{\partial z}\left(K\frac{\partial h}{\partial z}\right) = \frac{\partial \theta}{\partial t} \qquad (A2-8)$$

The hydraulic conductivity in Equations $A2-7$ and $A2-8$ is not constant in the unsaturated region but is a value that depends on the effective saturation of soil, S_e or the volume moisture content, θ. The total head, h in the same equation can be expressed as follows

$$h = \psi - z \qquad (A2-9)$$

Here, ψ is the pressure head [L], the coordinates, z in the vertical direction are positive downward.

Substituting equation $A2-9$ in $A2-8$, we get,

$$\frac{\partial}{\partial z}\left(K\frac{\partial \psi}{\partial z} - K\right) = \frac{\partial \theta}{\partial t} \qquad (A2-10)$$

This equation is referred to as the Richards' equation, which is the governing equation for saturated and unsaturated flow.

Richard's equation in Equation $A2 - 10$ can be formulated in different ways such as: Mixed form, ψ-based form, θ-based form based on the unknown parameter taken into consideration, and the advantages and limitations of some or all of these three methods are discussed previously in Celia et al. [1990], Milly et al. [1985], Rathfelder and Abriola [1994], Baca et al. [1997], Kirkland et al. [1992]. A general overview of the aforementioned methods is herein explored as follows:

A2.1.1 ψ-based form

The following equation is obtained by converting equation $A2 - 10$ into an equation in which only the pressure head is unknown.

$$\frac{\partial}{\partial z}\left(K\frac{\partial\psi}{\partial z} - K\right) = \frac{\partial\theta}{\partial\psi}\frac{\partial\psi}{\partial t} \qquad (A2 - 11)$$

If this relationship is substituted on the right side of equation $A2 - 6$,

$$\frac{\partial\theta}{\partial\psi}\frac{\partial\psi}{\partial t} = \frac{\partial(nS_r)}{\partial\psi}\frac{\partial\psi}{\partial t} = \left(S_r\frac{\partial n}{\partial\psi} + n\frac{\partial S_r}{\partial\psi}\right)\frac{\partial\psi}{\partial t} \qquad (A2 - 12)$$

Assuming that the change in the pressure head does not cause a change in the pore space in the unsaturated region, Eq. $A2 - 12$ is as follows.

$$\frac{\partial\theta}{\partial\psi}\frac{\partial\psi}{\partial t} = \left(\frac{\partial\theta}{\partial\psi} + \alpha\frac{\partial n}{\partial\psi}\right)\frac{\partial\psi}{\partial t} = (C + \alpha S_s)\frac{\partial\psi}{\partial t} \qquad (A2 - 13)$$

Here, C is the specific water capacity [L^{-1}], S_s is the specific storage coefficient [L^{-1}], $\alpha = 0$ (unsaturated), 1 (saturated) [dimensionless]. The specific water content, C is obtained from the gradient of the soil water characteristic curve representing the unsaturated characteristic, and the specific storage coefficient, S_s uses the representative value or experimental value for each soil.

Substituting Equation $A2 - 13$ in Equation $A2 - 11$ finally yields

$$\frac{\partial}{\partial z}\left(K(\psi)\frac{\partial\psi}{\partial z} - K(\psi)\right) = (C(\psi) + \alpha S_s)\frac{\partial\psi}{\partial t} \qquad (A2 - 14)$$

The advantage of the pressure head reference format is

➢ Even in heterogeneous ground, the value of the pressure head in the ground changes continuously,

so it can be used.

➢ It can be used for both saturated and unsaturated regions.

However, on the other hand, there is also a drawback

➢ Mass balance can't be satisfied strictly, and a detailed explanation is given in Abriola and Rathfelder [1993].

A2.1.2 θ-based form

The following equation is obtained by converting equation $A2 - 10$ into an equation in which only the volume moisture content is unknown.

$$\frac{\partial}{\partial z}\left(D(\theta)\frac{\partial \theta}{\partial z} - K(\theta)\right) = \frac{\partial \theta}{\partial t} \qquad (A2 - 15)$$

Here, D is the water diffusion coefficient [L²T] and is defined as follows:

$$D(\theta) = K(\theta)\frac{\partial \psi}{\partial \theta} = \frac{K(\theta)}{C(\theta)} \qquad (A2 - 16)$$

The advantage of the volume moisture content standard format is

➢ The conservation of mass is strictly maintained.

On the other hand, there are drawbacks such as:

➢ In the saturation region, the specific moisture capacity, C in the denominator on the right side of equation $A2 - 16$ is 0, so the moisture diffusion coefficient, D becomes infinite. Therefore, equation $A2 - 15$ cannot be used for the saturation region.

➢ In heterogeneous ground, it is difficult to use because the value of volumetric moisture content in the ground may be discontinuous.

A2.1.3 Mixed form

Equation $A2 - 10$ is a mixed Richards equation.

The advantage of the mixed format is that it strictly satisfies the conservation of mass, while retaining the advantages of the pressure head reference format.

A2.2 Unsaturation characteristics

Soil water retention and permeability are necessary data for analyzing unsaturated infiltration. As a representation of these measured data by a mathematical model, there is a soil water characteristic curve-unsaturated hydraulic conductivity model, which can express both water retention and hydraulic conductivity with a small number of parameters.

The Mualem-van Genuchten model and the Burdine-Brooks and Corey model have been proposed as a soil water characteristic curve-unsaturated hydraulic conductivity connected model, but the former is the most widely used today. The water retention curve function presented by van Genuchten is as follows:

$$S_e = [1 + (-\alpha\psi)^n]^{-m} \qquad (A2-17)$$

Here, S_e is the effective saturation [dimensionless], α [L^{-1}], n [dimensionless], and $m(= 1 - \frac{1}{n})$ [dimensionless] are parameters.

In addition, the unsaturated hydraulic conductivity estimation model presented by Mualem is

$$K_r = S_e{}^l \left[\frac{\int_0^{S_e} \frac{1}{|\psi|} dS_e}{\int_0^1 \frac{1}{|\psi|} dS_e} \right]^2 \qquad (A2-18)$$

Substituting Eq. $A2-17$ in $A2-18$, the following relative permeability coefficient function is obtained.

$$K_r = S_e{}^l \left[1 - \left(1 - S_e{}^{1/m} \right)^m \right]^2 \qquad (A2-19)$$

Here, K_r is the relative permeability coefficient [dimensionless] and l [dimensionless] is a parameter, which is empirically determined by Mualem and is often used to be 0.5.

A2.3 Spacial discretization using FEM

For each form of governing equation, discretize the space by using finite element method.

A2.3.1 ψ-based form

The governing equation is Equation A2 − 14, but if the volume change due to the change in pressure head is extremely small even in the saturated region, it is ignored.

$$L(\psi) = \frac{\partial}{\partial z}\left(K(\psi)\frac{\partial \psi}{\partial z} - K(\psi)\right) - C(\psi)\frac{\partial \psi}{\partial t} = 0 \qquad (A2-20)$$

The analysis target area is set to $0 \le z \le 1$, and it is divided into $m \ (= n - 1)$ elements by n nodes. The value of the pressure head, $\widehat{\psi^e}$ in each element can be linearly interpolated by the value of the pressure head at both ends of the element as follows.

$$\widehat{\psi^e}(z,t) = \frac{z_{i+1} - z}{\Delta z}\psi_i(t) + \frac{z - z_i}{\Delta z}\psi_{i+1}(t)$$

$$= N_i^e(z)\psi_i(t) + N_{i+1}^e(t)\psi_{i+1}(t)$$

$$= [N_i^e \quad N_{i+1}^e]\begin{Bmatrix} \psi_i \\ \psi_{i+1} \end{Bmatrix} \qquad (A2-21)$$

Hence,

$$z_i \le z \le z_{i+1}$$

$$\Delta z = z_{i+1} - z_i$$

The above equation is represented as:
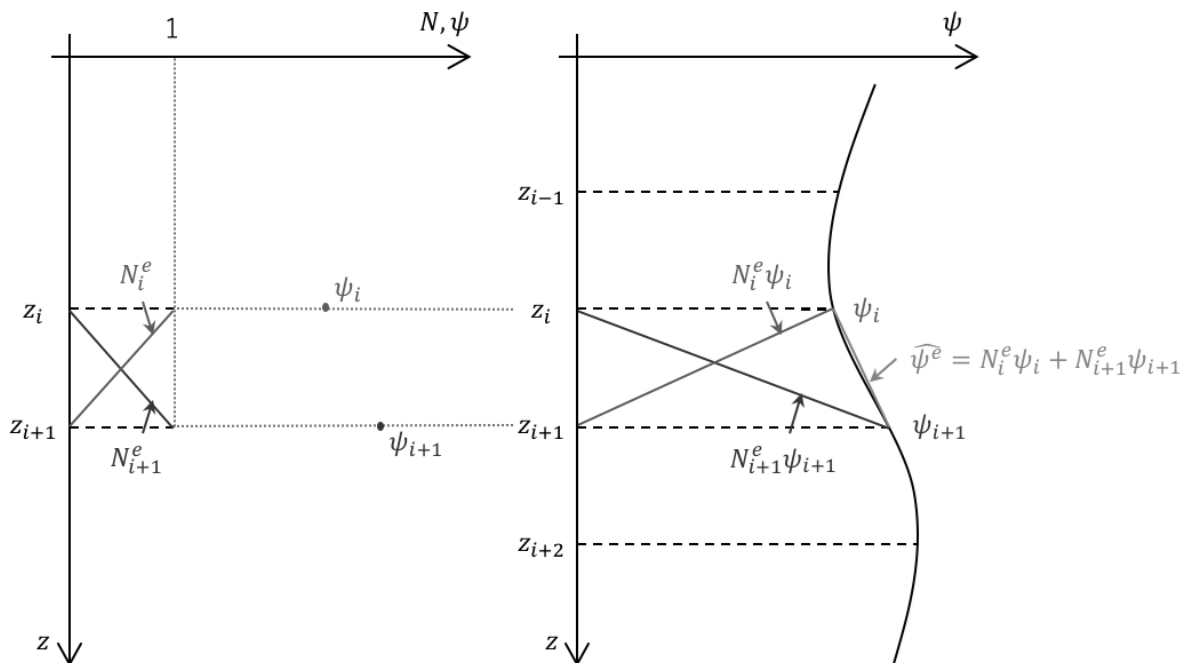
Figure A2-2: Linear interpolation of pressure head

When this is expanded to the entire area, E in which the elements are connected, the following equation is obtained.

$$\hat{\psi}(z,t) = \sum_e^E \widehat{\psi^e} = \sum_e^E \sum_i N_i^e \, \psi_i = \sum_{i=1}^n \phi_i(z)\psi_i(t) \qquad (A2-22)$$

Here, ϕ_i is a basis function and is given by the following equation.

$$\phi_i(z) = \begin{cases} 0 & : z < z_{i-1} \\ \dfrac{z - z_{i-1}}{z_i - z_{i-1}} & : z_{i-1} \le z \le z_i \\ \dfrac{z_{i+1} - z}{z_{i+1} - z_i} & : z_i \le z \le z_{i+1} \\ 0 & : z_{i+1} < z \end{cases} \qquad (A2-23)$$

Substituting the approximate value of the pressure head, $\hat{\psi}$ into Equation A2 $-$ 20, determining the weight (test) function by the Galerkin method, and using the weighted residual method.

$$\int_0^l L(\hat{\psi})\phi_i \, dz = \int_0^l \frac{\partial}{\partial z}\left(K(\hat{\psi})\frac{\partial\hat{\psi}}{\partial z} - K(\hat{\psi}) \right) - C(\hat{\psi})\frac{\partial\hat{\psi}}{\partial t} \phi_i = 0 \qquad (A2-24)$$

Hence, $i = 1,2,3 \ldots, n-1, n$

The following equation is obtained by using integration by parts for the higher-order differential term of Equation A2 $-$ 24.

$$\int_0^l \left(K(\hat{\psi})\frac{\partial\hat{\psi}}{\partial z} - K(\hat{\psi}) \right)\left(\frac{\partial\phi_i}{\partial z}\right) dz + \int_0^l C(\hat{\psi})\frac{\partial\hat{\psi}}{\partial t}\phi_i \, dz = \left[\left(K(\hat{\psi})\frac{\partial\hat{\psi}}{\partial z} - K(\hat{\psi}) \right)\phi_i \right]_0^l \qquad (A2-25)$$

Substituting Equation A2 $-$ 22 in Equation A2 $-$ 25,

$$[A_{ij}]\{\psi_j\} + [F_{ij}]\left\{\frac{\partial\psi_j}{\partial t}\right\} = \{B_i\} + \{Q_i\} \qquad (A2-26)$$

Here,

$$\left.\begin{aligned} [A_{ij}] &= \int_0^l K_k\phi_k\frac{\partial\phi_i}{\partial z}\frac{\partial\phi_j}{\partial z}dz \\ [F_{ij}] &= \int_0^l C_k\phi_k\phi_i\phi_j \, dz \\ \{B_i\} &= \int_0^l K_k\phi_k\frac{\partial\phi_i}{\partial z}dz \\ \{Q_i\} &= \left[\left(K(\hat{\psi})\frac{\partial\hat{\psi}}{\partial z} - K(\hat{\psi}) \right)\phi_i \right]_0^l \end{aligned}\right\} \qquad (A2-27)$$

Hence, $j, k = 1,2,3 \ldots, n-1, n$

Here, the integral for the entire region of each term in Equation $A2 - 27$ can be expressed as the sum of the integral values of each element, and is as follows:

$$
\left.\begin{aligned}
[A_{ij}] &= \sum_e^E \left[\int_{z_p}^{z_{p+1}} K_k \phi_k \frac{\partial \phi_i}{\partial z} \frac{\partial \phi_j}{\partial z} dz \right] &= \sum_e^E [A_{ij}]^e \\
[F_{ij}] &= \sum_e^E \left[\int_{z_p}^{z_{p+1}} C_k \phi_k \phi_i \phi_j \, dz \right] &= \sum_e^E [F_{ij}]^e \\
\{B_i\} &= \sum_e^E \left\{ \int_{z_p}^{z_{p+1}} K_k \phi_k \frac{\partial \phi_i}{\partial z} dz \right\} &= \sum_e^E \{B_i\}^e \\
\{Q_i\} &= \sum_e^E \left\{ \left[\left(K(\hat{\psi}) \frac{\partial \hat{\psi}}{\partial z} - K(\hat{\psi}) \right) \phi_i \right]_{z_p}^{z_{p+1}} \right\} &= \sum_e^E \{Q_i\}^e
\end{aligned}\right\} \qquad (A2-28)
$$

Hence, $p = 1,2,3 \ldots, n-2(= m-1), n-1(= m)$

Calculating for each:

a) $[A_{ij}]$

$$
[A_{ij}]^e = \int_{z_p}^{z_{p+1}} (K_p \phi_p + K_{p+1} \phi_{p+1})
\begin{bmatrix}
\dfrac{\partial \phi_p}{\partial z} \dfrac{\partial \phi_p}{\partial z} & \dfrac{\partial \phi_p}{\partial z} \dfrac{\partial \phi_{p+1}}{\partial z} \\
\dfrac{\partial \phi_{p+1}}{\partial z} \dfrac{\partial \phi_p}{\partial z} & \dfrac{\partial \phi_{p+1}}{\partial z} \dfrac{\partial \phi_{p+1}}{\partial z}
\end{bmatrix} dz \qquad (A2-29)
$$

Here, based on the definition for Equation $A2 - 23$

$$
\frac{\partial \phi_p}{\partial z} = \frac{\partial}{\partial z} \left(\frac{z_{p+1} - z}{z_{p+1} - z_p} \right) = -\frac{1}{z_{p+1} - z_p} \qquad (A2-30)
$$

$$
\frac{\partial \phi_{p+1}}{\partial z} = \frac{\partial}{\partial z} \left(\frac{z - z_p}{z_{p+1} - z_p} \right) = \frac{1}{z_{p+1} - z_p} \qquad (A2-31)
$$

Since,

$$
\begin{aligned}
A_{pp}^e &= \int_{z_p}^{z_{p+1}} (K_p \phi_p + K_{p+1} \phi_{p+1}) \frac{\partial \phi_p}{\partial z} \frac{\partial \phi_p}{\partial z} dz \\
&= \frac{K_p + K_{p+1}}{2(z_{p+1} - z_p)} \qquad (A2-32)
\end{aligned}
$$

$$A^e_{p(p+1)} = \int_{z_p}^{z_{p+1}} \left(K_p\phi_p + K_{p+1}\phi_{p+1}\right)\frac{\partial\phi_p}{\partial z}\frac{\partial\phi_{p+1}}{\partial z}\,dz$$

$$= -\frac{K_p + K_{p+1}}{2(z_{p+1} - z_p)} \tag{A2 − 33}$$

Similarly, the other components are calculated as follows:

$$[A_{ij}]^e = \begin{bmatrix} \dfrac{K_p + K_{p+1}}{2(z_{p+1} - z_p)} & -\dfrac{K_p + K_{p+1}}{2(z_{p+1} - z_p)} \\[3mm] -\dfrac{K_p + K_{p+1}}{2(z_{p+1} - z_p)} & \dfrac{K_p + K_{p+1}}{2(z_{p+1} - z_p)} \end{bmatrix} \tag{A2 − 34}$$

If this is expanded to the entire area, E where the elements are connected

$$[A_{ij}] = \begin{bmatrix} \dfrac{K_1 + K_2}{2L_{12}} & -\dfrac{K_1 + K_2}{2L_{12}} & 0 & \cdots & 0 \\[3mm] -\dfrac{K_1 + K_2}{2L_{12}} & \dfrac{K_1 + K_2}{2L_{12}} + \dfrac{K_2 + K_3}{2L_{23}} & -\dfrac{K_2 + K_3}{2L_{23}} & 0 & \vdots \\[3mm] 0 & -\dfrac{K_2 + K_3}{2L_{23}} & \ddots & -\dfrac{K_{n-2} + K_{n-1}}{2L_{(n-2)(n-1)}} & 0 \\[3mm] \vdots & 0 & -\dfrac{K_{n-2} + K_{n-1}}{2L_{(n-2)(n-1)}} & \dfrac{K_{n-2} + K_{n-1}}{2L_{(n-2)(n-1)}} + \dfrac{K_{n-1} + K_n}{2L_{(n-1)n}} & -\dfrac{K_{n-1} + K_n}{2L_{(n-1)n}} \\[3mm] 0 & \cdots & 0 & -\dfrac{K_{n-1} + K_n}{2L_{(n-1)n}} & \dfrac{K_{n-1} + K_n}{2L_{(n-1)n}} \end{bmatrix} \tag{A2 − 35}$$

Here,

$$L_{ij} = z_j - z_i \tag{A2 − 36}$$

b) $\left[F_{ij}\right]$

$$[F_{ij}]^e = \int_{z_p}^{z_{p+1}} \left(C_p\phi_p + C_{p+1}\phi_{p+1}\right)\begin{bmatrix} \phi_p\phi_p & \phi_p\phi_{p+1} \\ \phi_{p+1}\phi_p & \phi_{p+1}\phi_{p+1} \end{bmatrix}dz \tag{A2 − 37}$$

Here, based on the definition for Equation A2 − 23

$$F^e_{pp} = \int_{z_p}^{z_{p+1}} \left(C_p\phi_p + C_{p+1}\phi_{p+1}\right)\phi_p\phi_p\,dz$$

$$= \left(\frac{C_p}{4} + \frac{C_{p+1}}{12}\right)\left(z_{p+1} - z_p\right) \tag{A2 − 38}$$

$$F^e_{p(p+1)} = \int_{z_p}^{z_{p+1}} \left(C_p\phi_p + C_{p+1}\phi_{p+1}\right)\phi_p\phi_{p+1}\,dz$$

$$= \left(\frac{C_p}{12} + \frac{C_{p+1}}{12}\right)\left(z_{p+1} - z_p\right) \tag{A2 − 39}$$

Similarly, the other components are calculated as follows:

$$[F_{ij}]^e = \begin{bmatrix} \dfrac{3C_p + C_{p+1}}{12}(z_{p+1} - z_p) & \dfrac{C_p + C_{p+1}}{12}(z_{p+1} - z_p) \\ \dfrac{C_p + C_{p+1}}{12}(z_{p+1} - z_p) & \dfrac{C_p + 3C_{p+1}}{12}(z_{p+1} - z_p) \end{bmatrix} \qquad (A2-40)$$

If this is expanded to the entire area, E where the elements are connected

$$[F_{ij}] = \begin{bmatrix} \dfrac{3C_1+C_2}{12}L_{12} & \dfrac{C_1+C_2}{12}L_{12} & 0 & & \cdots & & 0 \\ \dfrac{C_1+C_2}{12}L_{12} & \dfrac{C_1+3C_2}{12}L_{12}+\dfrac{3C_2+C_3}{12}L_{23} & \dfrac{C_2+C_3}{12}L_{23} & & 0 & & \vdots \\ 0 & \dfrac{C_2+C_3}{12}L_{23} & \ddots & & \dfrac{C_{n-2}+C_{n-1}}{12}L_{(n-2)(n-1)} & & 0 \\ \vdots & 0 & \dfrac{C_{n-2}+C_{n-1}}{12}L_{(n-2)(n-1)} & \dfrac{C_{n-2}+3C_{n-1}}{12}L_{(n-2)(n-1)}+\dfrac{3C_{n-1}+C_n}{12}L_{(n-1)n} & \dfrac{C_{n-1}+C_n}{12}L_{(n-1)n} \\ 0 & \cdots & & 0 & \dfrac{C_{n-1}+C_n}{12}L_{(n-1)n} & & \dfrac{C_{n-1}+3C_n}{12}L_{(n-1)n} \end{bmatrix} \quad (A2-41)$$

Here, mass-lumping is performed on the right side of Equation $A2-41$. It is empirically known that the problem of computational stability caused by substituting Equation $A2-41$ can be solved by performing lumping.

$$[F_{ij}] = \begin{bmatrix} \dfrac{2C_1+C_2}{6}L_{12} & 0 & \cdots & & \cdots & & 0 \\ 0 & \dfrac{C_1+2C_2}{6}L_{12}+\dfrac{2C_2+C_3}{6}L_{23} & 0 & & & & \vdots \\ \vdots & & 0 & \ddots & & 0 & & \vdots \\ \vdots & & & 0 & \dfrac{C_{n-2}+2C_{n-1}}{6}L_{(n-2)(n-1)}+\dfrac{2C_{n-1}+C_n}{6}L_{(n-1)n} & 0 \\ 0 & \cdots & & \cdots & & 0 & \dfrac{C_{n-1}+2C_n}{6}L_{(n-1)n} \end{bmatrix} \quad (A2-42)$$

c) $\{B_i\}$

$$\{B_i\}^e = \int_{z_p}^{z_{p+1}} \left(K_p\phi_p + K_{p+1}\phi_{p+1} \right) \begin{Bmatrix} \dfrac{\partial \phi_p}{\partial z} \\ \dfrac{\partial \phi_{p+1}}{\partial z} \end{Bmatrix} dz \qquad (A2-43)$$

Here, from Equation $A2-30$ and Equation $A2-31$

$$\begin{aligned} B_p^e &= \int_{z_p}^{z_{p+1}} \left(K_p\phi_p + K_{p+1}\phi_{p+1} \right) \frac{\partial \phi_p}{\partial z} dz \\ &= -\frac{K_p + K_{p+1}}{2} \end{aligned} \qquad (A2-44)$$

$$\begin{aligned} B_{p+1}^e &= \int_{z_p}^{z_{p+1}} \left(K_p\phi_p + K_{p+1}\phi_{p+1} \right) \frac{\partial \phi_{p+1}}{\partial z} dz \\ &= \frac{K_p + K_{p+1}}{2} \end{aligned} \qquad (A2-45)$$

If this is expanded to the entire area, E where the elements are connected

$$\{B_i\} = \begin{Bmatrix} -\dfrac{K_1 + K_2}{2} \\[2mm] \dfrac{K_1 + K_2}{2} - \dfrac{K_2 + K_3}{2} \\[2mm] \vdots \\[2mm] \dfrac{K_{n-2} + K_{n-1}}{2} - \dfrac{K_{n-1} + K_n}{2} \\[2mm] \dfrac{K_{n-1} + K_n}{2} \end{Bmatrix} \qquad (A2-46)$$

d) $\{Q_i\}$

$\{Q_i\}$ indicates the amount of inflow and outflow at each node, and has a value only at the node where there is inflow from the outside of the analysis target area or outflow to the outside according to the law of conservation of mass. Assuming that the inflow is positive and there is no inflow or outflow from other than the front and bottom surfaces,

$$\{Q_i\} = \begin{Bmatrix} q_1 \\ 0 \\ \vdots \\ 0 \\ q_n \end{Bmatrix} \qquad (A2-47)$$

A2.3.2 θ-based form

This is omitted since it is impractical.

A2.3.3 Mixed form

Substituting the approximate value of the pressure head ($\hat{\psi}$) and the approximate value of the volume moisture content ($\hat{\theta}$) into Equation A2 $-$ 10, the weight (test) function is determined by the Galerkin method, and the weighted residual method is used.

$$\int_0^l \left[\frac{\partial}{\partial z}\left(K(\hat{\psi})\frac{\partial \hat{\psi}}{\partial z} - K(\hat{\psi}) \right) - \frac{\partial \hat{\theta}}{\partial t} \right] \phi_i = 0 \qquad (A2-48)$$

Hence, $i = 1,2,3 \dots, n-1, n$

The approximate value ($\hat{\theta}$) of the volume moisture content is as follows. The derivation is the same as the pressure head.

$$\hat{\theta}(z,t) = \sum_{i=1}^{n} \phi_i(z)\theta_i(t) \qquad (A2-49)$$

The following equation is obtained by using integration by parts for the higher-order differential term of Equation A2 − 49:

$$\int_0^l \left(K(\hat{\psi})\frac{\partial \hat{\psi}}{\partial z} - K(\hat{\psi}) \right)\left(\frac{\partial \phi_i}{\partial z} \right)dz + \int_0^l \frac{\partial \hat{\theta}}{\partial t}\phi_i\,dz = \left[\left(K(\hat{\psi})\frac{\partial \hat{\psi}}{\partial z} - K(\hat{\psi}) \right)\phi_i \right]_0^l \qquad (A2-50)$$

Substituting Equation A2 − 22 and Equation A2 − 49 in Equation A2 − 50

$$[A_{ij}]\{\psi_j\} + [G_{ij}]\left\{\frac{\partial \theta_j}{\partial t}\right\} = \{B_i\} + \{Q_i\} \qquad (A2-51)$$

Here,

$$\left.\begin{aligned}
[A_{ij}] &= \int_0^l K_k \phi_k \frac{\partial \phi_i}{\partial z}\frac{\partial \phi_j}{\partial z}dz \\
[G_{ij}] &= \int_0^l \phi_i \phi_j\,dz \\
\{B_i\} &= \int_0^l K_k \phi_k \frac{\partial \phi_i}{\partial z}dz \\
\{Q_i\} &= \left[\left(K(\hat{\psi})\frac{\partial \hat{\psi}}{\partial z} - K(\hat{\psi}) \right)\phi_i \right]_0^l
\end{aligned}\right\} \qquad (A2-52)$$

Hence, $j, k = 1,2,3 \dots, n-1, n$

Here, the integral for the entire region of each term in Equation A2 − 52 can be expressed as the sum of the integral values of each element, and is as follows:

$$\left.\begin{aligned}
[A_{ij}] &= \sum_e^E \left[\int_{z_p}^{z_{p+1}} K_k \phi_k \frac{\partial \phi_i}{\partial z}\frac{\partial \phi_j}{\partial z}dz \right] &&= \sum_e^E [A_{ij}]^e \\
[G_{ij}] &= \sum_e^E \left[\int_{z_p}^{z_{p+1}} \phi_i \phi_j\,dz \right] &&= \sum_e^E [G_{ij}]^e \\
\{B_i\} &= \sum_e^E \left\{ \int_{z_p}^{z_{p+1}} K_k \phi_k \frac{\partial \phi_i}{\partial z}dz \right\} &&= \sum_e^E \{B_i\}^e \\
\{Q_i\} &= \sum_e^E \left\{ \left[\left(K(\hat{\psi})\frac{\partial \hat{\psi}}{\partial z} - K(\hat{\psi}) \right)\phi_i \right]_{z_p}^{z_{p+1}} \right\} &&= \sum_e^E \{Q_i\}^e
\end{aligned}\right\} \qquad (A2-53)$$

Hence, $p = 1,2,3 \dots, n-2(= m-1), n-1(= m)$

The calculation of A_{ij}, B_i, Q_i are the same as the pressure head reference format, hence, only G_{ij} is calculated here.

$$[G_{ij}]^e = \int_{z_p}^{z_{p+1}} \begin{bmatrix} \phi_p \phi_p & \phi_p \phi_{p+1} \\ \phi_{p+1} \phi_p & \phi_{p+1} \phi_{p+1} \end{bmatrix} dz \qquad (A2-54)$$

Here, based on the definition of Equation $A2-23$

$$G_{pp}^e = \int_{z_p}^{z_{p+1}} \phi_p \phi_p \, dz$$
$$= \frac{z_{p+1} - z_p}{3} \qquad (A2-55)$$

$$G_{p(p+1)}^e = \int_{z_p}^{z_{p+1}} \phi_p \phi_{p+1} \, dz$$
$$= \frac{z_{p+1} - z_p}{6} \qquad (A2-56)$$

Similarly, the other components are calculated as follows:

$$[G_{ij}]^e = \begin{bmatrix} \dfrac{z_{p+1} - z_p}{3} & \dfrac{z_{p+1} - z_p}{6} \\ \dfrac{z_{p+1} - z_p}{6} & \dfrac{z_{p+1} - z_p}{3} \end{bmatrix} \qquad (A2-57)$$

If this is expanded to the entire area, E where the elements are connected

$$[G_{ij}] = \begin{bmatrix} \dfrac{L_{12}}{3} & \dfrac{L_{12}}{6} & 0 & \cdots & & 0 \\ \dfrac{L_{12}}{6} & \dfrac{L_{12}}{3} + \dfrac{L_{23}}{3} & \dfrac{L_{23}}{6} & 0 & & \vdots \\ 0 & \dfrac{L_{23}}{6} & \ddots & \dfrac{L_{(n-2)(n-1)}}{6} & 0 \\ \vdots & 0 & \dfrac{L_{(n-2)(n-1)}}{6} & \dfrac{L_{(n-2)(n-1)}}{3} + \dfrac{L_{(n-1)n}}{3} & \dfrac{L_{(n-1)n}}{6} \\ 0 & \cdots & 0 & \dfrac{L_{(n-1)n}}{6} & \dfrac{L_{(n-1)n}}{3} \end{bmatrix} \qquad (A2-58)$$

Here, mass-lumping is performed on the right side of Equation $A2-58$. It is empirically known that the problem of computational stability caused by substituting Equation $A2-58$ can be solved by performing lumping.

$$[G_{ij}] = \begin{bmatrix} \dfrac{L_{12}}{2} & 0 & \cdots & & \cdots & 0 \\ 0 & \dfrac{L_{12}}{2} + \dfrac{L_{23}}{2} & 0 & & & \vdots \\ \vdots & 0 & \ddots & 0 & & \vdots \\ \vdots & & 0 & \dfrac{L_{(n-2)(n-1)}}{2} + \dfrac{L_{(n-1)n}}{2} & 0 \\ 0 & \cdots & & \cdots & 0 & \dfrac{L_{(n-1)n}}{2} \end{bmatrix} \qquad (A2-59)$$

A2.4 Time discretization using FEM

For each format, we will introduce time discretization and iterative calculation by the backward finite difference method.

A2.4.1 ψ-based form

Using the backward difference for the time term in Equation $A2-26$,

$$[A_{ij}^{t+1}]\{\psi_j^{t+1}\} + [F_{ij}^{t+1}]\left\{\frac{\psi_j^{t+1} - \psi_j^t}{\Delta t}\right\} = \{B_i^{t+1}\} + \{Q_i^{t+1}\} \qquad (A2-60)$$

Here, arranging ψ, we get,

$$\left[[A_{ij}^{t+1}] + \frac{1}{\Delta t}[F_{ij}^{t+1}]\right]\{\psi_j^{t+1}\} = \{B_i^{t+1}\} + \{Q_i^{t+1}\} + \frac{1}{\Delta t}[F_{ij}^{t+1}]\{\psi_j^t\} \qquad (A2-61)$$

The inflow in the unsaturated region is non-linear because the hydraulic conductivity, K and specific moisture capacity, C contained in Equation $A2-61$ change depending on the value of the pressure head, ψ but iterative calculation is conducted as follows:

The value can be obtained by:

1. Estimating each coefficient by assuming the value of the pressure head, $(\psi^{t+1,1})$

2. Substituting each estimated coefficient, thereby obtaining the value of the pressure head, $(\psi^{t+1,2})$

3. Estimating each coefficient again using the value obtained in (2)

4. After that, (2) and (3) are repeated until $\psi^{t+1,s+1} - \psi^{t+1,s}$ falls within the allowable error range.

Considering the iterative calculation, Equation $A2-61$ can be written as:

$$\{\psi_j^{t+1,s+1}\} = \left[[A_{ij}^{t+1,s}] + \frac{1}{\Delta t}[F_{ij}^{t+1,s}]\right]^{-1}\left\{\{B_i^{t+1,s}\} + \{Q_i^{t+1,s}\} + \frac{1}{\Delta t}[F_{ij}^{t+1,s}]\{\psi_j^t\}\right\} \qquad (A2-62)$$

A2.4.2 θ-based form

Omitted

A2.4.3 Mixed form

Using the backward Euler method for the time term in Equation $A2-51$

$$[A_{ij}^{t+1}]\{\psi_j^{t+1}\} + [G_{ij}^{t+1}]\left\{\frac{\theta_j^{t+1} - \theta_j^t}{\Delta t}\right\} = \{B_i^{t+1}\} + \{Q_i^{t+1}\} \qquad (A2-63)$$

Considering iterative calculations

$$[A_{ij}^{t+1,s}]\{\psi_j^{t+1,s+1}\} + [G_{ij}^{t+1,s}]\left\{\frac{\theta_j^{t+1,s+1} - \theta_j^t}{\Delta t}\right\} = \{B_i^{t+1,s}\} + \{Q_i^{t+1,s}\} \qquad (A2-64)$$

Here, using Taylor's expansion for $\theta_j^{t+1,s+1}$

$$\theta_j^{t+1,s+1} = \theta_j^{t+1,s} + \frac{\partial\theta}{\partial\psi}\Bigg|^{t+1,s}\left(\psi_j^{t+1,s+1} - \psi_j^{t+1,s}\right) + 0 \qquad (A2-65)$$

Substituting Equation $A2-65$ in Equation $A2-61$, we get,

$$[A_{ij}^{t+1,s}]\{\psi_j^{t+1,s+1}\} + [F_{ij}^{t+1,s}]\left\{\frac{\psi_j^{t+1,s+1} - \psi_j^{t+1,s}}{\Delta t}\right\} + [G_{ij}^{t+1,s}]\left\{\frac{\theta_j^{t+1,s} - \theta_j^t}{\Delta t}\right\}$$
$$= \{B_i^{t+1,s}\} + \{Q_i^{t+1,s}\} \qquad (A2-66)$$

Here,

$$\delta_j^{t+1,s} = \psi_j^{t+1,s+1} - \psi_j^{t+1,s} \qquad (A2-67)$$

$$[A_{ij}^{t+1,s}]\{\delta_j^{t+1,s} + \psi_j^{t+1,s}\} + [F_{ij}^{t+1,s}]\left\{\frac{\delta_j^{t+1,s}}{\Delta t}\right\} + [G_{ij}^{t+1,s}]\left\{\frac{\theta_j^{t+1,s} - \theta_j^t}{\Delta t}\right\} = \{B_i^{t+1,s}\} + \{Q_i^{t+1,s}\}(A2-68)$$

Rearranging the terms, we get,

$$\{\delta_j^{t+1,s}\} = \left[[A_{ij}^{t+1,s}] + \frac{1}{\Delta t}[F_{ij}^{t+1,s}]\right]^{-1}\left\{\{B_i^{t+1,s}\} + \{Q_i^{t+1,s}\}[A_{ij}^{t+1,s}]\{\psi_j^{t+1,s}\} - \frac{1}{\Delta t}[G_{ij}^{t+1,s}]\{\theta_j^{t+1,s} - \theta_j^t\}\right\}$$